

Voltammetric Sensing

A thesis submitted for the degree of Doctor of Philosophy
in Physical and Theoretical Chemistry

Min Lu
St Hugh's College

Trinity Term 2014

Abstract

Electrochemical analysis using mercury electrodes has been a prominent methodology since the beginning of voltammetry, however, due to its toxic nature their use is being slowly phased out in favour of environmentally friendlier alternatives. In this thesis, carbon electrodes feature heavily as a means to provide a cheaper and non-toxic approach to voltammmetric sensing. Pulse techniques have also been used for the sensitive detection of commonly studied analytes, including antimony and iron.

In the first instance, antimony (V) is determined at an unmodified edge plane pyrolytic graphite (EPPG) electrode using differential pulse anodic stripping voltammetry (DPASV). Antimony is a naturally occurring element of significant toxicity, however, its detection has been a very under-explored area electrochemically and often needs to be reduced from a +V to +III oxidation state prior to electroanalysis. Chapter 5 describes antimony detection in its pentavalent form at an unmodified carbon surface in 0.25 M HCl by depositing beyond the hydrogen wave such that interfering effects from hydrogen gas at the working electrode is avoided and stripping peaks can be analysed. Next, the simple fabrication of a vibrating electrode is presented by modifying a commercially available vibrating toothbrush with platinum foil as a means to enhance mass transport for electroanalytical work. Sensitive detection of trace analytes is an important aspect of electroanalytical chemistry, and the work presented in chapter 6 also suggests the possible fabrication of vibrating electrodes with a wide scope for different electrode materials.

Iron is a commonly studied analyte due to its prominence in the environment and biological systems, and many analytical techniques have been used for determining its concentration and speciation. Chapter 7 aims to summarise and give a review of re-

cent *electrochemical* methods for the determination of iron. Following this, a square wave voltammetric method was used for the detection of Fe(III) at an unmodified edge plane pyrolytic graphite (EPPG) electrode and a screen printed electrode (SPE). Sensitive results could be achieved *without* the need for surface modification, and the simple procedure was applied to real samples of commercially bottled mineral water.

The final chapters of this thesis looks at pH determination at carbon electrodes. pH is an important measurement used in nearly all industries and as such, the need for its determination is of great interest. Chapter 9 uses an unmodified edge plane pyrolytic graphite (EPPG) electrode as a simple sensor for pH determination by exploiting the pH sensitive nature of surface quinone groups intrinsic within carbon edge-plane like sites. Developing this further, an unmodified glassy carbon (GC) electrode was investigated in chapter 10 and shown to correspond well with Nernstian behaviour based on a 2 proton/2 electron system at 298 K and 310 K. Using this approach, both EPPG and GC electrodes are suggested as new materials for pH determination and can be used in aqueous solutions over the pH range 1.0 to 13.0, as a cheap and simple alternative to the classic glass electrode.

Acknowledgements

First and foremost, my sincere thanks go to Professor Richard Compton for all his help, patience and guidance throughout my time in group, during both Part II and DPhil.

Thank you also to everyone in the Compton group (past and present). I have made many great friendships along the way that I will take with me in the years ahead. Special mention go to Emma, Ying, Lin and Eddy for sharing this DPhil journey with me. I've thoroughly enjoyed our "first year" dinners, drinks and chats and it is people like you that make 3 years fly by.

I have enjoyed calling Oxford my home for the past 7 years, and this would not have been the case without some amazing people I have met during my time here. Thank you to all my friends at Hilda's and Univ who have been by my side since my first moments in Oxford, I feel privileged to have friends like you. Special thanks go to Jo, Heather, Dave Quick and Matt for not moving to London and being only a bike ride away from a hug. Thank you also to Jemma for being an awesome housemate.

My time in Oxford as a graduate would not have been the same without the balance provided by the Hugh's MCR and Oxgrow. Thank you to all the people I have met for providing me an escape when times got tough. Huge thanks also go to Julie for all the London getaways, laughter and chats. Thank you for being there for me, you've been like the sister I never had.

Finally, to my parents who have helped me through life and all its ups and downs. Their unconditional love and support is a debt I will never be able to repay. Thank you both for shaping me into the person I am today. I love you and hope I can always make you happy and proud. I would also like to acknowledge and thank the rest of my family in China, though separated by distance, you have all been behind me every step of the way for which I am truly grateful.

Glossary

Roman Symbols

Symbol	Definition	Units
a_i	Activity of species i	
A	Electrode area	m^2
$[C]$	Concentration of species C	mol m^{-3}
$[C]_{bulk}$	Bulk solution concentration of species C	mol m^{-3}
$[C]_0$	Concentration of species C at the electrode surface	mol m^{-3}
D	Diffusion coefficient	m^2 s^{-1}
E	Potential	V
$E^{\ominus}$	Standard potential	V
$E_{\mathrm{f}}^{\ominus}$	Formal potential	V
E_a	Activation energy barrier	J
F	Faraday constant ≈ 96485	C mol^{-1}
G	Gibbs Energy	J mol^{-1}
I	Current	A
I_a	Oxidative current	A
I_c	Reductive current	A
I_{p}	Peak Current	A
j	Flux	mol m^{-2} s^{-1}
k^0	Heterogeneous rate constant	m s^{-1}
K_{eq}	Equilibrium constant	
m	Mass	g

Continued on next page

m_T	Mass transport coefficient	m s^{-1}
N_A	Avogadro constant $\approx 6.022 \times 10^{23}$	mol^{-1}
R	Gas constant ≈ 8.314	J K^{-1} mol^{-1}
t	Time	s
T	Temperature	K
Q	Total electric charge	C
x	x coordinate in Cartesian space	m
y	y coordinate in Cartesian space	m
z	Vertical coordinate in cylindrical space	m
$\neq$	Transition state	

Greek Symbols

Symbol	Definition	Units
α	Butler-Volmer transfer coefficient for reduction	
β	Butler-Volmer transfer coefficient for oxidation	
Γ	Surface coverage	mol m^{-2}
Λ	Matsuda-Ayabe parameter	V s^{-1}
μ	Chemical potential	
$\bar{\mu}$	Electrochemical potential	
ν	Scan rate	V s^{-1}
ϕ	Potential of certain phase	V

Abbreviations

Abbreviations used throughout the thesis is listed below. Abbreviations used in Chapter 7 is defined within the text.

Abbreviation	Definition
AAS	Atomic Absorption Spectroscopy
AdSV	Adsorptive Stripping Voltammetry
ASV	Anodic Stripping Voltammetry
BPPG	Basal Plane Pyrolytic Graphite
CSV	Cathodic Stripping Voltammetry
CV	Cyclic Voltammetry
DPV	Differential Pulse Voltammetry
EPPG	Edge Plane Pyrolytic Graphite
GC	Glassy Carbon
HMDE	Hanging Mercury Drop Electrode
HOPG	Highly Ordered Pyrolytic Graphite
HPLC	High Performance Liquid Chromatography
IHP	Inner Helmholtz Plane
LoD	Limit of Detection
LSV	Linear Sweep Voltammetry
MFE	Mercury Film Electrode
OHP	Outer Helmholtz Plane
RDE	Rotating Disk Electrode
SCE	Saturated Calomel Electrode
SPE	Screen Printed Electrode
SWV	Square Wave Voltammetry

Contents

1 Introduction : Fundamentals of Electrochemistry **1**

1.1 Equilibrium Electrochemistry 1

1.1.1 Chemical Equilibrium 1

1.1.2 Electrochemical Equilibrium 2

1.1.3 The Nernst Equation 5

1.2 Dynamic Electrochemistry 9

1.2.1 Three Electrode Setup 10

The Working Electrode 11

The Reference Electrode 12

The Counter Electrode 13

1.2.2 Solvents and Supporting Electrolyte 13

1.2.3 Removal of Oxygen 14

1.3 Faradaic and Non-Faradaic Processes 15

1.3.1 Electrode Processes 15

Current and Flux 15

1.3.2 Non-Faradaic Processes 17

The Electrical Double Layer 18

1.4 Mass Transport 20

1.4.1 Diffusion 21

Fick's 1st Law 21

Fick's 2nd Law 22

Diffusion Coefficients 22

The Cottrell Equation 23

The Nernst Diffusion Layer and Limiting Current 23

1.4.2 Convection 25

1.4.3 Migration 26

1.5 Electrode Kinetics 27

1.5.1 Heterogeneous Electron Transfer 27

1.5.2 Transition State Theory 28

1.5.3 Butler-Volmer Kinetics . . . 29
1.5.4 Tafel Analysis . . . 30
1.6 Voltammetric Techniques . . . 32
1.6.1 Linear Sweep Voltammetry . . . 32
1.6.2 Cyclic Voltammetry . . . 34
1.6.3 The Randles - Ševčik Equations . . . 38
Bibliography . . . 39

2 Introduction : Electroanalytical Methods 42
2.1 Amperometry . . . 43
2.1.1 Voltammetry . . . 43
2.1.2 Polarography . . . 45
2.1.3 Stripping Voltammetry . . . 47
Anodic Stripping Voltammetry (ASV) . . . 48
Cathodic Stripping Voltammetry (CSV) . . . 50
Adsorptive Stripping Voltammetry (AdSV) . . . 51
2.1.4 Pulse Techniques in Voltammetry . . . 53
Differential Pulse Voltammetry . . . 53
Square Wave Voltammetry . . . 55
2.1.5 Chronoamperometry . . . 57
2.2 Potentiometry . . . 60
2.3 Data Analysis Methods . . . 62
2.3.1 The Standard Addition Method . . . 63
2.3.2 Limits of Detection . . . 64
Bibliography . . . 65

3 Introduction : Carbon Electrodes 69
3.1 Introduction to Carbon Electrodes . . . 69
3.2 Carbon . . . 70
3.3 Pyrolytic Graphite . . . 70
3.3.1 BPPG vs. EPPG . . . 71
3.4 Glassy Carbon (GC) . . . 74

3.5 Screen Printed Carbon Electrodes (SPE) 77
Bibliography 79

4 Experimental Methods **83**
4.1 Chemical Reagents 83
4.2 Apparatus 83
4.2.1 Voltammetric Measurements 83
4.2.2 pH Measurements 85
4.3 Working Electrodes 85
4.3.1 Carbon Electrodes 86
Edge Plane Pyrolytic Graphite (EPPG) Electrodes 86
Screen Printed Electrodes (SPE) 86
Glassy Carbon (GC) Electrodes 87
Bibliography 87

5 Determination of Sb(V) using Differential Pulse Anodic Stripping Voltammetry at an Unmodified Edge Plane Pyrolytic Graphite Electrode **89**
5.1 Introduction 90
5.2 Experimental 93
5.2.1 Apparatus and Reagents 93
5.2.2 Experimental Procedure 94
5.3 Results and Discussions 95
5.4 Conclusions 98
Bibliography 98

6 Easy Fabrication of a Vibrating Foil Electrode **101**
6.1 Introduction 101
6.2 Experimental 103
6.2.1 Apparatus and Reagents 103
6.2.2 Experimental Procedure 103
6.3 Results and Discussions 105
6.4 Conclusions 110
Bibliography 110

7 Determination of Iron: Electrochemical Methods 112

7.1 Introduction . . . 112

7.2 Electrochemical Methods . . . 117

7.2.1 Mercury Electrodes . . . 118

7.2.2 Platinum Electrodes . . . 125

7.2.3 Carbon Electrodes . . . 128

7.3 Conclusions . . . 133

Bibliography . . . 134

8 Voltammetric Determination of Iron(III) in Water 140

8.1 Introduction . . . 140

8.2 Experimental . . . 141

8.2.1 Apparatus and Reagents . . . 141

8.2.2 Experimental Procedure . . . 142

8.3 Results and Discussions . . . 143

8.3.1 Optimisation of the EPPG Electrode . . . 143

8.3.2 Fe(III) Analysis on EPPG Electrode . . . 144

8.3.3 Analysis of Real Samples . . . 146

8.4 Conclusions . . . 151

Bibliography . . . 152

9 Voltammetric pH Sensor based on an Edge Plane Pyrolytic Graphite Electrode 153

9.1 Introduction . . . 153

9.2 Experimental . . . 158

9.2.1 Apparatus and Reagents . . . 158

9.2.2 Experimental Procedure . . . 158

9.3 Results and Discussions . . . 159

9.3.1 Investigating the Effects of changing Ionic Strength and Buffer Concentration . . . 164

9.4 Conclusions . . . 167

Bibliography . . . 167

10 Voltammetric pH Sensing using Carbon Electrodes : Glassy Carbon behaves similarly to EPPG **170**

10.1 Introduction 171

10.2 Experimental 174

10.2.1 Apparatus and Reagents 174

10.2.2 Experimental Procedure 174

10.3 Results and Discussions 175

10.3.1 Investigating the GC Electrode Response to pH at Higher Temperature 179

10.4 Conclusions 183

Bibliography 183

11 Summary and Conclusions **186**

Chapter 1

Introduction : Fundamentals of Electrochemistry

Electrochemistry is an area of chemistry which deals with the interconversion of electrical energy and chemical energy. Chemical reactions occur at interfaces where electrons are transferred, known as oxidation-reduction reactions. It is these electron transfers that drive or are driven by the interactions between electrical energy and chemical change. Electrochemical processes occur in a wide range of fields, ranging from fuel cells to photosynthesis, and the application of electrochemical methods can often be used to study these chemical systems. It is therefore essential to understand the principles of electrochemistry to gain an insight to the processes that occur.

This chapter will introduce fundamental principles of electrochemistry with respect to electrode reactions carried out in this thesis.

1.1 Equilibrium Electrochemistry

1.1.1 Chemical Equilibrium

For a reaction in chemical equilibrium, a state is reached where both the concentration of the reactants and products have no further tendency to change with time. For a reversible

reaction, this state can be achieved when the forward and backward reaction occurs at the same rate, resulting in a dynamic equilibrium. If species A and B are in equilibrium with species X and Y, the chemical equation to show this is:

$$aA + bB \rightleftharpoons xX + yY \tag{1.1}$$

Quantitatively, for a system in equilibrium at constant pressure and temperature, the Gibbs energy is at its minimum, and the standard Gibbs energy change for the reaction is given as:

$$\triangle\ G^0 = -RTlnK_{eq} \tag{1.2}$$

where R is the universal gas constant, T is the temperature and K_{eq} is the equilibrium constant for a given reaction. Such an equilibrium can exist for liquid, gaseous or solid species by expressing the equilibrium constant in partial pressures or in concentration. The corresponding equilibrium expression for the reaction in Equation 1.1, when relating to the species in aqueous form is given as:

$$K_{eq} = \frac{[X]^x[Y]^y}{[A]^a[B]^b} \tag{1.3}$$

1.1.2 Electrochemical Equilibrium

An electrochemical equilibrium differs significantly to a chemical equilibrium in that it involves the transfer of charged electrons between two separate phases (solution and electrode) such that both the chemical and electrical energies must be considered in each phase. Take, as an example, the reaction in Equation 1.4.

$$Fe(CN)_6^{3-}(aq) + e^-(m) \rightleftharpoons Fe(CN)_6^{4-}(aq) \tag{1.4}$$

An electrochemical equilibrium is set up when an inert metal electrode, such as a platinum wire, is immersed in a solution of potassium ferrocyanide, $K_4Fe(CN)_6$, and potassium ferricyanide, $K_3Fe(CN)_6$, as shown in Figure 1.1. The equilibrium established at the electrode surface (Equation 1.4) involves the two dissolved ions and the electrons in the metal electrode. The rate at which $Fe(CN)_6^{4-}$ gives up electrons to the electrode, is opposed by the rate at which electrons are released to the $Fe(CN)_6^{3-}$ anions. The $Fe(CN)_6^{4-}$ loses an electron and is "oxidised" whilst the $Fe(CN)_6^{3-}$ gains an electron and is "reduced". The reaction proceeds until a dynamic equilibrium is established between the chemical species where no further changes occur, but note that the concentration of Fe^{3+} and Fe^{2+} will not be significantly changed from their values before the introduction of the electrode into the solution since the amount of charge transferred in reaching equilibrium is tiny.

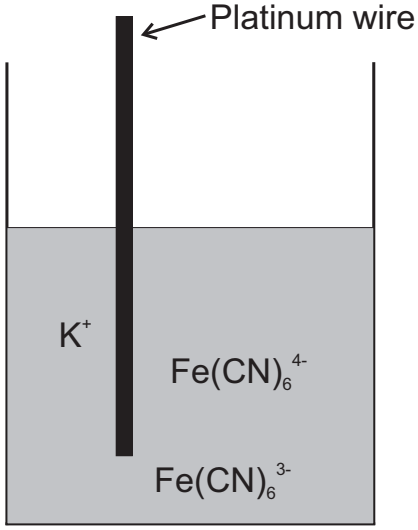


Figure 1.1: Aqueous solution of potassium ferrocyanide (Fe^{2+}) and ferricyanide (Fe^{3+}) into which a platinum wire electrode is immersed. The K^+ ions ensure electro-neutrality in bulk solution

It can be seen that irrespective of the position of equilibrium, there is likely to be a net electrical charge on both phases due to the transferred charged electrons such that a charge separation will exist between the electrode and the solution species. It is this charge separation that leads to the origin of an electrode potential being established.

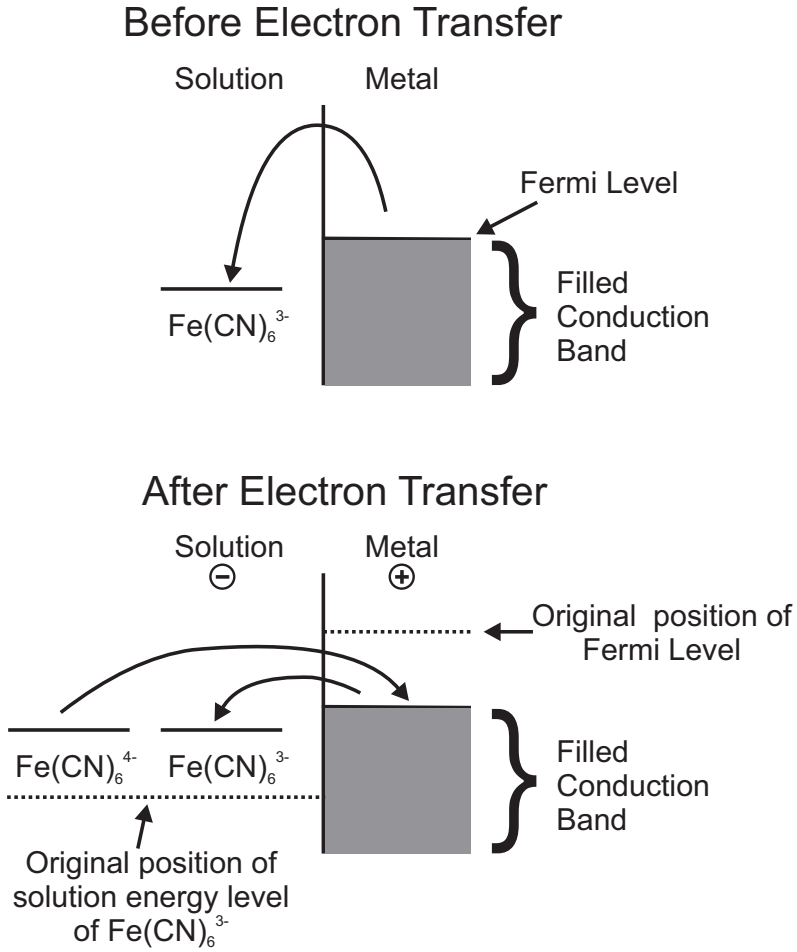


Figure 1.2: Energy level diagram illustrating the energy difference between the metal and the solution phase before and after the establishment of equilibrium

Changes in the electron energies at the electrode/solution interface can be depicted using an energy level diagram as shown in Figure 1.2 [1]. The electronic structure of metals consist of conduction bands in which the energy levels form an effective continuum and are filled up to an energy maximum, known as the Fermi level. In contrast, the

solution phase $Fe(CN)_6^{3-}$ and $Fe(CN)_6^{4-}$ ions have discrete electronic energy levels. It is thermodynamically favourable for electrons to pass from the Fermi level of the metal to the lower unoccupied molecular orbitals of the solution species at the interface. This energy difference is the driving force of the electron transfer for the reaction. The electron transfer proceeds until the electrode and the solution are in energetic equilibrium and no further current is observed.

1.1.3 The Nernst Equation

Whilst in an electrochemical equilibrium, the transfer of charged electrons means that the balance between both chemical and electrical energies defines the equilibrium position [2]. As the electron moves between the solution and electrode, these two phases may have different electrical potentials which leads to the electron having differing electrical energies.

Ions will spontaneously act to lower both their electrical and chemical potential energy by redistributing the chemical species until it reaches an equilibrium state. By combining both potential energies into a single entity, we get the electrochemical potential, expressed in units of J mol^{-1}. As such, the electrochemical potential, $\bar{\mu}$, accounts for both the chemical and electrical energies, as seen in Equation 1.5.

$$\bar{\mu}_j = \mu_j + Z_j F \phi \tag{1.5}$$

For a species, j, the first term is the chemical potential, μ_j (Gibbs energy per mole). The second term, $Z_j F \phi$, represents the molar electrical energy term where Z_j is the charge on species j, F is the Faraday constant (96485 C mol^{-1}) and ϕ is the potential of

the particular phase in which species j is found. At constant temperature and pressure, a system under electrochemical equilibrium can be analysed since the electrochemical potentials of the reactants and products will be balanced.

Taking the familiar ferro/ferri-cyanide equilibrium reaction as an example,

$$Fe(CN)_6^{3-}(aq) + e^-(m) \rightleftharpoons Fe(CN)_6^{4-}(aq)$$

A balance between the electrochemical potentials of the reactants and products at equilibrium gives:

$$\bar{\mu}_{Fe(CN)_6^{3-}} + \bar{\mu}_{e-} = \bar{\mu}_{Fe(CN)_6^{4-}} \tag{1.6}$$

The chemical potential of the two species, $Fe(CN)_6^{3-}$ and $Fe(CN)_6^{4-}$, is expressed as:

$$\mu_{Fe(CN)_6^{3-}} = \mu^0_{Fe(CN)_6^{3-}} + RTln\left(\frac{[Fe(CN)_6^{3-}]}{[\quad]^0}\right)$$

and

$$\mu_{Fe(CN)_6^{4-}} = \mu^0_{Fe(CN)_6^{4-}} + RTln\left(\frac{[Fe(CN)_6^{4-}]}{[\quad]^0}\right) \tag{1.7}$$

where $[\quad]^0$ is the standard solution, taken to be one molar.

Taking Equations 1.5, 1.6 and 1.7, and combining we arrive at:

$$\phi_M - \phi_S = \frac{\triangle\ \mu^0}{F} + \frac{RT}{F}ln\left(\frac{[Fe(CN)_6^{3-}]}{[Fe(CN)_6^{4-}]}\right) \tag{1.8}$$

which gives us the Nernst equation for a single electrode/surface interface where $\Delta\mu^0 = \mu^0_{Fe(CN)_6^{3-}} + \mu_{e^-} - \mu^0_{Fe(CN)_6^{4-}}$ is a constant at a given T and P.

At equilibrium, the charge separation existing between the metal and the solution

leads to a potential drop, $\Delta\phi_{M/S}$, across the electrode/solution interface, where:

$$\Delta\phi_{M/S} = \phi_M - \phi_S \tag{1.9}$$

ϕ_M represents the potential of the metal electrode, whilst ϕ_S gives the potential of the solution.

Though the value for $\Delta\phi_{M/S}$ has a fixed and absolute value, it is not directly measurable. It is therefore necessary to introduce a second electrode to create two electrode/solution interfaces such that the potential difference can be calculated. By using an electrode with a known and constant potential, it can act as a reference point in which the potential difference at the working electrode can determined. This electrode is also known as the reference electrode.

$$E = (\phi_M - \phi_S)_{WE} - (\phi_M - \phi_S)_{RE} \tag{1.10}$$

The potential, E, measured as the potential difference across the two electrode/solution interfaces where $(\phi_M - \phi_S)_{WE}$ and $(\phi_M - \phi_S)_{RE}$ represents the potential drop between the working electrode (WE) and reference electrode (RE). The reference electrode provides a constant potential such that any changes in E corresponds to changes in $(\phi_M - \phi_S)_{WE}$.

In equilibrium chemistry, potentials such as E are measured under conditions of low current flow where the term $(\phi_M - \phi_S)_{WE}$ is given by equations of the form of Equation 1.8. For a general one electron reversible process where :

$$Ox + e^- \rightarrow Red \tag{1.11}$$

we have:

$$(\phi_M - \phi_S)_{WE} = \text{constant} + \frac{RT}{F} ln \left(\frac{[Ox]}{[Red]} \right) \tag{1.12}$$

It then follows that the Nernst equation for an ideal solution can be expressed as

$$E = E^o + \frac{RT}{F} ln \frac{a_{ox}}{a_{red}} \tag{1.13}$$

where a is the activity of the species and E^o is defined as the standard electrode potential where the reference electrode is chosen to be the standard hydrogen electrode. The standard hydrogen electrode (SHE) is the standard reference electrode by which all standard electrode potentials, E^0, are established and is therefore considered to possess a potential of absolute zero. For the SHE, a platinum wire in HCl (where the activity is unity) is bubbled under a constant flow of gaseous hydrogen at a pressure of one atmosphere.

Equation 1.8 relates to an ideal solution, whereas in Equation 1.13, we have replaced concentration by activity for generality. The activity of a species can be defined as:

$$a_C = \gamma_C [C] \tag{1.14}$$

where a_C is the activity of species C, γ_C is the activity coefficient and $[C]$ is the concentration.

In very dilute solutions, the Nernst equation can be expressed directly in terms of concentrations since the activity coefficients are close to unity. However, at high concentration, solutions are not ideal due to ion-ion and ion-solvent interactions in the electrolyte and the true activity of the ions must be used. The activity coefficient, γ, can be used to express the equation in terms of its "effective concentration" to account for deviations

from ideal behaviour.

By substituting the activities of O and R into the Nernst equation, we get:

$$E = E^o + \frac{RT}{F} ln \frac{\gamma_O}{\gamma_R} + \frac{RT}{F} ln \frac{[O]}{[R]} \tag{1.15}$$

We can introduce the concept of the formal potential given by:

$$E_f^o = E^o + \frac{RT}{F} ln \frac{\gamma_O}{\gamma_R} \tag{1.16}$$

which leads to:

$$E = E_f^o + \frac{RT}{F} ln \frac{[O]}{[R]} \tag{1.17}$$

where the formal potential, E_f^o, is dependent on solution composition and will change as the activity changes. E_f^o only approximates to the standard potential and takes into account deviations from solution ideality.

Though activities should be used to define equilibrium constants, in practice it is very inconvenient as values tend to be unknown, so concentrations are often used instead.

1.2 Dynamic Electrochemistry

In the previous section, equilibrium electrochemistry was discussed whereby the charge separation leads to potentials being established. Next, we consider an electrical potential applied to an electrode. This external potential perturbs the equilibrium such that a driven electrochemical reaction occurs at the interface. Exchange of electrons in this case brings about oxidation or reduction of a species in solution, and is termed electrolysis.

All electrolytic electrochemical experiments require at least two electrodes if they are to be studied qualitatively. A two-electrode system with only a working electrode and a reference electrode may be used when very low currents (*ca.* 10^{-9} A) are involved. This arises when the working electrode is a microelectrode as the tiny currents involved in electrolysis are so small that negligible change occurs at the reference electrode. However, typically a three electrode setup is used, and a counter electrode is introduced.

1.2.1 Three Electrode Setup

A three electrode configuration consists of a working electrode (WE), a reference electrode (RE) and a counter (auxiliary) electrode (CE), as shown in Figure 1.3. This arrangement is necessary when applying a voltage to the working electrode in an electrolytic cell [3].

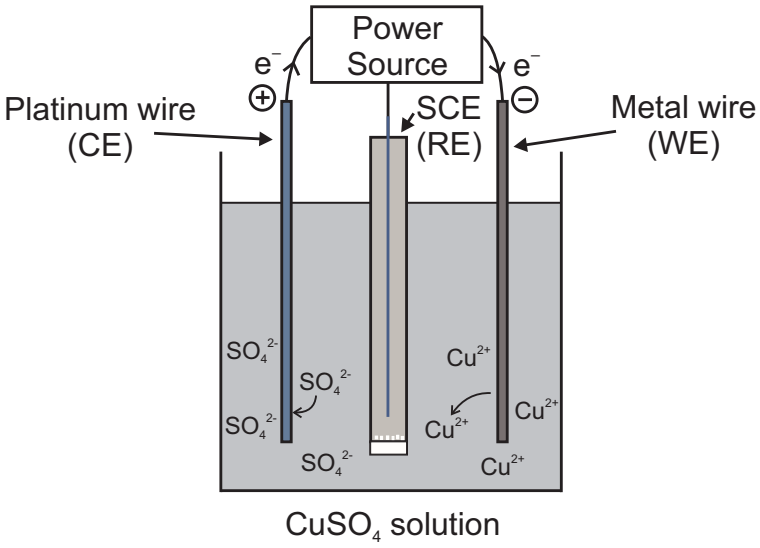


Figure 1.3: A three electrode electrolytic cell consisting of a platinum wire counter electrode, metal working electrode and saturated calomel electrode (SCE) as the reference electrode, in a solution of $CuSO_4$

For dynamic electrochemical experiments, a potentiostat is used to control the three electrodes. A fixed potential, E, is first applied between the working and reference elec-

trodes whilst drawing up negligible current through the reference electrode. Next, the potentiostat drives the counter electrode to a voltage required to pass the same current as that induced to flow through the working electrode. It is the presence of the counter electrode for this purpose that a controlled potential can be applied to the working electrode.

Since the potential of the reference electrode may be altered through changing concentrations as a result of electrolysis, no current must pass through the reference electrode. If appreciable current were to pass through the reference electrode, the stability of the measurement could be compromised, altering the $(\phi_M - \phi_S)_{RE}$ term. As well as this, a third term, IR, corresponding to the electrical resistance of the bulk solution between the working and reference electrode, would be gained such that Equation 1.10 becomes:

$$E = (\phi_M - \phi_S)_{WE} + IR - (\phi_M - \phi_S)_{RE} \tag{1.18}$$

Changes in E would cause unpredictable changes in IR, as well as alter $(\phi_M - \phi_S)_{WE}$ such that the potential through the working electrode would no longer be controlled. The counter electrode thus ensures that no current is drawn though the reference electrode and current instead passes between the working and counter electrode only. As such, the potential of the working electrode is held relative to a stable reference electrode and study of current through the working electrode can be then quantified.

The Working Electrode

The working electrode is the electrode in an electrochemical system at which processes of interest occurs. The electrode can be referred to as cathodic or anodic depending on

whether the reaction at the electrode is a reduction or an oxidation. Working electrodes should be electrochemically inert such that when a potential is applied, they do not generate a current in response to an applied potential. The choice of electrode material often depends upon the potential window required, however an extensive range of materials can be used [4]. Commonly used working electrode materials for voltammetry include mercury [5–7], platinum [8–10], gold [11, 12] and various forms of carbon [13, 14]. Carbon based electrodes have gained popularity in recent decades and an introduction to pyrolytic graphite, glassy carbon and screen printed electrodes is described in Chapter 3.

The Reference Electrode

The reference electrode has a known and stable equilibrium electrode potential such that it can be used as a reference point to measure the potential difference at the working electrode, as described earlier.

The standard hydrogen electrode was previously introduced in section 1.1.3. Extensive tabulated values of standard electrode potentials exist, however, the SHE is not typically used in electrochemical experiments due to its complicated design. More common reference electrodes include the saturated calomel electrode (SCE) and the silver/silver chloride electrode (Ag/AgCl). The potential in relation to the SHE is 0.244 V for a saturated calomel electrode and 0.197 V for a Ag/AgCl electrode at 298 K.

A saturated calomel electrode consists of a solid Hg_2Cl_2 paste and a column of liquid mercury immersed within a saturated KCl solution. It is necessary for the solution to be saturated so that the potential at the SCE is kept constant since the chloride ion concentration is constant. The silver/silver chloride reference electrode offers a mercury free alternative to the saturated calomel electrode [15]. It is composed of a silver wire,

sometimes coated with a layer of solid silver chloride, and immersed in a solution that is saturated with potassium chloride and silver chloride. Both the SCE and the Ag/AgCl reference electrodes offer stable half-cell potentials that do not change over time or with temperature, and as such, act as suitable reference electrodes.

The Counter Electrode

The counter electrode is used in a three electrode arrangement and acts to pass the counter current in the circuit when a current is induced at the working electrode. Any inert conducting material that will not interfere with redox reactions within the electrochemical cell, and of sufficient size can generally be used. Platinum or silver wire and graphite rods are common counter electrodes.

1.2.2 Solvents and Supporting Electrolyte

Electrochemical experiments are carried out in a solvent into which the electrodes are placed to complete an electrochemical cell. An extensive range of solvents may be used and the choice depends on a wide range of properties including the solubility and redox activity of the analyte, and solvent properties such as the electrical conductivity when electrolyte is added (see below), electrochemical activity and chemical activity. The solvent should be electrochemically inert over a wide potential window such that it does not react with any analytes or product species.

Many electrochemical experiments use aqueous solutions as the solvent, however, other non-aqueous solvents can also be used including methanol [16], dimethylsulfoxide (DMSO) [17], acetonitrile [18], and dimethylformamide (DMF) [19]. For aqueous solutions where water is required, doubly or triply distilled water is needed to ensure no interferences from

impurities occur. Highly sensitive experiments combined with the low concentrations of species often encountered in electrochemical experiments means that solvents need to be of high analytical grade.

Solvents generally contain a supporting electrolyte such that the electrochemical medium is sufficiently ionic for charged species of interest to move to the electrode interface to form a double layer (detailed in section 1.3.2). The effect of a supporting electrolyte also acts to avoid migration effects, decrease solution resistance, prevent a large double layer capacitance and maintain a constant ionic strength [20, 21]. Supporting electrolytes may be an inorganic salt, mineral acid or a buffer, and typically have concentrations approximately 100 times greater than the analyte [22].

1.2.3 Removal of Oxygen

The electrochemical reduction of oxygen is known to proceed via a two step mechanism where the first step is the formation of hydrogen peroxide [23]. This may be followed by the reduction of peroxide to water in a second step.

$$\begin{aligned} O_2 + 2H^+ + 2e^- &\rightarrow H_2O_2 \\ H_2O_2 + 2H^+ + 2e^- &\rightarrow 2H_2O \end{aligned} \tag{1.19}$$

Both steps above can lead to a significant current during the cathodic sweep where the products formed can interfere with analytical measurements and may also affect chemical processes under investigation. To prevent such interferences occurring, the cell is most commonly purged with an inert gas such as nitrogen or argon to remove any dissolved oxygen from the electrochemical cell prior to measurements [24].

1.3 Faradaic and Non-Faradaic Processes

1.3.1 Electrode Processes

Two types of processes occur at the electron/solution interface that produce current, namely faradaic and non-faradaic. Faradaic currents are generated during the reduction or oxidation of electroactive species at an electrode. Current generated from faradaic processes is governed by Faraday's laws of electrolysis and provides a direct measure of the rate of a redox reaction.

If the charge transfer reaction is thermodynamically or kinetically unfavourable, it will not occur. However, non faradaic processes such as adsorption and desorption can occur with changing potential. Although electronic charge does not cross the interface in non-faradaic processes, transient currents associated with the movement of electrolyte ions, reorientation of solvent dipoles, adsorption/desorption at the electrode/solution interface are present.

Both faradaic and non-faradaic processes occur when electrochemical reactions take place, and as such, both current contributions have to be considered in order to analyse an electrochemical response.

Current and Flux

As current is passed through a cell and electrolysis takes place, the concentration of the oxidized and reduced species changes at the electrode/solution interface such that the concentration is no longer the same as that in bulk. Quantitatively, this can be described by Faraday's law (Equation 1.20) where the mass of the species oxidised/reduced at an electrode during electrolysis is directly proportional to the quantity of charge transferred

at the surface [25]. The equation is given as

$$m = \frac{QM}{zF} \tag{1.20}$$

where m is the mass of species reacted at the electrode, Q represents the total electric charge passed, M is the molar mass of species, z is the number of electrons transferred per ion.

For a general redox reaction:

$$O(aq) + e^{-}(m) \rightarrow R(aq)$$

an associated current, i, is observed that relates A, the electrode area, F, Faraday's constant, n, the number of moles of electrons, and j, the flux of the species O reaching the electrode surface. The magnitude of the current is thus given as:

$$i = nFAj \tag{1.21}$$

The flux of the species can be thought of as the rate of the electrolysis reaction which is derived from the heterogeneous rate constant, k, and the concentration of the species at the electrode. It represents the quantity of species O reaching the electrode area per second, and has units of moles cm^{-2} s^{-1}.

$$j = k[O]_0 \tag{1.22}$$

Here, the subscript, 0, on the concentration term represents the surface concentration of

the reactant.

It therefore follows that the flux, and therefore the current observed, is dependent on the rate at which the oxidised species reaches the electrode surface from the bulk solution, and the rate at which electron transfer, k, occurs. As a redox process takes place, the electroactive species close to the electrode surface depletes such that the electrode surface concentration is not equal to the bulk reactant concentration.

$$[reactant]_0 \neq [reactant]_{bulk}$$

Depletion of reactants local to the electrode surface leads to material diffusing from further away to reach the electrode/solution interface. The result of this will be discussed further in later sections.

1.3.2 Non-Faradaic Processes

Non-faradaic processes give rise to a current without charge being transferred across the interface. For electrochemical reactions, although faradaic processes are of main interest, the effect of non-faradaic currents (also known as the capacitive current) must also be taken into account.

An important non-faradaic process is the charging and discharging of the electrochemical double layer when the potential is changed. This current only causes accumulation (or removal) of electrical charges on the electrode and in the electrolyte solution near the electrode, but does not involve any chemical reactions. There is always some capacitive current flowing when the potential of an electrode is changing, this is the background current in voltammetric measurements. The electrical double layer will be discussed next.

The Electrical Double Layer

When an electrode is inserted into a solution a charge will be established in the solution equal and opposite to that at the electrode. If a potential is applied, a build up of charge is seen at the electrode/solution interface where an excess of ions in solution of opposite charge to the electrode migrate to the surface in order to maintain charge neutrality. This counter charge of ions that accumulate at the electrode surface crudely forms two layers of charge at the interface, more commonly referred to as the electrical double layer. Models describing the structure of the double layer have been proposed by Helmholtz [26], Gouy [27] and Chapman [28], and Stern [29].

Today, the BDM model proposed by Bockris, Devanthan and Müller [30] is widely used where the double layer consists of three distinct regions; the Inner Helmholtz Plane (IHP), Outer Helmholtz Plane (OHP) and diffuse layer. The IHP is defined as the zone in which an axis through the centre of specifically adsorbed species is drawn. It lies closest to the electrode surface and consists of solvent molecules and specifically adsorbed ions. Specifically adsorbed ions do not possess a solvation shell and are in direct contact with the electrode. Electrostatic and chemical interactions between the electrode and the ion govern the nature of specific adsorption.

When ions do possess a solvation shell, their minimum distance of approach to the electrode is limited by their increased size. The plane through the centre of non-specifically adsorbed solvated ions closest to the electrode surface is termed as the OHP, and is considered to be the approximate site for electron transfer. Molecules within the OHP involve electrostatic interactions, such that solvated ions are attracted to the electrode by coulombic forces. The "compact layer" encompasses these two Helmholtz layers, consisting of

a charged layer strongly bound to the surface, even when the electrode is removed from solution [31, 32].

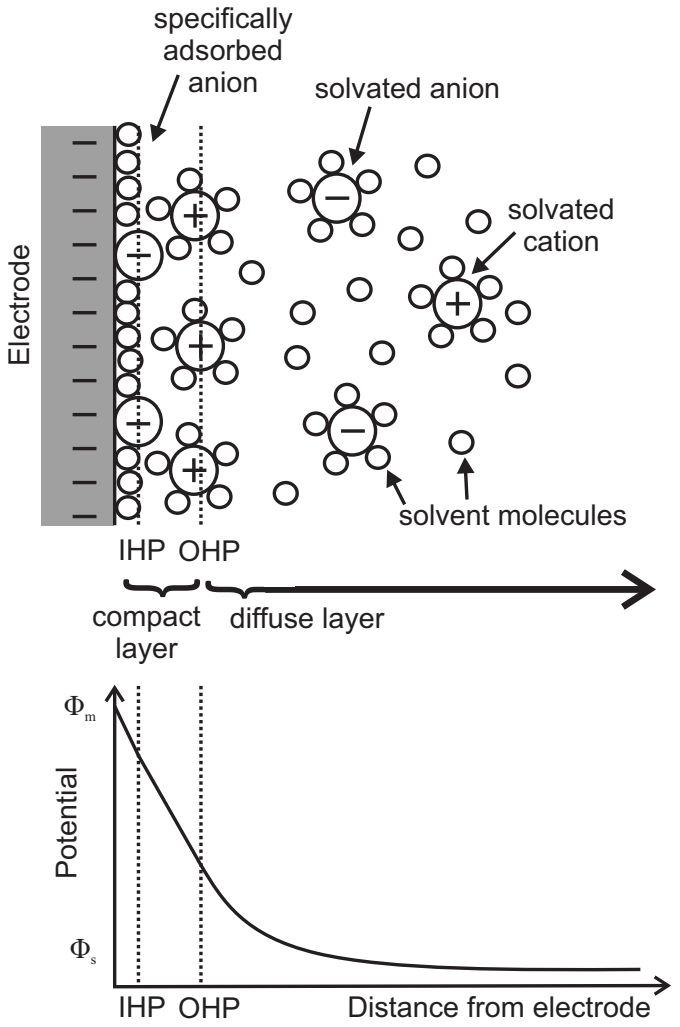


Figure 1.4: Schematic representation of the electrical double layer at a negatively charged electrode surface. A corresponding graph shows the steep drop in potential between the electrode and OHP, and the gradual fall in potential within the diffuse layer as the value returns to that seen in the bulk

Beyond these adsorbed layers, a diffuse layer exists. This results from Brownian motion in solution acting to disperse the excess ions formed on the surface. Non-specifically adsorbed ions which have their primary solvation shells generally reside in the diffuse layer extending some distance from the electrode surface. The total thickness of the diffuse layer

depends on the ionic strength of the solution. In this diffuse layer, a potential drop exists as the net charge density returns to the bulk concentration further from the electrode. The transition from an ordered distribution of ions at the electrode surface controlled by the interfacial electrical field to an equilibrated distribution of ions controlled by natural convection can be seen.

The combined charge resulting from the Helmholtz and diffuse layers is equal (but in opposite sign to) the net charge on the electrode surface. The charge of the electrode surface is given as the sum of the individual charges:

$$Q_M = -(Q_{IHP} + Q_{OHP} + Q_{diff}) \tag{1.23}$$

where Q_M is the charge of the electrode surface and Q_{IHP}, Q_{OHP} and Q_{diff} are the charges arising from the Inner Helmholtz Plane, Outer Helmholtz Plane and diffuse layer, respectively.

A schematic diagram of the electrical double layer at a negatively charged electrode, together with a plot of the potential *vs.* distance from the electrode is shown in Figure 1.4. From the plot, two distinct regions can be seen corresponding to the Helmholtz plane between the OHP and electrode, and the diffuse layer as the potential returns to that seen in the bulk.

1.4 Mass Transport

Mass transport involves the movement of material from one location to another arising from differences in electrical or chemical potentials. For electrolysis to take place, the

reactant species needs to be transported from the bulk solution to the electrode interface prior to a reaction.

Three main transport processes control the flux to the electrode, these are diffusion, convection and migration. Of these processes, diffusion is the most important and influential mode of mass transport in controlled potential methods, and will be discussed in detail below.

1.4.1 Diffusion

Diffusion arises due to the spontaneous movement of a species down a concentration gradient, maximising the entropy of the system. The diffusional flux is directly proportional to the concentration difference and the rate at which this occurs can be mathematically modelled using Fick's laws where the flux of the species is dependent on the concentration gradient at that given point [1].

Fick's 1st Law

Under steady state conditions, Fick's first law relates the diffusive flux to the concentration whereby in one (spatial) dimension, the law is:

$$J_d = -D\frac{\partial c}{\partial x} \tag{1.24}$$

where D ($cm^2\ s^{-1}$), the diffusion coefficient, is characteristic of the diffusing species, j is the flux and has units of mol $cm^{-2}\ s^{-1}$, and the local concentration gradient is represented by $\frac{\partial c}{\partial x}$. The negative sign in Equation 1.24 is representative of the flux moving down the concentration gradient.

Fick's 2nd Law

Fick's second law predicts how diffusion causes the concentration to change with time. By considering a volume of unit cross-sectional area with thickness δx, the change in concentration at a given point, x, is given by the flux difference in and out of the volume.:

$$\frac{\partial c}{\partial t} = \frac{J(x) - J(x + \delta x, t)}{\delta x} = -\frac{\partial J}{\partial x} \tag{1.25}$$

Substituting Fick's 1st law (Equation 1.24), we obtain Fick's second law of diffusion in one dimension.

$$\frac{\partial c}{\partial t} = D\frac{d^2 c}{dx^2} \tag{1.26}$$

When considering Fick's 2nd law in three directions, (x,y,z), the equation becomes

$$\frac{\partial c}{\partial t} = D\frac{\partial^2 c}{\partial x^2} + D\frac{\partial^2 c}{\partial y^2} + D\frac{\partial^2 c}{\partial z^2} \tag{1.27}$$

Diffusion Coefficients

The diffusion coefficient, D, of a molecule is an important parameter indicative of the diffusion mobility and provides a measure of how far a molecule will diffuse in a certain time. Einstein's theory for the diffusion of Brownian particles [33], specifically, the root mean square displacement in time, t, is

$$\sqrt{< x^2 >} = \sqrt{2Dt} \tag{1.28}$$

The value of D can vary considerably depending on the viscosity and temperature of the medium, and the size of the diffusing molecule. However, generally speaking the bigger

the molecule, the smaller the value of the diffusion coefficient. The diffusion coefficient is temperature dependent and often follows an Arrhenius type relationship as seen in Equation 1.29.

$$D = D_{\infty} exp\left(\frac{-E_A}{RT}\right) \tag{1.29}$$

where D_{∞} is the hypothetical value of the diffusion coefficient at an infinite temperature, and E_A (kJ mol^{-1}) is the activation energy for diffusion.

The Cottrell Equation

The Cottrell equation describes the change in electrical current with respect to time in a controlled potential experiment where a potential step is applied such that the potential changes from a value of zero current to a diffusion controlled value [34]. The change in current is due to the depletion of material near the electrode surface with time as the potential is applied. The Cottrell equation for planar diffusion to a macroelectrode is given as:

$$i = \frac{nFA\sqrt{D}[C]_{bulk}}{\sqrt{\pi t}} \tag{1.30}$$

where n represents the number of electrons transferred, A is the electrode area and $[C]_{bulk}$ is the bulk concentration of the electroactive species.

The Nernst Diffusion Layer and Limiting Current

When potential step experiments are carried out, the Cottrell equation predicts that the observed current decays to zero with a dependence that is inversely proportional to

the square root of time ($1/\sqrt{t}$). This is generally observed for up to a few seconds. An exception to this occurs at very short times (< 10 ms) when the current caused by faradaic processes at the electrode is obscured by charging currents due to movement of the ions comprising the supporting electrolyte near the electrode.

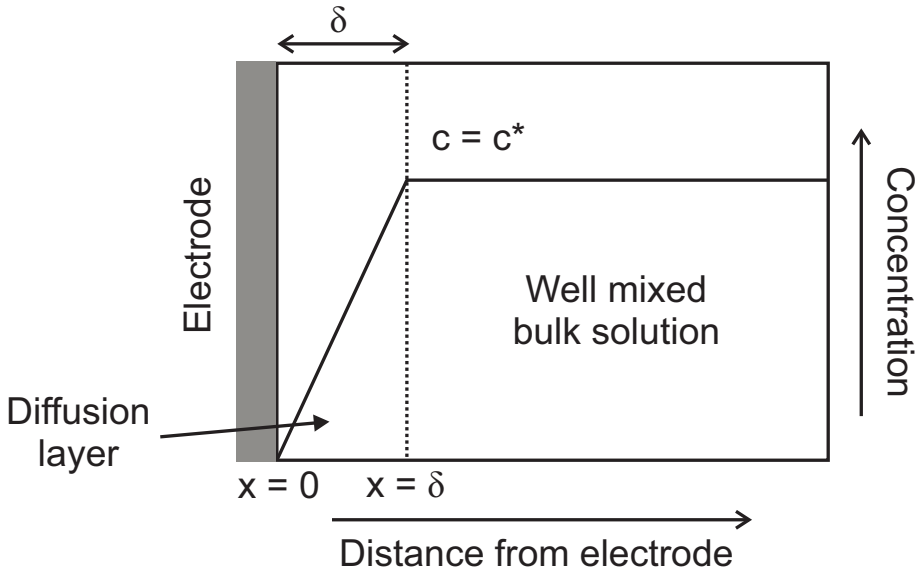


Figure 1.5: Schematic diagram of the Nernst diffusion layer model

At longer times, the Cottrell equation implies that the current will fall to zero, however experimentally measured current in fact tend to an approximately steady value [35]. This is consistent with the model shown in Figure 1.5 where beyond the critical distance from the electrode, δ, the bulk solution is well mixed by natural convection such that the concentration of the electroactive species is maintained at a constant bulk value [36].

Close to the electrode, natural convection is lost due to the rigidity of the solid electrode and frictional forces. The zone in which this occurs, between x = 0 and x = δ, is known as the "diffusion layer". Within this diffusion layer, changes in concentration occur by diffusional transport based on Fick's Laws. From Fick's 1st Law, the steady

state diffusional flux can be expressed as:

$$j = D\frac{\partial[C]}{\partial x} = \frac{D[C]_{bulk}}{\delta} \tag{1.31}$$

It follows that the corresponding steady state current can be expressed as:

$$I_{ss} = \frac{nFAD[C]_{bulk}}{\delta} = nFAm_T[C]_{bulk} \tag{1.32}$$

where m_T (cm s^{-1}) is defined as the mass transport coefficient and is given by:

$$m_T = \frac{D}{\delta} \tag{1.33}$$

The Nernst diffusion layer is a simplified model which provides a helpful and insightful concept. In reality, the zone of mixing via natural convection and the stagnant zone of diffusion merge into one another. Experimental evidence has shown that the diffusion layer is *ca.* 10 - 100 μm, and for voltammetric experiments based on the diffusion only model, it is important for the time scale to be restricted such that concentration changes are confined within the diffusion zone, x = 0 and x = δ.

1.4.2 Convection

Convective effects occur due to movement of solution by external mechanical forces, and can be either natural or forced. Natural convection can occur in all solutions, arising from thermal gradients and density differences in the solution. The endo- or exo-thermicity of a given process leads to the formation of thermal gradients and density differences result directly from the electrode reactions. Natural convection typically becomes a significant

mass transport process at timescales beyond *ca.* 20 s. This perturbation is often difficult to model and thus is an unwanted effect during electrolysis.

For processes with longer timescales, forced convection can be introduced to control convection. This is achieved by external means such as stirring, vibration or bubbling gas through solution. Often, electrochemical experiments deliberately utilise this external form of perturbation such that contributions from natural convection become negligible for quantitative analysis and to ensure reproducibility in experiments.

The one dimensional convective flux, J_c, is given by the equation below where ν_x is the solution velocity in the x direction of species C at concentration $[C]$.

$$J_c = [C]\nu_x \tag{1.34}$$

1.4.3 Migration

As a result of the potential gradient set up between the electrode and solution, charged species interact with the electric field and are free to move to or from the electrode with anions being attracted to a positive electrode and cations to a negative electrode. This induced migration of ions is likely to accompany electrochemical reactions in bulk solution where concentration gradients are generally small.

The migratory flux is proportional to the concentration of the species, the electric field and the mobility of the ion. The one dimensional migrative flux, J_m, is given as below, determined by the concentration $[i]$ and the charge on the ion, z_i.

$$J_m = \frac{-z_i F}{RT} D_i [i] \frac{\partial E}{\partial x} \tag{1.35}$$

The effects of migration can complicate electroanalytical quantification, making it difficult to control and interpret. A charge transfer process occurring at the electrode can cause a change in the concentration of the electroactive species local to the electrode surface, which in turn alters the electrical potential in solution and the electrical field to the electrode.

Steps can however, and usually must, be taken in order to compensate for these effects. In most experiments a chemically and electrochemically inert background supporting electrolyte (such as KCl in water) can be used. The presence of a background electrolyte with a concentration of approximately 100 times more concentrated than the reactant species under investigation swamps the solution with charged species and has the effect of maintaining electroneutrality by minimising the electrochemical double layer effect [22]. An excess of background electrolyte also ensures that an electric field does not build up in the bulk solution and bulk resistivity is reduced.

1.5 Electrode Kinetics

1.5.1 Heterogeneous Electron Transfer

For a general redox reaction in which species O and R are interconverted by a one electron transfer,

$$O^{n+}(aq) + e^{-}(m) \underset{k_{ox}}{\overset{k_{red}}{\rightleftarrows}} R(aq)$$

k_{red} and k_{ox} represent the first order rate constants for the reductive (cathodic) and oxidative (anodic) processes, respectively.

The forward and backward reactions can be expressed in terms of current as equations:

$$i_c = -FAk_{red}[O]_0 \tag{1.36}$$

$$i_a = FAk_{ox}[R]_0 \tag{1.37}$$

where $k_{red}[O]_0$ and $k_{ox}[R]_0$ are the respective fluxes for the reductive and oxidative processes and n is assumed to be one.

The cathodic, c, and anodic, a, currents, i_c and i_a, can be combined to give an expression for the net current for the redox reaction:

$$i = i_c + i_a = FAk_{ox}[R]_0 - FAk_{red}[O]_0 \tag{1.38}$$

At equilibrium this net current, and therefore the net rate of reaction, is zero. No current is passed and the concentration of the reactants and products are in complete equilibrium.

1.5.2 Transition State Theory

Using transition state theory [1], it is possible to relate the Gibbs energies of activation to the rate constants k_{red} and k_{ox}. Transition state theory requires that for a reaction to occur, the activation energy barrier, E_a, (which exists between products and reactants) must be overcome. The constants k_{red} and k_{ox} are both potential dependent such that at relatively negative potentials, the cathodic reaction predominates and conversely, at relatively positive potentials, the anodic reaction predominates. The energy required to drive the reaction forwards or backwards may be represented by a reaction profile.

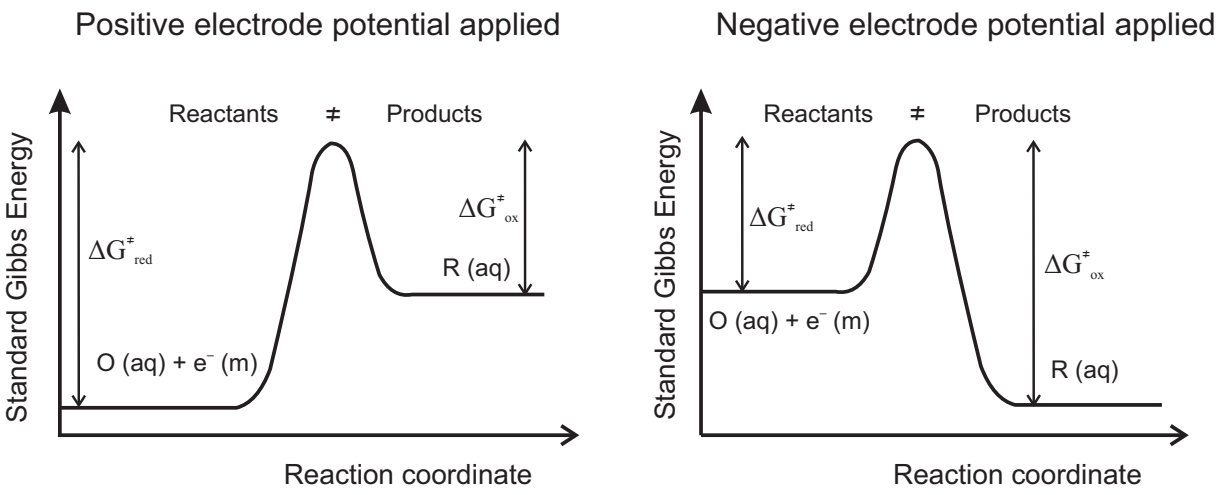


Figure 1.6: Reaction profiles for the electrode process $O(aq) + e^{-}(m) \rightleftharpoons R(aq)$, where $\neq$ represents the transition state. Left: relative energy when the electrode has a positive potential applied Right: relative energy when the electrode has a negative potential applied

The two energy profiles shown in Figure 1.6 illustrate the energy of the reactants and products when the electrode is held positively ($k_{ox} \gg k_{red}$) or negatively ($k_{ox} \ll k_{red}$) relative to the potential of the solution. By increasing the relative energy of the reactants or products, the process is driven in the most energetically favourable direction.

1.5.3 Butler-Volmer Kinetics

By assuming Arrhenius behaviour, the rate of reaction for the reduction and oxidation reactions is given below:

$$k^0_{red} = A_{red} exp(\frac{-\alpha \Delta G^{\neq}_{red}}{RT}) \tag{1.39}$$

$$k^0_{ox} = A_{ox} exp(\frac{+\beta \Delta G^{\neq}_{ox}}{RT}) \tag{1.40}$$

At equilibrium, the rate constants k^0_{red} and k^0_{ox} are equal as no net current flows, and may be considered as simply k^0 (cm s^{-1}), the standard electrochemical rate constant. The magnitude of k dictates the rate at which a reaction will reach equilibrium. A reaction

with a large k value will reach equilibrium rapidly, whereas equilibrium will be reached slower for a reaction with a small k value.

The rate constants given by Equations 1.39 and 1.40 can be rearranged to describe the relationship between reaction kinetics and the potential difference at the electrode/solution interface with respect to net flux, j. The result is the *Butler-Volmer equation*,

$$j = k^0 exp(\frac{-\alpha F(E - E_f^0)}{RT})[O]_0 - k^0 exp(\frac{\beta F(E - E_f^0)}{RT})[R]_0 \tag{1.41}$$

where $\alpha + \beta = 1$ and k^0 is the standard electrochemical rate constant. This condition is required by the principle of microscopic reversibility.

It is evident that the rate of electron transfer will be influenced by $(E - E_f^0)$, the applied potential, α, the charge transfer coefficient and k^0, the standard heterogeneous charge transfer rate constant (cm s^{-1}). The charge transfer coefficient gives the position of the transition state and provides a measure of the symmetry of the energy barrier. Though it can possess values from zero to one, the typical, often encountered value of near 0.5 implies that the transition state lies intermediate in its electrical behaviour between the reactants and products. Where α tends to zero, the transition state will be more reactant like in nature, whereas the transition states is more product like if it tends to one (for a reduction).

1.5.4 Tafel Analysis

For a simple one-electron redox process, the flux is given as in Equation 1.41. It can be seen that with an arbitrary potential, E, imposed on the electrode, the net flux is a balance between the reduction current and the oxidation current due to the addition of an

electron to species O, and the removal of an electron from species R, respectively. Under extreme potentials where $E \gg E_f^0$ or $E \ll E_f^0$, it is possible to neglect one or other of the two terms.

For the reduction of A, where A gains an electron to form B, the flux becomes:

$$j = k^0 exp\left[\frac{-\alpha F(E - E_f^0)}{RT}\right][A]_0 \tag{1.42}$$

and for the oxidation process:

$$j = k^0 exp\left[\frac{\beta F(E - E_f^0)}{RT}\right][B]_0 \tag{1.43}$$

Provided that $[A]_0$ and $[B]_0$ do not substantially change from their constant bulk values, the reduction and oxidation current, I_{red} and I_{ox}, respectively, can be described using the expressions:

$$ln|I_{red}| = -\frac{\alpha FE}{RT} + constant \tag{1.44}$$

and

$$ln|I_{ox}| = \frac{\beta FE}{RT} + constant \tag{1.45}$$

Using experimental results, ln $|I_{ox}|$ *vs.* E or ln $|I_{red}|$ *vs.* E plots can be formed from current and potential data – these are known as Tafel plots. The magnitude of the transfer coefficients, α and β, can thus be calculated from the slope as shown in Figure 1.7.

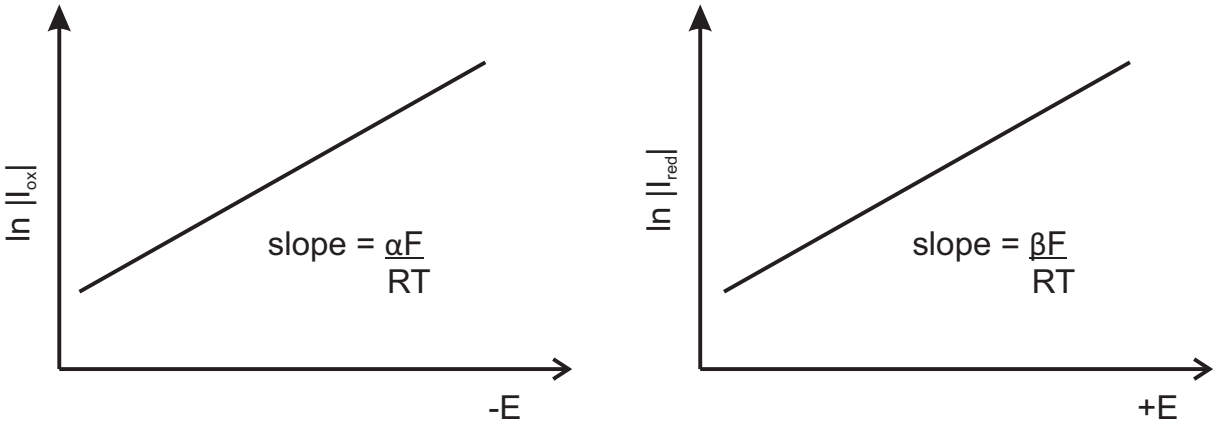


Figure 1.7: Tafel plots for both anodic (left) and cathodic (right) processes

1.6 Voltammetric Techniques

Electrochemistry can be used as an analytical tool to provide important insight into reaction mechanisms and kinetics [37]. These techniques can be broken down into several categories depending on which aspects of the cell are controlled and which are measured. In voltammetry, information about an analyte is obtained by measuring the current (arising from electrolysis), as the potential is varied. Here, the two most common electroanalyical techniques, linear sweep voltammetry (LSV) and cyclic voltammetry (CV), will be introduced. Further *electroanalytical* methods are described in the next chapter.

1.6.1 Linear Sweep Voltammetry

Linear sweep voltammetry (LSV) is closely related to cyclic voltammetry (CV) whereby a voltage is applied to the working electrode over a potential range that encompasses the start and end of the faradaic process of interest. A plot of I *vs.* E, called a voltammogram, can be constructed using the recorded current that flows through the working electrode and a knowledge of the applied potential. The potential is generally swept (scanned) at a specific rate, known as the "scan rate", ν (V s^{-1}).

Linear sweep voltammetry (LSV) studied in a stationary solution considers diffusion as the only mass transport method involved for the electroactive species. However, LSV can also be used at hydrodynamic electrodes as a method to increase the flux to the electrode surface, as shown later in Chapter 6. The potential of the working electrode is swept linearly from a starting potential, E_1, to a second potential, E_2, as a function of time whilst the current is measured. When the potential applied is not great enough to cause electron transfer for:

$$O + e^- \rightarrow R$$

no current flows. However, when the potential is swept to more negative potentials, the species is reduced at the electrode and a corresponding increase in current is seen.

As the potential is driven even more negatively, a maximum current, the peak current, i_p, is reached with a corresponding peak potential, E_p. At potentials more negative than E_p, the rate of diffusion to the electrode surface dictates the shape of the voltammogram. As electrolysis proceeds, the electroactive species is depleted such that the diffusion layer at the electrode/solution interface thickens and the observed current decreases. As such, the flux of the material to the electrode becomes diffusion limited.

For irreversible, non-Nernstian cases with slow reaction kinetics (small k^0), a much more negative potential is required to drive the electron transfer compared to reversible, Nernstian cases with fast reaction kinetics (large k^0). No current flows in the irreversible case until the potential is considerably more negative than the equilibrium potential. The region prior to the peak is activation controlled, whereas after the peak, diffusion becomes the rate determining step. This contrasts to reversible cases as rapid electrode kinetics causes the reaction to occur at less negative potentials, such that current flows as soon

as it becomes thermodynamically favourable and the entire wave is diffusion controlled. The peak produced for irreversible systems is broader than that of a reversible system, as shown in Figure 1.8.

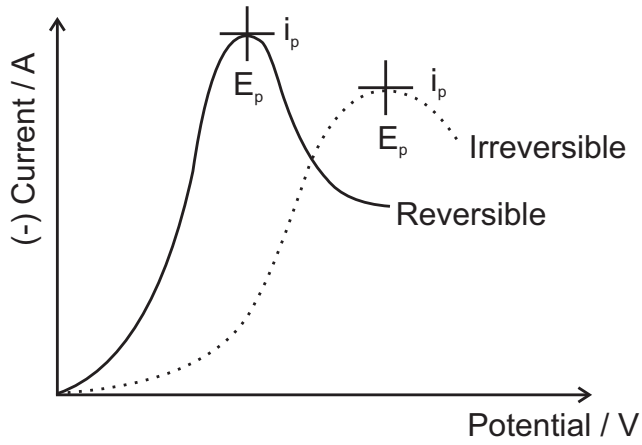


Figure 1.8: Linear sweep voltammograms for the reduction of a species in a reversible and irreversible electron transfer

In a non-steady state system, the voltammogram is peak shaped. In a stirred solution or at a microelectrode, convection and diffusion are mass transport considerations, and a limiting current is observed except at fast scan rates. We will see the change in voltammetry from a transient to steady state at a platinum foil electrode in Chapter 6, as it is held stationary and vibrating, respectively.

1.6.2 Cyclic Voltammetry

Cyclic voltammetry is widely used and can provide information on the system of interest, including thermodynamics of redox and adsorption processes and the kinetics of heterogeneous electron transfer. Both forward and reverse scans are shown in a current *vs.* potential plot. Often, multiple CV cycles can be taken to give fuller information on a reaction.

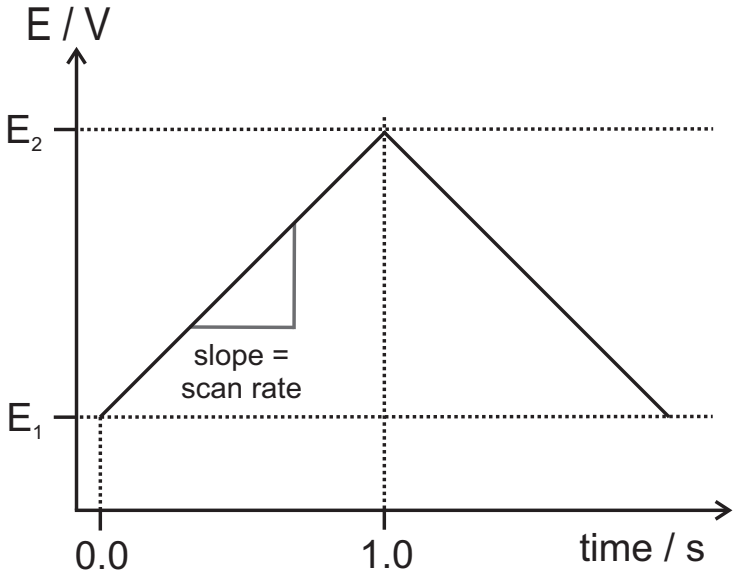


Figure 1.9: A triangular cyclic voltammetric waveform, with scan rate corresponding to the slope

For a CV experiment, the potential is scanned from a starting potential, E_1, to a second potential, E_2, then again back to the starting potential, E_1, following a triangular potential ramp as shown in Figure 1.9. The value of the starting potential, E_1, is generally chosen where there is negligible current flow such that the chemical species under investigation is not initially oxidised or reduced. Typically, E_2 is selected so that the potential window (E_2 - E_1) contains the redox reaction of interest.

For a typical reversible redox couple, where $O + e^- \rightleftharpoons R$, the cathodic current rapidly increases as the applied potential approaches the characteristic E_f^0 of the process. The current will increase until a peak is reached which corresponds to the concentration of species O at the electrode surface as it tends to zero. The current then decreases as the solution surrounding the electrode is depleted of O. At a point beyond the peak, the scan direction is reversed and an anodic current is generated when the electrode becomes a sufficiently strong oxidant. An anodic peak current results when the surface concentration of species R at the electrode approaches zero, as it is re-oxidised back to O. The current

then decays as the solution surrounding the electrode is depleted of species R.

The kinetics of the electroactive species can be identified as reversible, irreversible or quasi-reversible from their voltammetric behaviour. The rate at which the electron transfer occurs between the working electrode and the solution redox species, corresponding to the electrochemical rate constant, k^0, dictates the reversibility of the reaction. Reactions with large k^0 values are electrochemically reversible since electron transfer occurs rapidly without significant thermodynamic barriers.

On the other hand, reactions involving slow electron transfers are electrochemically irreversible and have small k^0 values. It should be noted that the magnitude of the k^0 value is with respect to the rate of mass transport and the timescale of the experiment, such that:

$$k^0 \gg m_T \qquad \text{represents a reversible reaction}$$

$$k^0 \ll m_T \qquad \text{represents an irreversible reaction}$$

where m_T is the mass transport coefficient (as mentioned in section 1.4.1).

The reversibility and irreversibility of a reaction can also be defined using the parameter, Λ, introduced by Matsuda and Ayabe [38]:

$$\Lambda = \frac{k^0}{\left(\frac{FD\nu}{RT}\right)^{1/2}} \tag{1.46}$$

Ranges for Λ and k^0 suggested by Matsuda and Ayabe dictate whether a reaction is reversible, quasi-reversible or irreversible. For stationary macroelectrodes, and under the

assumption $\alpha \sim 0.5$ at 298 K, the limits for the different types of reactions are:

$$\begin{aligned}
&\text{Reversible:} && \Lambda \geq 15 \quad ; k^0 \geq 0.3\nu^{1/2} cm\ s^{-1} \\
&\text{Quasi-reversible:} && 15 > \Lambda < 10^{-3} \quad ; \quad 0.3\nu^{1/2} > k^0 < 2\text{x}10^{-5}\nu^{1/2} cm\ s^{-1} \\
&\text{Irreversible:} && \Lambda \leq 10^{-3} \quad ; \quad k^0 \leq 2\text{x}10^{-5}\nu^{1/2} cm\ s^{-1}
\end{aligned}$$

In reversible systems, little or no overpotential is required for reactions to occur and current flows readily in both the forward and backward directions. Rapid electrode kinetics is seen as soon as the reaction is thermodynamically feasible. CVs show a back peak with a $59/n$ mV ($T = 298$ K where n is the number of electrons transferred: $Ox + ne^- \rightleftharpoons Red$) peak-to-peak separation, representing fast electrode kinetics.

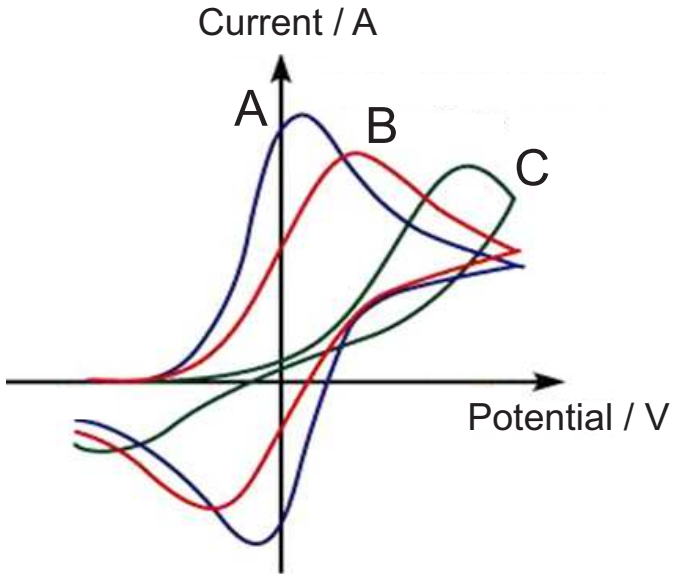


Figure 1.10: Cyclic voltammograms for a reversible electron transfer (A), quasireversible electron transfer (B) and irreversible electron transfer (C)

In the case of irreversible systems a large overpotential is required to drive the electron transfer which results in a large peak-to-peak separation. A wide potential window is

therefore often required to encompass both the oxidative and reductive processes due to the wide difference in potential.

A reaction is referred to as quasi-reversible when its response is intermediate to that of a reversible and irreversible system. For such reactions, the peak potential and peak current dependence on scan rate are neither reversible or irreversible, but somewhere in between. Electron transfer is slow for both irreversible and quasi-reversible systems. Voltammograms for these reactions display a reduced peak current and wider separation between peaks, as seen in Figure 1.10.

A summary of criteria distinguishing the different systems is given in Table 1.1, where $T = 298$ K is assumed.

FEATURE	REVERSIBLE	QUASI-REVERSIBLE	IRREVERSIBLE
Peak-to-peak , separation ΔE_p	$59/n$ mV, Nernstian behaviour	ΔE_p is slightly greater than 59/n mV	No reverse peak within a few hundred mV, ν dependent
Peak potential, E_p	Independent of scan rate, ν	Dependent of ν	Proportional to ν by $30/\alpha$ mV per decade of ν
Peak current, I_p	Directly proportional to $\nu^{1/2}$	Not proportional to $\nu^{1/2}$	Directly proportional to $\nu^{1/2}$
$\frac{I_p(R)}{I_p(O)}$	-1	$\neq$ -1	$\neq$ -1

Table 1.1: Summary of CV features for reversible, quasi-reversible and irreversible reactions, where ν is scan rate and α is the transfer coefficient in the reaction $A \pm ne^- \rightleftharpoons B$

1.6.3 The Randles - Ševčik Equations

The peak current, I_p, varies with scan rate in accordance with the Randles - Ševčik equation for reversible and irreversible systems as given in Equations 1.47 and 1.48 where n (the number of electrons) is assumed to be one.

Reversible

$$I_p = 2.69\text{x}10^5 A D^{1/2} [C]_{bulk} \nu^{1/2} \tag{1.47}$$

Irreversible:

$$I_p = 2.99\text{x}10^5 \alpha^{1/2} A D^{1/2} [C]_{bulk} \nu^{1/2} \tag{1.48}$$

Various parameters can be obtained using the Randles - Ševčik equations. For reversible and irreversible reactions, a plot of I *vs.* $\nu^{1/2}$ gives a linear plot from which the gradient can provide values for the diffusion coefficient, transfer coefficient, electrode area or species concentration depending on the known data. For a simple one electron reversible couple, the ratio of reverse : forward peak currents ($i_p(R)$ / $i_p(O)$), is one. The change in peak potential with scan rate indicates whether a reaction is reversible or irreversible. For reversible reactions, E_p is independent of scan rate, whereas in irreversible reactions, E_p is proportional to the scan rate by approximately $30/\alpha$ (1.16 RT/α F) for each factor of 10 in the scan rate.

In the next chapter, a selection of electroanalytical methods, including stripping voltammetry, pulse techniques, chronoamperometry and potentiometry is described.

Bibliography

[1] R. G. Compton and C. E. Banks, *Understanding Voltammetry* (Imperial College Press, London, 2011), 2nd edition.

[2] A. J. Bard and L. R. Faulkner, *Electrochemical Methods: Fundamentals and Applications* (Wiley, New York, 2001), 2nd edition.

[3] P. H. Rieger, *Electrochemistry* (Chapman & Hall, New York, 1994), 2nd edition.

[4] N. Yamada, *Tokoshi Nyusu, Kagaku Kogyo Shiryo* **13** (1978) 30.

[5] J. Barek, A. G. Fogg, A. Muck and J. Zima, *Critical Reviews in Analytical Chemistry* **31** (2001) 291.

[6] V. Vyskocil and J. Barek, *Critical Reviews in Analytical Chemistry* **39** (2009) 173.

[7] E. Mirmomtaz and A. A. Ensafi, *Electrochimica Acta* **54** (2009) 4353.

[8] H. Berge and B. Struebing, *Fresenius' Zeitschrift fuer Analytische Chemie* **234** (1968) 321.

[9] J. D. Strycker, P. Westbroek and E. Temmerman, *Journal of Non-Crystalline Solids* **347** (2004) 231.

[10] E. J. Vasini and M. C. Giordano, *Electrochimica Acta* **34** (1989) 577.

[11] D. Merli, F. Ravasio, S. Protti, M. Pesavento and A. Profumo, *Talanta* **130** (2014) 90.

[12] M. Palcic, S. Milardovic, I. Kerekovic and Z. Grabaric, *International Journal of Electrochemical Science* **9** (2014) 3701.

[13] S. Alegret, A. Merkoci, M. I. Pividori and M. del Valle, *Encyclopedia of Sensors* **3** (2006) 23.

[14] K. Vytras, I. Svancara and R. Metelka, *Journal of the Serbian Chemical Society* **74** (2009) 1021.

[15] G. J. Janz and D. J. G. Ives, *Annals of the New York Academy of Sciences* **148** (1968) 210.

[16] A. A. Ramadan, H. Mandil and W. Asaad, *Asian Journal of Chemistry* **18** (2005) 50.

[17] A. Kotani, M. Odagiri, K. Takamura and F. Kusu, *Journal of Electroanalytical Chemistry* **624** (2008) 323.

[18] B. Dakova, P. Carbonnelle, A. Walcarius, L. Lamberts and M. Evers, *Electrochimica Acta* **37** (1992) 725.

[19] S. Roffia, V. Concialini, C. Paradisi and M. Ciano, *Journal of Electroanalytical Chemistry and Interfacial Electrochemistry* **161** (1984) 305.

[20] S. M. L. Agostinho, R. F. V. Villamil, A. A. Neto and H. Aranha, *Quimica Nova* **27** (2004) 813.

[21] A. M. Bond, *Trends in Molecular Electrochemistry*, 445-502 (CRC Press, 2004).

[22] E. J. F. Dickinson, J. G. Limon-Petersen, N. V. Rees and R. G. Compton, *Journal of Physical Chemistry C* **113** (2009) 11157.

[23] H. S. Wroblowa, Y.-C. Pan and G. Razumney, *Journal of Electroanalytical Chemistry and Interfacial Electrochemistry* **69** (1976) 195.

[24] I. B. Butler, M. A. A. Schoonen and D. T. Rickard, *Talanta* **41** (1994) 211.

[25] C. Brett and A. M. Oliveira-Brett, *Electroanalysis* (Oxford University Press, Oxford, 1998).

[26] H. Helmholtz, *Wied. Ann.* **7** (1879) 337.

[27] L. G. Gouy, *Compt. Rend.* **149** (1910) 654.

[28] D. L. Chapman, *Philosophical Magazine* **25** (1913) 475.

[29] O. Stern, *Elektrochem* **30** 508.

[30] J. O. Bockris, M. A. V. Devanthan and K. Mueller, *Proc. Roy. Soc, Ser. A.* **274** (1963) 55.

[31] K.-L. Yang, S. Yiacoumi and C. Tsouris, *Journal of Chemical Physics* **117** (2002) 8499.

[32] S. Dewan, V. Carnevale, A. Bankura, A. Eftekhari-Bafrooei, G. Fiorin, M. L. Klein and E. Borguet, *Langmuir* **30** (2014) 8056.

[33] A. Einstein, *Annalen der Physik* **17** (1905) 549.

[34] A. C. Fisher, *Electrode dynamics* (Oxford : Oxford University Press, Oxford, 1996).

[35] C. Amatore, S. Szunerits, L. Thouin and J. S. Warkocz, *Journal of Electroanalytical Chemistry* **500** (2001) 62.

[36] C. Amatore, C. Pebay, C. Sella and L. Thouin, *ChemPhysChem* **13** (2012) 1562.

[37] J. Wang, *Analytical electrochemistry* (Wiley-VCH, New York, 2000), 2nd edition.

[38] H. Matsuda and Y. Ayabe, *Zeitschrift fuer Elektrochemie und Angewandte Physikalische Chemie* **59** (1955) 494.

Chapter 2

Introduction : Electroanalytical Methods

Many sensitive electroanalytical methods and techniques can be used for the trace detection of electroactive species by measuring the potential and/or current in an electrochemical cell containing the analyte. A wide range of biological and non-biological target analytes can be analysed, and using these techniques, exceptionally low detection limits (in the order of 10^{-12} M [1–3]) and characterization information including chemical kinetics can be deduced.

Whilst analytical methods such as spectroscopy, chromatography and fluorescence can be employed, they are often very expensive and impractical for use since the nature of the equipment is typically large, bulky, expensive and/or relatively immobile. As such, electroanalytical methods can sometimes be preferred for studying analytes showing redox behaviour due to their low cost and ability to provide sensitive analytical measurements. Their capability to be made miniature and used for in-situ analysis leads to an extensive range of applications being developed including, but not limited to, electrochemical sensors and biosensors [4, 5], fuel cells [6, 7] and electrochemical detection schemes based on novel nanomaterials [8, 9].

Electrochemical methods may be split up into two major classes : amperometric and

potentiometric. In amperometry, a potential is applied to drive the kinetics of the electron transfer reaction and the often diffusion controlled current flowing across the electrode/solution interface is measured. This current is directly proportional to the bulk concentration of the analyte present in the solution. Potentiometry can be used to measure the potential of kinetically facile electron transfer reactions, under conditions of zero current flow. The cell potential responds to changes in the activity of the analyte species present in the solution in a well defined manner described by the Nernst equation.

Experiments described in this thesis is based on voltammetric techniques and as such, amperometric methods for electroanalysis will be discussed in detail below. Many of the techniques contained in this chapter follows on from concepts introduced in section 1.6 of the previous chapter.

2.1 Amperometry

The term "amperometry" embraces a variety of electrochemical methods in which a controlled potential, at a value where redox processes can occur, is applied to an electrode and the current occurring as a consequence of oxidation/reduction at the electrode surface is recorded as the analytical signal.

2.1.1 Voltammetry

Voltammetry is considered an active technique since the applied potential electrochemically oxidises or reduces the electroactive species at the electrode, forcing a change in the concentration. The resulting current can then be monitored [10]. In many cases, the applied potential is varied or the current is monitored over a period of time. As such, voltammetric techniques can be described as some function of potential, current or time,

giving useful information about the mechanism and kinetics of electrochemical reactions.

In the 1960s and 1970s, significant advances in the theory and instrumentation were made in all areas of voltammetry which enhanced the sensitivity and expanded the repertoire of analytical methods [11]. Together with the commercial development of cheaper instruments, voltammetric methods became widely incorporated into routine analytical work.

In the earliest voltammetric techniques, including polarography, a mercury working electrode was used. Today, a whole host of materials can be used for the working electrode, including mercury, platinum, gold, silver, and carbon [12–16]. A wide variety of carbon based electrodes exists, and an introduction to some commonly used carbon electrode materials is described in the next chapter. The choice of material often depends on the potential window and other characteristics required for the experiment. Alternatives to mercury electrodes, such as platinum, gold and carbon are often preferred since they are less hazardous to the environment and can be used at more positive potentials. However, the electrode surface can be easily altered by the adsorption of a solution species or by the formation of an oxide layer and requires frequent reconditioning either by applying an appropriate potential or by polishing.

Chemists use voltammetric techniques for a wide variety of purposes including fundamental studies of oxidation and reduction processes in various media [17], adsorption processes on surfaces [18], electron transfer and reaction mechanisms [19], kinetics of electron transfer processes [20], speciation [21], and thermodynamic properties of solvated species. Voltammetric methods are also used for determining compounds of pharmaceutical interest and when coupled with HPLC, they are effective tools for the analysis of complex mixtures [22].

The analytical advantages of the various voltammetric techniques include being able to measure small currents to give excellent sensitivity for both inorganic and organic species, rapid analysis times, and being able to function within a wide range of temperatures. As well as this, it is applicable to a large number of solvents and electrolytes and can be used to simultaneously determine several analytes. Using experimentally obtained data, many unknown kinetic and mechanistic parameters can thus be determined.

2.1.2 Polarography

Jaroslav Heyrovský, a Czech chemist, was the inventor of polarography in 1922 and a subsequent recipient of the 1959 Nobel Prize in chemistry awarded for his ground-breaking work. By recording the current-voltage curve for a solution of 1.0 M aqueous NaOH, Heyrovský correctly interpreted the current increase between – 1.9 and – 2.0 V as a result of Na^+ ion reduction forming an amalgam [23]. His early contribution to electroanalytical chemistry made a great impact and all modern analytical voltammetric methods originate from polarography.

Polarography is a type of measurement that falls into the linear-sweep voltammetry category whose response is determined by combined diffusion/convection mass transport. Using a mercury based working electrode, the electrode potential is altered in a linear fashion from the initial potential to the final potential. As a sweep is taken, the current *vs.* potential response of a polarographic experiment produces a sigmoidal shape [24]. Qualitative information can be determined from the half-wave potential, giving the standard potential for the redox reaction being studied if it has fast electrode kinetics.

Mercury based electrodes such as dropping mercury electrodes (DME) or static mercury drop electrodes (SMDE), such as hanging mercury drop electrodes (HMDE), are used

as working electrodes in polarography. For a dropping mercury electrode, the influence of gravity causes liquid mercury from a reservoir to be steadily released from the end of a glass capillary tube. A spherical mercury droplet electrode forms but has a finite lifetime of several seconds. At the end of its lifetime, the suspended mercury droplet falls and is replaced by a new drop providing constant surface renewal for analysis. The hanging mercury drop electrode (HDME) on the other hand, produces a partial mercury drop of controlled geometry and surface area at the end of a capillary by rotating a micrometer screw to control the flow of mercury from the reservoir.

HMDEs have static surface areas which can be accurately controlled during experiments, in contrast to DMEs where they are subject to a constantly changing surface. However, the static surface of the HDME means it is more likely to suffer from surface adsorption phenomena than a DME. Unlike solid electrodes which need to be cleaned and polished between most experiments, mercury electrodes can be self-renewing by simply releasing the contaminated drop to allow a clean drop to grow between each experiment.

There is one additional type of mercury electrode that is commonly used: the mercury film electrode (MFE). Formation of MFEs involve a solid substrate electrode, typically carbon or platinum, being placed in a solution of Hg^{2+} and held at a potential where the reduction of Hg^{2+} to Hg is favourable, forming a thin mercury film on the solid electrodes surface.

Mercury has several advantages as a working electrode since it has a wide cathodic range and a renewable surface. Its high overpotential for the reduction of H_3O^+ to H_2 makes potentials as negative as - 1.0 V *vs.* SCE in acidic solutions and - 2.0 V versus SCE in basic solutions accessible [25]. Other advantages include the ability of metals to dissolve in mercury, resulting in the formation of stable amalgams to give highly sensitive

and reproducible measurements [26], and the ability to easily renew the surface of the electrode by extruding a new drop. Mercury however, is highly toxic and handling the drop system can be a little complicated [27, 28]. Due to the ease at which mercury is oxidised, it cannot be used as an electrode at potentials more positive than approximately - 0.3 V to + 0.4 V *vs.* SCE (depending on the electrolyte).

2.1.3 Stripping Voltammetry

The detection of trace and ultratrace analyte species can often pose a challenge since the voltammetric signal produced is limited by the concentration of the species in bulk solution. However, a highly sensitive method for electroanalytical detection using pre-concentration techniques can be carried out in the form of stripping voltammetry [29]. Low detection limits can be achieved through an initial pre-concentration step where the species of interest is deposited onto the electrode surface. This is followed by a suitable potential being applied to the working electrode to "strip" the accumulated analyte back into solution. The stripping peak currents and peak widths are a function of the size, coverage and distribution of the analyte on the electrode surface.

Stripping voltammetry is one of the most sensitive electroanalytical techniques for trace metal ion analysis in aqueous media whereby very low detection limits can be achieved, often within and below the nanomolar region [30–32]. Analytical detection of analytes using electrochemical procedures compare favourably with Atomic Absorption Spectroscopy (AAS) and Inductively Coupled Plasma (ICP) analysis. Soltyk et al. [33] determined zinc within concentration ranges of 20-40ppb, 0.5-20ppb and 10-50ppb by AAS, ICP-MS and AdSV, respectively.

There are three main approaches to stripping analysis which are classified by the nature

of the pre-concentration step; anodic stripping voltammetry (ASV), cathodic stripping voltammetry (CSV) and adsorptive stripping voltammetry (AdSV).

Anodic Stripping Voltammetry (ASV)

Anodic Stripping Voltammetry (ASV) is a voltammetric method for the quantitative determination of specific ionic species. It is often used with mercury electrodes for the determination of amalgam forming metals where the analyte of interest is electrodeposited at the working electrode during a pre-concentration deposition step, and oxidized from the electrode during the stripping step.

Pre-concentration:

$$M^{n+}(aq) + ne^- \rightarrow M(electrode) \tag{2.1}$$

Stripping:

$$M(electrode) \rightarrow M^{n+}(aq) + ne^- \tag{2.2}$$

The determination of cations can be achieved by holding the working electrode at a reducing potential such that the positive cations in solution are reduced and accumulate to the electrode. A deposition potential is chosen such that the current is limited by mass transfer and not electron transfer kinetics. The choice of deposition potential allows selectivity in the stripping voltammogram, where the value can be varied depending on which species are to be analyzed. Generally, a deposition potential *ca.* 0.3 V more negative than the reduction potential of the redox couple is used. After deposition for a set time period, the potential is driven positively where the analyte is re-oxidised back into solution. The current is measured during the stripping step and oxidation of the species is registered as a peak in the current signal at a potential where the species begins

to be oxidized. The shape of the stripping peak will depend on the type of electrode used, the voltammetric waveform, and the kinetics of the electrode reaction. The potential at which the species is stripped is dependent on its formal potential (for reversible couples), allowing it to be identified based on the stripping peak potential. The pre-concentration time, potential and convection are controlled parameters of the experiment. In some cases, a preliminary cleaning step is incorporated prior to the deposition where the potential is held at a more oxidizing potential than the analyte of interest for a period of time in order to fully remove any accumulated species from the electrode.

The current peaks produced is proportional to the concentration of the analyte species that has been reduced onto the electrode. By selecting a potential window where the analyte of interest (generally a metal) is expected to appear, ASV can be used to identify and quantify the metal concentration in a sample. In certain cases, stripping voltammetry can be further optimised to obtain maximum analytical sensitivity and to decrease limits of detection. This can be achieved during the pre-concentration step by stirring the solution and having a longer deposition time to further aid the accumulation of the species onto the electrode surface for stripping.

The use of mercury electrodes, such as mercury film electrodes (MFEs), enhances the process as when the metal ion is reduced to the metallic state, it forms an amalgam with the mercury which stabilizes it during the stripping phase [34, 35]. Ghoneim et al [36] successfully used differential pulse anodic stripping voltammetry (DPASV) to simultaneously determine Cd, Pb, Cu, Sb, Bi, Se, Zn, Mn, Ni, Co and Fe in water samples at a hanging mercury drop electrode. Five of the elements were directly detected first before the pH of the sample was modified and complexing agents were added to determine the other elements. Upon oxidation, a sharp peak is produced which improves the resolution

between analytes. In cases where the analyte of interest has an oxidizing potential above that of mercury, or where mercury electrodes would be unsuitable, other materials such as gold, platinum or carbon may be used as the working electrode [37–41].

Cathodic Stripping Voltammetry (CSV)

Cathodic stripping voltammetry is similar to that of ASV, with the difference being the pre-concentration potential is held at an oxidising potential, and the oxidised species is stripped from the electrode by cathodically sweeping the potential to more negative values, observing the reduction of the accumulated species.

Pre-concentration:

$$2M^{n+}(aq) + mH_2O(l) \rightarrow M_2O_m(electrode) + 2mH^+ + 2(m-n)e^-$$

or

$$M + L^{m-} \rightarrow ML^{(n-m)-}(ads) + ne^- \tag{2.3}$$

Stripping:

$$M_2O_m(electrode) + 2mH^+ + 2(m-n)e^- \rightarrow 2M^{n+}(aq) + mH_2O(l)$$

or

$$ML^{(n-m)-}(ads) + ne^- \rightarrow M + L^{m-} \tag{2.4}$$

The pre-concentration step employs electrolytic formation of a sparingly soluble salt (e.g. oxide, halide, sulfide) between the oxidised electrode material and the analyte. The salt is deposited on the surface of the electrode during the pre-concentration step and on

reduction of the salt, the species is stripped back into the solution.

Iron is one of the most commonly detected analytes using cathodic stripping voltammetry [42, 43], with detection limits as low as 0.1 nM [26]. A brief review on the determination of iron using voltammetric methods such as stripping voltammetry is given in Chapter 7. In seawater, the majority of dissolved iron (Fe^{2+} and Fe^{3+}) is naturally complexed with organic ligands, however CSV can be used to take advantage of ligand competition between an added ligand and natural ligands in solution. A commonly used complexing agent in this case is 1-nitroso-2-naphthol (NN) [44–46].

Many trace metals have been determined in natural waters and their speciation evaluated [47]. As well as iron, chromium was determined in seawater using CSV and its speciation could be achieved by forming complex species with diethylenetriaminepentaacetic acid (DTPA) at a hanging mercury drop electrode [48]. The different stabilities of the Cr(VI) and Cr(III) complexes allowed for their characterisation. Using another complexing ligand, catechol, dissolved concentrations of copper and zinc was evaluated in estuary water by Van den Berg et al. [49].

Adsorptive Stripping Voltammetry (AdSV)

Adsorptive stripping voltammetry is similar to the aforementioned ASV and CSV except that the pre-concentration step occurs via adsorption to the electrode surface rather than as a result of redox reactions. The pre-concentration step in adsorptive stripping voltammetry involves the adsorption of an organic compound or a metal complex onto the working electrode surface, and often involves a mediating ligand or complexing agent. The subsequent stripping step involves determination of the adsorbed species by reduction or oxidation as appropriate.

Pre-concentration:

$$A(aq) \rightarrow A(ads)$$

or

$$M(aq) + L(aq) \rightarrow ML(ads) \tag{2.5}$$

Stripping:

$$A(ads) \pm ne^{-} \rightarrow B(aq)$$

or

$$ML(ads) \pm ne^{-} \rightarrow B'(aq) \tag{2.6}$$

Adsorptive stripping methods have been widely utilised for the trace determination of metals [50, 51]. Abbasi et al [52] recently used N-nitrozo-N-phenylhydroxylamine (cupferron) as a selective complexing agent for the detection of zinc. Subsequent stripping of the adsorbed complex from the hanging mercury drop electrode created sensitive peak currents. The use of cupferron as a complexing agent for the determination of gallium was investigated by Grabarczyk and Wardak [53]. Cathodic stripping of the adsorbed gallium complex from the electrode resulted in a calculated detection limit of 1.3 x 10^{-10} mol L^{-1}. Biochemical species [54–56] have also been detected using AdSV at a various electrodes. Electrochemically inactive oestrogen can be detected voltammetrically by complexing them with sodium nitrate [57]. The electroactive nitro derivatives can then be adsorbed onto the electrode surface prior to stripping to give a well defined voltammetric wave. Ligands and complexing agents have been shown to form electroactively stable

complexes for AdSV, and successful stripping can be followed after the adsorption step.

2.1.4 Pulse Techniques in Voltammetry

Pulse voltammetry techniques can be used to aid analytical electrochemistry by achieving lower detection limits. As non-faradaic charging currents can obscure small faradaic currents of interest, trace amounts of analyte can be difficult to determine electroanalytically [10]. Pulse techniques work by applying pulses at periodic intervals, such that after sampling the currents before and after a potential change, a more enhanced signal results. By measuring the current late into the pulse life, there is negligible non-faradaic signal since the charging current decays faster than the faradaic current. This increase in sensitivity is a result of reducing the charging current and/or increasing the faradaic current which improves the signal-to-noise ratio. Differential pulse voltammetry (DPV) and square wave voltammetry (SWV) are among the most sensitive means for electroanalysis, and are consequently widely used for trace detection of different electroactive species.

Differential Pulse Voltammetry

DPV can be used to obtain greater sensitivity, by orders of magnitude greater than that of linear voltammetry with LoD vaulues around 10^{-8} M. It can be considered as a derivative of linear sweep voltammetry where a series of potential pulses of small fixed amplitude superimposed on a potential staircase is applied. Figure 2.1 illustrates the waveform for this technique.

Current is measured at two points, 1 and 2, for each pulse (see Figure 2.1) once immediately before the pulse, the potential is then stepped by a small amount (typically < 100 mV), and the current is sampled again just before the end of the pulse. The

potential of the working electrode is then stepped back by a lesser value than during the forward pulse such that baseline potential of each pulse is incremented throughout the sequence. The resulting current difference, $\triangle I$, is plotted as a function of potential which gives rise to a peak shaped response, the height of which is directly proportional to the concentration of the analyte.

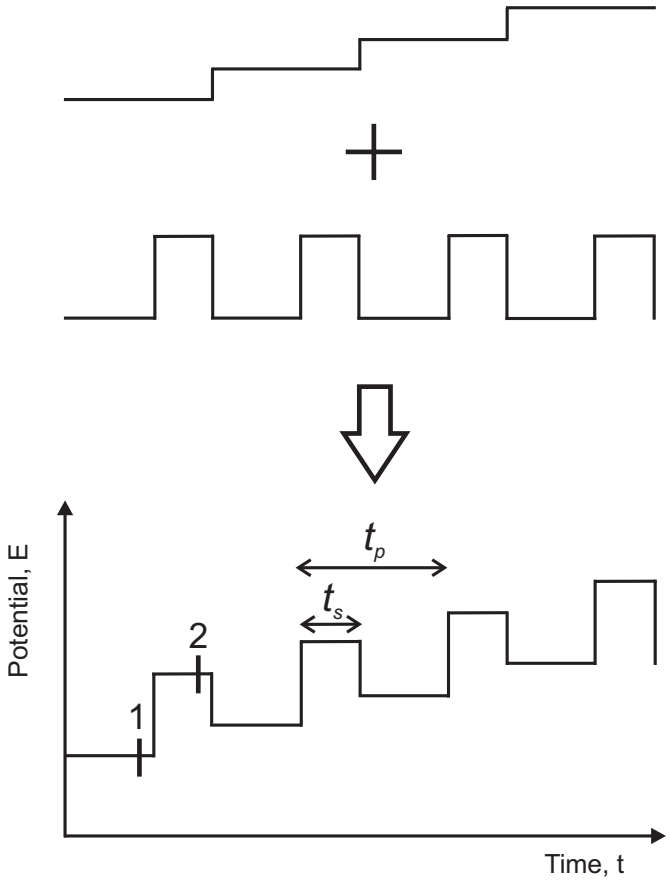


Figure 2.1: DPV waveform, where t_s is the step time and t_p is the pulse time. Currents are sampled at points 1 and 2, as indicated on the waveform

In such a scan, by sampling the current just before the potential is changed, the effect of the charging current can be minimised and enhanced signals from a reduced contribution from background currents results in greater sensitivity. If the background current from interfacial capacitance or from competing faradaic processes does not change much from

the first current sample to the second, then the subtractive process tends to cancel the background contribution. Since only the faradaic current is extracted, electrode reactions can be more accurately analysed.

With DPV, the step size, pulse amplitude or height, pulse width, and rest width are all variable factors that can be used to increase sensitivity of a particular application. Electrochemically reversible reactions show symmetrical peaks, whilst electrochemically irreversible reactions show asymmetrical peaks. The peaked response of DPV results in improved resolution between species with similar redox potentials such that mixtures of electroactive species can be analysed. Quantitatively, Equation 2.7 can be used to calculate the number of electrons corresponding to the peak, based on the width of the peak at half height.

$$W_{1/2} = \frac{3.52RT}{nF} \tag{2.7}$$

Square Wave Voltammetry

The square wave voltammetric waveform is another type of pulse voltammetry and can be seen as a variation of DPV. SWV consists of a staircase superimposed by a symmetrical double pulse, one in the forward and one in the reverse direction. Equal time is spent at the potential of the ramped baseline and of the superimposed pulse.

The current is again sampled at two separate points per pulse, as shown in Figure 2.2. The forward current sample, i_f, is recorded after the first pulse which is in the direction of the staircase. The reverse current sample, i_r, is recorded after the second pulse from each cycle, which is in the backward direction. The difference between the two forward and backward current measurements, $\triangle i$, calculated from $i_f - i_r$, together with the separate

forward and reverse currents thus produces three plots of current against potential for a single SWV sweep.

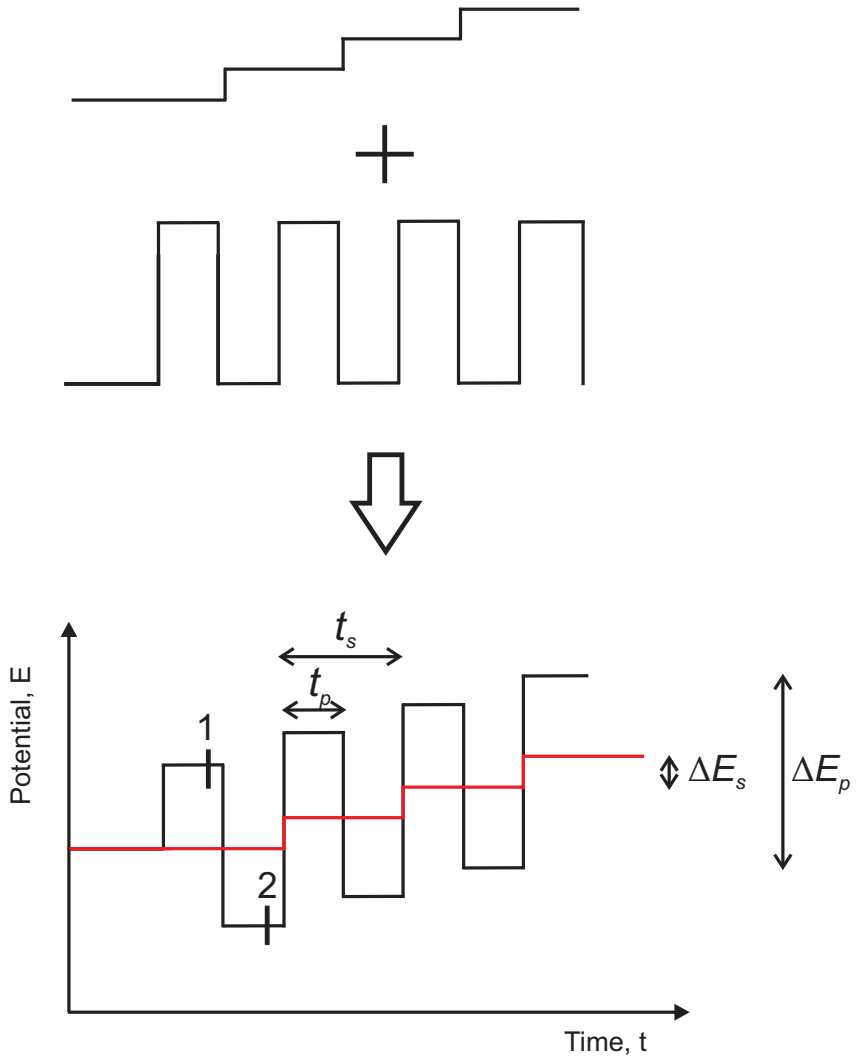


Figure 2.2: Schematic waveform for SWV showing square wave pulses superimposed on a staircase

The differential voltammogram produced by SWV is peak shaped with a symmetrical peak observed at the half-wave potential (Figure 2.3), where the peak current corresponds to the analyte concentration. This differential peak has a larger peak current than the individual forward and back peaks, hence increasing the sensitivity of the technique.

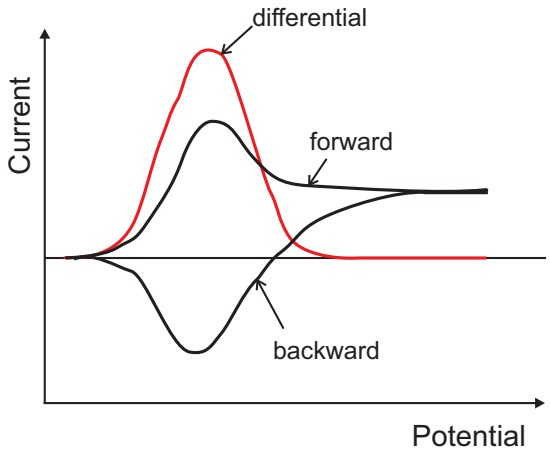


Figure 2.3: The forward, backward and differential voltammograms produced upon a single SWV sweep. The differential current is larger than the forward and backward currents, allowing more sensitive analyses

Square wave voltammetry is very similar to DPV, however, the time spent at each interval is smaller. For DPV, the time spent before the pulse is significantly longer than the length of the pulse forming a larger diffusion layer, and leading to a pseudo equilibrium occurring at the electrode surface before each pulse. In SWV, the pulses are of equal length in time and the difference in the charging currents is considered small enough to allow for a rapid succession of pulses. As such, SWV is generally a faster technique than DPV, but can only be applied to solid electrodes. As well as this, DPV has a longer pulse width than SWV, limiting the timescale of the technique. Shorter pulses can therefore be utilised in the latter to give lower limits of detection in the order of nanomolar concentrations.

2.1.5 Chronoamperometry

Chronoamperometry is an electrochemical technique in which the potential of the working electrode is stepped from a potential of no current to a potential where there is a high, usually diffusion controlled, current as shown in Figure 2.4, and as described by the Cottrell equation in section 1.4.1.

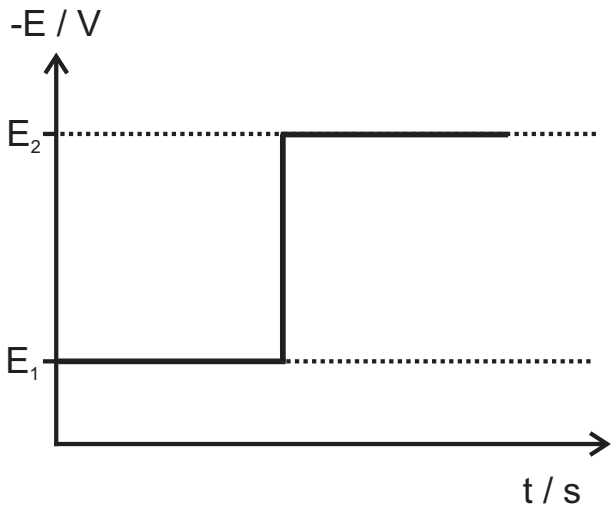


Figure 2.4: Variation in applied potential in a typical potential step experiment

Chronoamperometry generates high charging currents which then decays rapidly with time. Figure 2.5 shows a typical current-time response to a potential step at a macroelectrode. For the reduction, $O + e^- \rightarrow R$, the Cottrell equation assumes diffusion control at all times. As $[O]$ depletes at the electrode surface and reduces to form $[R]$ in solution, the diffusion layer thickens, causing the measured current to decrease proportionally to the increasing diffusion layer. Eventually, the current falls to zero.

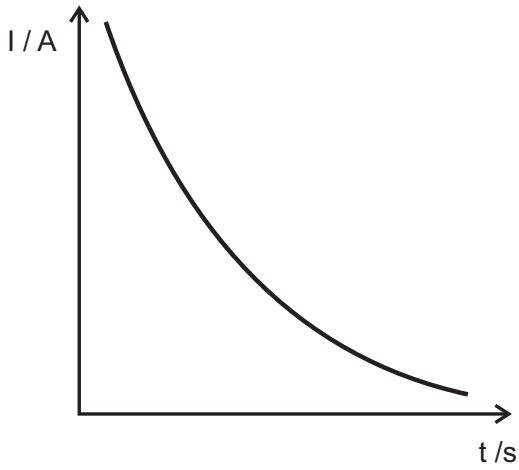


Figure 2.5: Typical example of a voltammetric response following a potential step at a macroelectode

The response at macroelectrodes is seen above, however, chronoamperometry is also investigated at microelectrodes (where at least one dimension is in the order of microns or less). Here, instead of the current decaying to zero, it tends to a steady state value at long timescales, or small electrode radii.

By solving Fick's second law of diffusion and supposing a spherical or hemispherical microelectrode, the flux of reactant at the electrode surface can be deduced.

$$j = D[C]_{bulk}\left(\frac{1}{\sqrt{D\pi t}} + \frac{1}{r_e}\right) \tag{2.8}$$

where r_e is the radius of the sphere or hemisphere electrode.

Using Equation 2.8 and considering the short-time limit, we arrive at:

$$j = \frac{[C]_{bulk}\sqrt{D}}{\sqrt{\pi t}} \tag{2.9}$$

Under the conditions : $\sqrt{D\pi t} \ll r_e$ where the diffusion layer is small compared to the radius of the spherical electrode, diffusion is approximately linear. This result corresponds to the earlier case of linear, one dimensional diffusion.

In the case of a long-time limit,

$$j = D\frac{[C]_{bulk}}{r_e} \tag{2.10}$$

or

$$I = 4\pi r_e DF[C]_{bulk} \qquad \text{(sphere)} \tag{2.11}$$

$$I = 2\pi r_e DF[C]_{bulk} \qquad \text{(hemisphere)} \tag{2.12}$$

where $\sqrt{D\pi t} \gg r_e$, it can be seen that a steady state current is established. Instead of the current decreasing towards zero as for linear diffusion, here the diffusion layer thickness expands as electrolysis continues. As time proceeds, more electroactive species will "feed" the constant diffusion gradient at the electrode surface once steady-state is attained. Steady state current dominates more for electrodes with small r_e and as such, it can be seen that for microelectrodes of spherical or hemispherical geometry, a steady state is rapidly established.

2.2 Potentiometry

Potentiometry is a type of measurement where the potential difference between a measuring (indicator) electrode and a reference electrode in solution is measured whilst no significant current is drawn from the cell. As no faradaic current flows, the potential is usually controlled by the thermodynamic properties of the system [58]. The measured potential depends on the activity of ions according to the Nernst equation (as described in section 1.1.3), and can be used to calculate the concentration of the analyte in the sample.

A popular potentiometric method for the determination of ions can be carried out at ion selective electrodes (ISEs), which are often membrane based electrodes that respond selectively to the activity of a specific ion in the presence of various interfering ions from the sample. The activity of the ions is then converted into an electrical potential. The first electrode of this type was the glass electrode which responds selectively to the hydrogen ion and has been used to measure pH since the early 20th century [59].

The glass electrode is used by dipping it in a sample solution and completing the elec-

trochemical cell with a reference electrode. In a glass pH electrode, a partially hydrated thin glass membrane that is responsive to changes in H^+ activity separates the sample solution from an inner solution of 1 M HCl within which a Ag/AgCl electrode is immersed. The glass consists of a mixture of Na_2SiO_3, $CaSiO_3$ and SiO_2, and when immersed in aqueous solution the hydrated membrane surface results in the formation of negatively charged sites (SiO^-) with sodium ions (Na^+) serving as counter ions. An equilibrium is established between H^+ and Na^+ electrostatically bound to anionic sites in the glass and in solution:

$$H^+(aq) + Na^+(gl) \rightleftarrows H^+(gl) + Na^+(aq) \tag{2.13}$$

This equilibrium shifts depending on the concentration of H^+, with the Na^+ ions migrating from the interior of the glass to the hydrated region to maintain electrical neutrality. It then follows that the H^+ ions move to replace the Na^+ ions that have migrated. This combination of ion migrations provides sufficient electric current for the potential to be measured. As H^+ ions are intrinsically smaller and faster moving than Na^+, most of the current in the hydrated region is carried by the hydrogen ions and the glass surface behaves as it were permeable to H^+ [59]. It thus acts as a selective indicator electrode sensitive to pH. Developing upon the glass electrode for pH determination, a typical modern pH probe today combines both the indicator and reference electrodes into one body to simplify pH measurements.

Since the success of glass pH electrodes, other types of glass electrodes have been developed with different composition such that they can respond selectively to a wide variety of ions [60, 61] including Na^+ [62], K^+ [63] and Ca^{2+} and Mg^{2+} [64]. These electrodes all consist of an internal reference electrode separated from the test solution

by a membrane which acts reversibly and with good selectivity to specific ions. Other ion selective membrane electrodes used for potentiometric measurements include solid-state membrane electrodes [65, 66] and liquid membrane electrodes [67–69]. In solid-state electrodes, the internal reference solution is separated from the test solution by an insoluble, inorganic salt. The salt, such as a silver halide, acts as an ionic conductor for specific ions, and the potential developed across it depends on the activity of the specific ion in the sample solution according to the Nernst Equation. Replacing the glass or inorganic crystal with a thin layer of water immiscible liquid ion exchanger leads to the construction of a liquid membrane electrode.

The use of ion-selective electrodes is limited by interference from other undesired ions [70]. No ion-selective electrodes are completely ion-specific and all are sensitive to some other ions to some extent. For many cases, these interferences are insignificant enough to be ignored, however in some cases the electrode may be far more sensitive to the interfering ion than to the desired ion, such that the probe can only be used if the interfering ion is present in trace quantities, or entirely absent.

2.3 Data Analysis Methods

The need for data analysis of analytical measurements is required to be able to interpret the results and quantify analytes. Two techniques that have been used within this thesis are described below.

2.3.1 The Standard Addition Method

When an increasing sensor response is seen with increasing analyte concentration, calibration plots can be constructed to determine the analytical parameters of the system. Peak height *vs.* concentration graphs can be used to find the unknown concentration of a sample through extrapolation from the graph or the standard addition method.

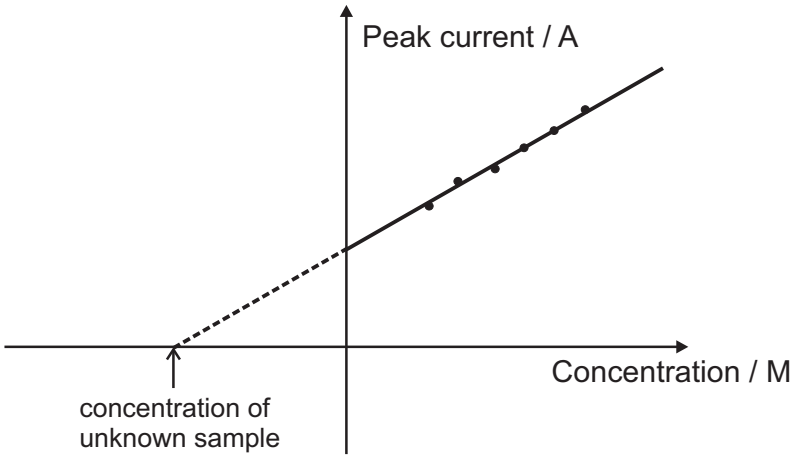


Figure 2.6: Peak current *vs.* concentration plot for the standard addition

The standard addition method is a quantitative approach where a sample of unknown concentration is spiked several times with known aliquots of a standard solution to form a standard addition plot, as shown in Figure 2.6. The concentration of the spiked aliquots should be less than *ca.* 10 % of the unknown analyte. After consecutive standard additions, the total analyte concentration is a combination of the unknown and the standard, such that the total concentration increases approximately linearly and the analytical response can be measured.

The concentration of the analyte in the sample can then be estimated from the graph by fitting a line of best fit through the experimental data points and extrapolating to the

concentration axis. The intercept on the x axis will give the concentration of the analyte present. Accuracy of the line of best fit dictates the reliability of the results. A perfect line of best fit, of a positive gradient, is defined as having a correlation coefficient, or R^2 value, of one. To ensure accuracy of the analysis, there should be a minimum of four standard additions to the sample. Reproducibility can be achieved by repeated measurements of each point.

The standard addition method is very useful in determining unknown analyte concentrations in the analysis of real samples. Interferences caused by matrix effects that lead to errors in measurements (caused by temperature, pH and other interfering materials affecting the electrode signal), can be partly eliminated.

2.3.2 Limits of Detection

The detection limit (LoD) is defined as the minimum value of the signal from the species that is being measured, that is significantly different from the blank signal. Most analytical instruments produce a response even in the blank experiments; this signal is often referred to as "noise". Since the type of noise that contributes to the measurement and calibration of detection limits can be rather subjective, the LoD value calculated depends on the accuracy of the results from raw analytical signals and of the model used. A number of different models for calculating detection limits have been suggested.

One commonly used approach is the statistical method known as the "three sigma method (3σ)". This model estimates a LoD value based on the sensitivity and experimental error of a standard addition plot. For a linear plot, $y = a + bx$, as shown in Figure 2.6, the detection limit can be estimated by:

$$LoD = \frac{3\sigma}{b} \tag{2.14}$$

where σ represents the standard deviation in the y-coordinate and b is the gradient of the plot.

The value calculated using the three sigma method is only a statistical estimation for the detection limit, and may not necessarily be the lowest experimentally distinguishable signal from the blank background. A better estimate for the LoD can be calculated using more precise experimental data by lowering the experimental error such that there is a smaller standard deviation. Limitations from instrumentation and experimental error often means that the theoretically calculated value for the LoD is lower than that can be experimentally achieved, however.

A range of different carbon electrodes have been used in the work presented in this thesis, and an introduction to their properties and uses is discussed in the next chapter.

Bibliography

[1] P. L. Croot, *Analytical Chemistry* **83** (2011) 6395.

[2] R. G. Kempegowda and P. Malingappa, *Electrochemistry Communications* **25** (2012) 83.

[3] L. M. Laglera, J. Santos-Echeandia, S. Caprara and D. Monticelli, *Analytical Chemistry* **85** (2013) 2486.

[4] S. Chen, L. Zhang, Y. Long and F. Zhou, *Electroanalysis* **26** (2014) 1236.

[5] C. Wang and C. Yu, *Reviews in Analytical Chemistry* **32** (2013) 1.

[6] F. Zhao, R. C. T. Slade and J. R. Varcoe, *Chemical Society Reviews* **38** (2009) 1926.

[7] W. Zhou, Z. Zhou, S. Song, W. Li, G. Sun, P. Tsiakaras and Q. Xin, *Applied Catalysis, B: Environmental* **46** (2003) 273.

[8] W. Dai, M. Li, H. Li and B. Yang, *Sensors and Actuators, B: Chemical* **201** (2014) 31.

[9] A. Merkoci, *Electroanalysis* **25** (2013) 15.

[10] R. G. Compton and C. E. Banks, *Understanding Voltammetry* (Imperial College Press, London, 2011), 2nd edition.

[11] F. Settle, *Handbook of Instrumental Techniques for Analytical Chemistry* (Prentice Hall, 1997).

[12] R. K. Shervedani, A. Hatefi-Mehrjardi and A. Asadi-Farsani, *Analytica Chimica Acta* **601** (2007) 164.

[13] R. Segura, M. I. Toral and V. Arancibia, *Talanta* **75** (2008) 973.

[14] J. A. Cox and M. Majda, *Analytica Chimica Acta* **118** (1980) 271.

[15] X. Diao and K. Sumi, *Analytical Sciences* **26** (2010) 681.

[16] H. C. Leventis, I. Streeter, G. G. Wildgoose, N. S. Lawrence, L. Jiang, T. G. J. Jones and R. G. Compton, *Talanta* **63** (2004) 1039.

[17] A. P. Aldrich and C. M. G. V. den Berg, *Electroanalysis* **10** (1998) 369.

[18] A. S. Kumar and P. Swetha, *Colloids and Surfaces, A: Physicochemical and Engineering Aspects* **384** (2011) 597.

[19] X. Ji, C. E. Banks, A. Crossley and R. G. Compton, *Chemphyschem : a European journal of chemical physics and physical chemistry* **7** (2006) 1337.

[20] R. L. McCreery, *Electroanalytical Chemistry* **17** (1990) 221.

[21] C. M. G. van den Berg, *Analytical Chemistry* **78** (2006) 156.

[22] M. J. Nash, J. E. Maskall and S. J. Hill, *Journal of Environmental Monitoring* **2** (2000) 97.

[23] J. Heyrovsky, *Comptes Rendus Chimie* **179** (1924) 1267.

[24] A. J. Bard and L. R. Faulkner, *Electrochemical Methods: Fundamentals and Applications* (Wiley, New York ; Chichester, 2001), 2nd edition.

[25] A. Economou and P. R. Fielden, *Analyst (Cambridge, United Kingdom)* **128** (2003) 205.

[26] J. Gun, P. Salauen and C. M. G. van den Berg, *Analytica Chimica Acta* **571** (2006) 86.

[27] R. F. Palmer, S. Blanchard, Z. Stein, D. Mandell and C. Miller, *Health & place* **12** (2006) 203.

[28] F. Zahir, R., F. Zahir, S. J. Rizwi, S. K. Haq and R. H. Khan, *Environmental toxicology and pharmacology* **20** 351.

[29] J. Wang, *Analytical electrochemistry* (Wiley-VCH, New York, 2000), 2nd edition.

[30] C. M. G. V. den Berg and Z. Q. Huang, *Journal of Electroanalytical Chemistry and Interfacial Electrochemistry* **177** (1984) 269.

[31] C. M. G. V. den Berg, M. Nimmo, O. Abollino and E. Mentasti, *Electroanalysis* **3** (1991) 477.

[32] M. S. El-Shahawi, A. S. Bashammakh, A. A. Al-Sibaai, S. O. Bahaffi and E. H. Al-Gohani, *Electroanalysis* **23** (2011) 747.

[33] K. Soltyk, A. Lozak, M. Warowna-Grzeskiewicz and Z. Fijalek, *Acta Poloniae Pharmaceutica* **57** (2000) 261.

[34] C. Locatelli and S. Casolari, *Current Topics in Analytical Chemistry* **4** (2004) 57.

[35] C. Locatelli and G. Torsi, *Microchemical Journal* **78** (2004) 175.

[36] M. M. Ghoneim, A. M. Hassanein, E. Hammam and A. M. Beltagi, *Fresenius' journal of analytical chemistry* **367** (2000) 378.

[37] P. Salaun, K. B. Gibbon-Walsh, G. M. S. Alves, H. M. V. M. Soares and C. M. G. van den Berg, *Analytica Chimica Acta* **746** (2012) 53.

[38] N. Scheers, T. Andlid, M. Alminger and A.-S. Sandberg, *Electroanalysis* **22** (2010) 1090.

[39] J.-H. Yoon, J. E. Yang, J. P. Kim, J. S. Bae, Y.-B. Shim and M.-S. Won, *Bulletin of the Korean Chemical Society* **31** (2010) 140.

[40] E. V. Vikulova, N. A. Malakhova, L. I. Kolyadina, N. Y. Stozhko, F. A. Gareeva, T. M. Kudryavtseva and K. Z. Brainina, *Zavodskaya Laboratoriya, Diagnostika Materialov* **78** (2012) 12.

[41] M. Lu, K. E. Toghill, M. A. Phillips and R. G. Compton, *International journal of environmental analytical chemistry* **93** (2013) 213.

[42] Z.-M. Dong, G.-C. Zhao and H. Wang, *Fenxi Kexue Xuebao* **29** (2013) 30.

[43] A. P. Aldrich and C. M. G. V. den Berg, *Electroanalysis* **10** (1998) 369.

[44] K. Yokoi and C. M. G. V. den Berg, *Electroanalysis* **4** (1992) 65.

[45] T. Nagai, A. Imai, K. Matsushige, K. Yokoi and T. Fukushima, *Limnology* **5** (2004) 87.

[46] M. Gledhill and C. M. G. V. den Berg, *Marine Chemistry* **47** (1994) 41.

[47] E. P. Achterberg and C. Braungardt, *Analytica Chimica Acta* **400** (1999) 381.

[48] M. Boussemart, C. M. G. V. den Berg and M. Ghaddaf, *Analytica Chimica Acta* **262** (1992) 103.

[49] C. M. V. den Berg, A. G. A. Merks and E. K. Duursma, *Estuarine, Coastal and Shelf Science* **24** (1987) 785.

[50] M. G. Paneli and A. Voulgaropoulos, *Electroanalysis* **5** (1993) 355.

[51] A. Z. A. Zuhri and W. Voelter, *Fresenius' Journal of Analytical Chemistry* **360** (1998) 1.

[52] S. Abbasi, A. Farmany, M. Roushani and S. S. Mortazavi, *Water Science and Technology* **69** (2014) 438.

[53] M. Grabarczyk and C. Wardak, *Journal of Environmental Science and Health, Part A: Toxic/Hazardous Substances & Environmental Engineering* **49** (2014) 1142.

[54] D. Asangil, I. H. Tasdemir and E. Kilic, *Journal of Pharmaceutical Analysis* **2** (2012) 193.

[55] M. L. Yola and N. Ozaltin, *Reviews in Analytical Chemistry* **30** (2011) 29.

[56] J. Barek, K. Peckova and V. Vyskocil, *Current Analytical Chemistry* **4** (2008) 242.

[57] T. Hong, J. B. Kyong, H. J. Lee and M. zoon Czae, *Analytical Science & Technology* **12** (1999) 34.

[58] P. H. Rieger, *Electrochemistry* (Chapman & Hall, New York, 1994), 2nd edition.

[59] G. A. Perley, *Anal. Chem* **21** (1949) 395.

[60] M. A. Arnold and R. L. Solsky, *Analytical Chemistry* **58** (1986) 84.

[61] Y. G. Vlasov, *Fresenius' Zeitschrift fuer Analytische Chemie* **335** (1989) 92.

[62] G. Eisenman, D. O. Rudin and J. U. Casby, *Science* **126** (1957) 831.

[63] C. O. Lee, *Biophysical journal* **27** (1979) 209.

[64] H. M. A. Elbary and O. I. Mostafa, *Egyptian Journal of Chemistry* **43** (2000) 79.

[65] A. Michalska, *Electroanalysis* **24** (2012) 1253.

[66] J. Bobacka, *Electroanalysis* **18** (2006) 7.

[67] A. A. Al-Sibaai, *Proceedings of the Analytical Division of the Chemical Society* **12** (1975) 65.

[68] M. D. L. A. Arada-Perez, I. C. Nodarse and M. Yazdani-Pedram, *Journal of the Chilean Chemical Society* **49** (2004) 31.

[69] P. G. Veltsistas, T. I. Sikalos, M. I. Prodromidis, C. D. Papadimitriou and M. I. Karayannis, *Mikrochimica acta* **135** (2000) 113.

[70] A. Michalska, M. Ocypa and K. Maksymiuk, *Analytical and Bioanalytical Chemistry* **385** (2006) 203.

Chapter 3

Introduction : Carbon Electrodes

3.1 Introduction to Carbon Electrodes

Many different types of carbon based electrodes have been used for electroanalytical studies, ranging from glassy carbon to the discovery of new carbon based materials such as carbon nanotubes [1]. Reports using carbon materials in electrochemistry has been studied extensively due to many factors including the ease of their modification, wide potential window, relatively inert electrochemistry, non-toxicity and generally their low cost [2, 3]. The wide variety of carbon materials lead to diverse physical properties with differing surface structures, significantly changing the sensitivity of electroanalytical methods for detection of different analyte ions [4–6].

Carbon based electrodes have been used in the majority of work presented in this thesis, and as such, this chapter aims to give a brief overview of the properties and structure of the carbon based materials used within the work presented, including pyrolytic graphite, glassy carbon electrodes and screen printed electrodes.

3.2 Carbon

Carbon is one of the most abundant and important elements in the universe, present in all living organisms. It is essential to life where nearly every molecule in living organisms contains this. With 4 electrons in its valence shell, it is able to provide 4 electrons to form covalent bonds and combine with itself and other elements leading to millions of unique compounds. Carbon exists as several different allotropes which can be crystalline or amorphous in nature, such as diamond, graphite, graphene etc, however the various allotropes of carbon have very different chemical and physical properties. Many isotopes of carbon can also be formed, of which three occurs naturally in nature, carbon-12, carbon-13, and the radioactive carbon-14.

Whilst bulk carbon is relatively inert, the intrinsic carbon surface is extensively decorated with functional groups which can be exploited for electrochemical analysis [7]. Facile chemical modification of the carbon material allows the surface chemistry of carbon to impart specific properties to suit particular analyses [8–11]. As well as this, surface defects have also shown to increase the rate of electron transfer processes which is of great importance in electroanalytical chemistry [12, 13].

3.3 Pyrolytic Graphite

Pyrolytic graphite is a generic term for an unique form of graphite manufactured by decomposition of a hydrocarbon gas at very high temperatures in a vacuum furnace to form an ultra-pure product which is near theoretical density and extremely anisotropic [14]. The material is grown onto a substrate where the deposited form of graphite, composed of crystallites, tend to be aligned parallel to the surface of deposition, giving it a layered

composition where different planes lead to different properties. The graphite layers are approximately parallel, equidistant and randomly ordered. Parallel to the basal planes, pyrolytic graphite has very high thermal conductivity, acting as a superb electrical conductor, and is mechanically strong [2, 15]. Comparatively, perpendicular to the basal planes, the material has low thermal conductivity, acting as an electrical insulator where it is also mechanically weak. This unique property allows pyrolytic graphite to have many uses in electrochemistry [16–18].

3.3.1 BPPG vs. EPPG

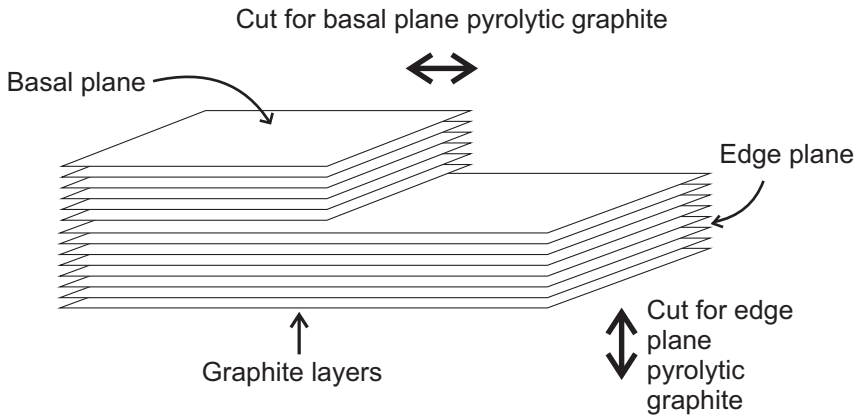


Figure 3.1: Schematic of pyrolytic graphite cut showing basal and edge planes

Covalent bonds formed between the graphite sheets result in highly ordered layers. The orientation at which the graphite crystal is cut gives two distinct surfaces, namely the edge plane and basal plane. If cut perpendicular to the sheets, an edge plane electrode is formed (EPPG), whereas if cut parallel to the sheets, a basal plane electrode results (BPPG) where graphite layers lying parallel to the surface are separated by 3.35 $\mathring{A}$, as shown in Figure 3.1.

Important features are demonstrated from the nature of the graphite structure and bonding. As conductivity is directional, it can be seen that current will travel parallel to the graphite sheets resulting in high resistivity perpendicular to the sheets. As such, BPPG electrodes have a higher resistance and exhibit slower electrode kinetics compared to EPPG electrodes. The fast kinetics shown in EPPG electrodes suggest that there are many reactive sites present at the edge plane sites, whereas there are far fewer edge plane like defects at basal plane surfaces [15]. The highly reactive edge plane defects allow low detection limits, high sensitivities, improved signal to noise characteristics, low background currents and low over-potentials, making it more advantageous over many other carbon materials [19]. It has been reported that the electrode kinetics at edge planes are at least three orders of magnitude faster than those at basal planes [20].

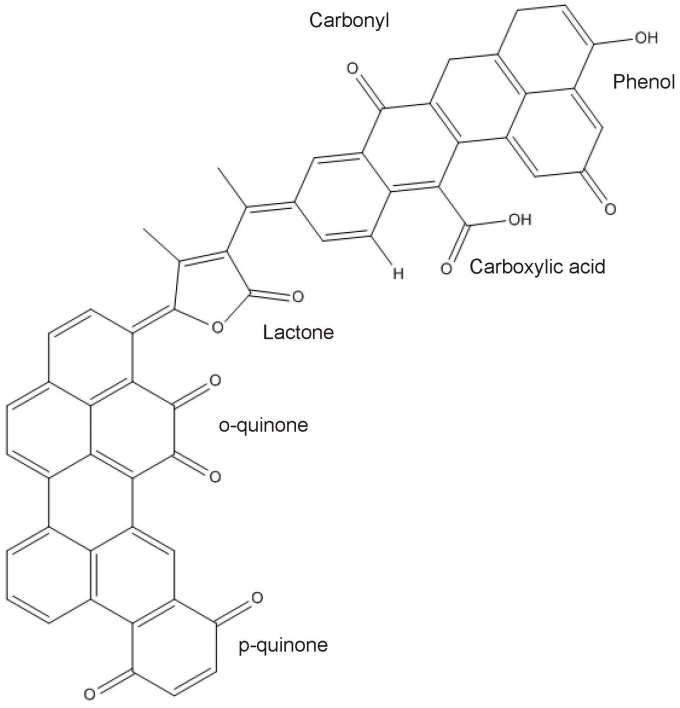


Figure 3.2: Representation of various functional groups present on graphitic carbon surfaces, adapted from ref [21]

Edge plane defect sites are high energy defects where electron transfer takes place, and thus making these sites much more chemically reactive than the relatively inert basal plane surfaces [15]. Given the highly reactive chemical sites at the EPPG edge planes, it has been shown that the edge plane defect sites can potentially react with atmospheric oxygen in the air [7]. As such, these sites are often decorated with a wide range of oxygen containing surface functional groups such as quinones, carbonyls, hydroxyl, etc as seen in Figure 3.2. Surface oxo-groups have a great importance in chemical reactivity. Banks and Compton [15] have previously reported evidence defining the role of the edge plane sites as the site of electron transfer and basal plane terraces as voltammetrically inert. This suggests that most electron transfer processes that occur are preferred at the edge plane step defects. As such, EPPG electrodes are commonly used as an electrode substrate for electroanalysis.

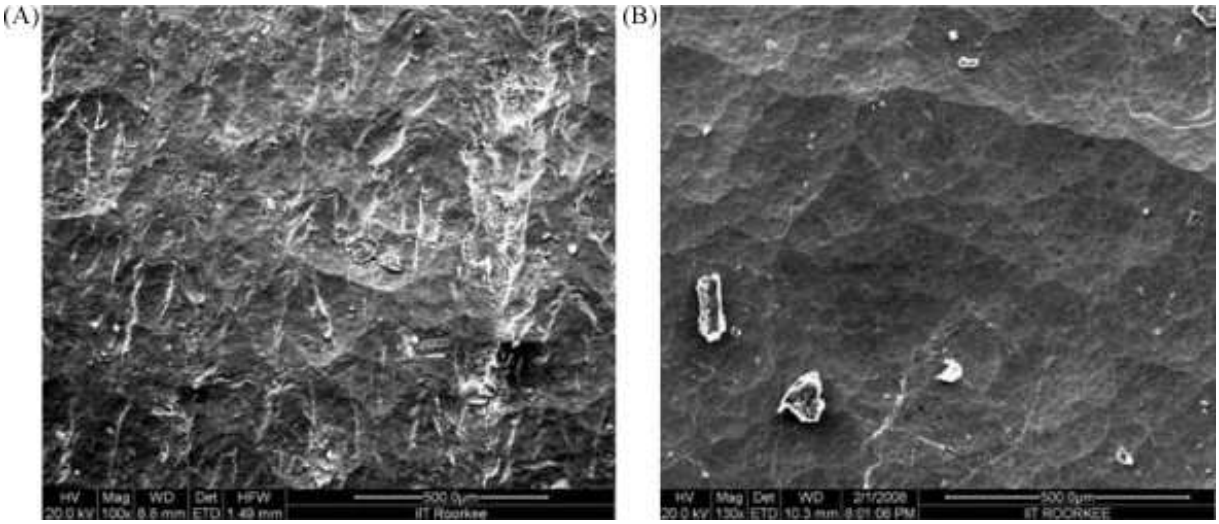


Figure 3.3: A comparison of FE-SEM images of (A) edge plane and (B) basal plane of pyrolytic graphite electrode

Characterisation of the graphitic surface has been extensively covered by many groups

using physical and chemical techniques such as XPS [22, 23], thermal desorption methods [24], spectroscopy [25] and electrochemistry [26, 27]. An FE-SEM image [28] comparing the basal and edge plane of a pyrolytic graphite is shown in Figure 3.3. It can be seen from the SEM images that (A) the edge plane surface is rough, showing the graphite plates edges, whereas (B) the basal plane surface is much smoother.

In regards to voltammetry, there is a significant difference in voltammetric response between BPPG electrodes compared to EPPG electrodes. This arises since there is higher resistance at the basal plane due to the alignment of graphite sheets with respect to the electrode surface, as mentioned earlier, and as such, electron transfer kinetics are much slower compared to edge plane sites [20]. A higher overpotential is required at BPPG electrodes [29] resulting in often electrochemically irreversible voltammograms, whereas EPPG electrodes display nearly reversible voltammograms with a peak-to-peak separation of 58 mV. For this reason, EPPG electrodes are often preferred to BPPG electrodes in practise.

3.4 Glassy Carbon (GC)

Glassy carbon (GC) is used extensively as an electrode material in electroanalysis. It is formed by heating an aromatic polymer, such as a phenolic or a furfurylic resin, to high temperatures and pressure in an inert atmosphere [30]. Being a non-graphitizing carbon, it combines glassy and ceramic properties with those of graphite which results in higher strength and hardness compared to ordinary graphite, allowing it to reach temperatures of over 3000 ^{o}C. Glassy carbon exhibits many useful characteristics such as its impermeability to gas and liquids, wide potential range, resistance to chemical attack,

high thermal stability, well-defined conductivity, low electrical resistance and low density [31, 32]. The hard glassy like nature and inertness of the material also contributes to its ease with which the surface can be modified [33, 34].

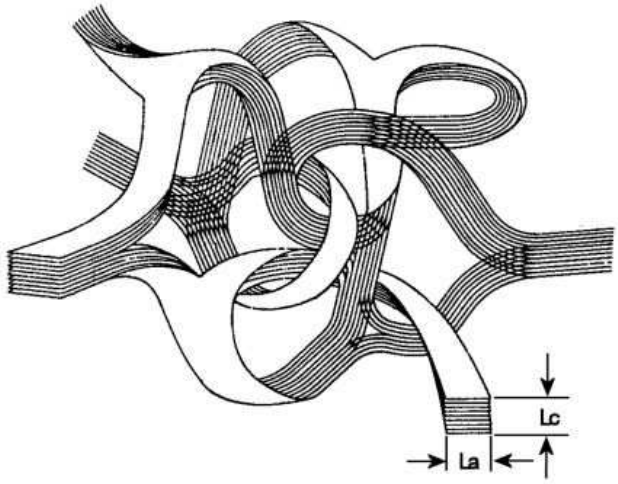


Figure 3.4: The Jenkins - Kawamura model showing the interwoven structure of glassy carbon, with L_a = 2.9 nm and L_c = 1.4 nm for GC formed at 1000 ^{o}C

The structure of glassy carbon has been investigated by many researchers since its production in the 1960s. Ergun and Tiensuu [35] first suggested that GC contains diamond-like and graphite-like structures with sp^2 and sp^3 bonded atoms. Using X-ray diffraction, graphitic domains were thought to be linked by short oxygen containing bridges. Following on from this, a widely accepted model for glassy carbon was proposed by Jenkins and Kawamura [36] in 1971, composing of interwoven ribbons of graphite containing highly conjugated sp^2 carbon atoms and forming a polymer-like crystalline structure as shown in Figure 3.4. Here, L_a and L_c are the lengths of the graphitic domains perpendicular and parallel to the graphite c axis, with a value of 2.9 nm and 1.4 nm for GC formed at 1000^{o}C, respectively. XPS and TEM techniques were used to characterise the glassy carbon material and it was suggested to exist like amorphous carbon, consisting of regions

of small graphite-like basic structural units of partly stacked but mismatched structure with the edges terminated by hydrogen or hydroxyls [31]. The model is based on the assumption that the molecular orientation of the polymeric precursor material is memorized to a certain extent after carbonisation. In such a structure, the many conjoined micropores causes GC to have a lower density (1.3 - 1.5 g cm^{-3}) than graphite (2.27 g cm^{-3}) or diamond (3.52 g cm^{-3}) [37], reflecting its porous microstructure. As such, it is expected to be gas permeable, however GC has in fact shown to be highly impermeable.

In light of this, the structure of GC was again revised, and using HRTEM (High Resolution Transmission Electron Microscopy) [38, 39] it is thought that fullerene-related structures are present. This follows from the discovery of fullerenes and the subsequent related structures such as carbon nanotubes, where it has been shown that sp^2 bonded carbons containing non-six membered rings can be highly stable. Despite this updated fullerine related model, its detailed atomic structure is still not known and further work is being conducted.

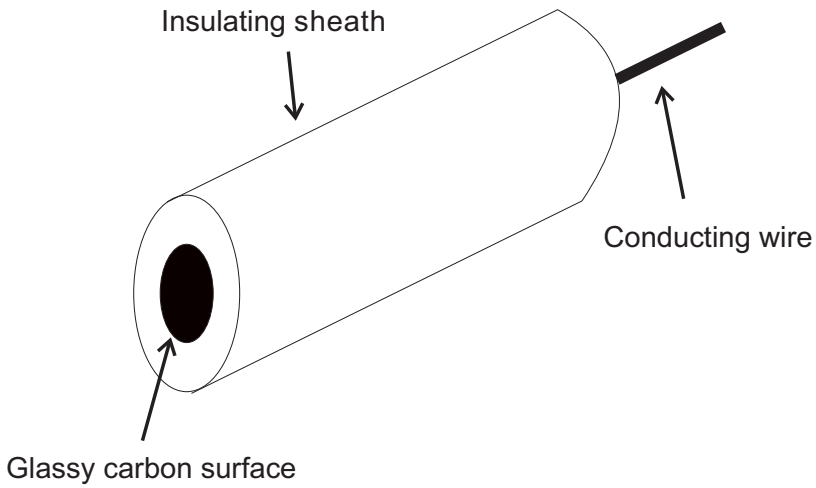


Figure 3.5: Schematic of a typical commercial glassy carbon electrode

GC is extensively used in electrochemistry as an electrode for the fabrication of sensors and trace analysis of electroactive substances. The electrodes are available commercially from CH instruments (Austin, TX, USA) in the form of a rod sealed in an insulating sheath, as shown in Figure 3.5, and it is in this practical form that most experiments are conducted. It can also be easily modified and forms a base for surface modified electrodes [40–44].

3.5 Screen Printed Carbon Electrodes (SPE)

Electrode systems based on either a two or three electrode configuration can be screen printed onto small and inexpensive solid surfaces. By miniaturising the working electrode, reference electrode and counter electrode, only a very small sample is required which can very useful especially in the analytical biosensing sector [45, 46]. The cheap and disposable nature of screen printed electrodes (SPEs) make them popular electrochemical sensors [47, 48], and can be easily integrated into portable systems for direct in-situ analysis of samples. The advantage of this means that excessive cleaning and electrode pre-treatment is not required between measurements. As well as this, SPEs avoid some of the common problems related to classical solid electrodes, such as memory effects [49]. For commercially bought SPEs, screen printing technology is a well-established mass produced technique which deposits ink layer by layer on a solid substrate through the use of a screen or mesh to define the shape and size of the desired electrode, as shown in Figure 3.6. The screen mesh is placed just above the substrate to be printed and whilst the squeegee is moved across the surface, ink is pushed through the mesh and forms the pattern below. The excess ink is removed from the edges by the squeegee and the mesh is allowed to

peel away from the surface leaving a layer of deposited ink on the printing surface. This technique can be very useful since there is good reproducibility, design flexibility and a wide choice of materials can be used.

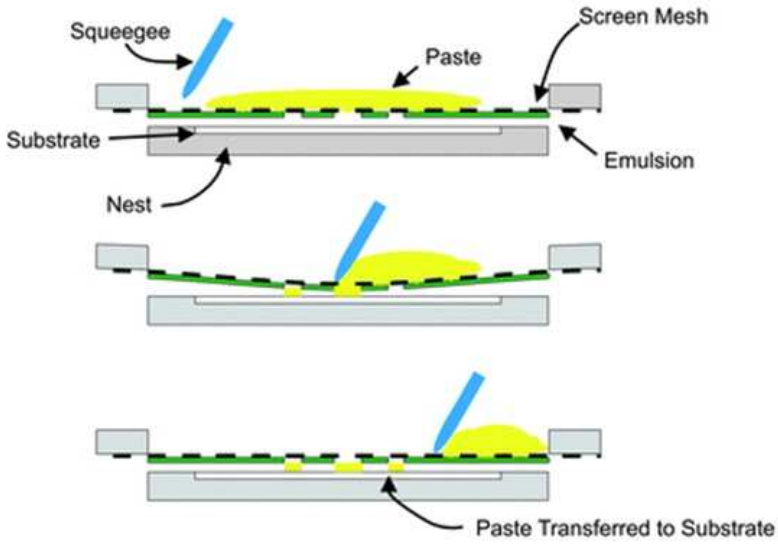


Figure 3.6: Schematic representation of the manufacture of screen printed electrodes

The majority of SPEs are manufactured using graphite inks with silver ink generally forming the conductive track, however gold inks and other materials can also be used. Carbon paste is a widely used material because it is relatively cheap, easy to modify and chemically inert. For fabrication of carbon based SPEs [50], the inks selected consist of graphite particles, polymer binder and other additives which are utilised for dispersion, printing and adhesion tacks. The ink composition e.g. type, size or loading of graphite particles and printing conditions dictate the selectivity and sensitivity required for each analysis and can affect the electron transfer reactivity and overall analytical performance of the resulting carbon sensors.

A wide variety of commercially bought screen printed electrodes is available. However,

due to the versatility of SPEs, there is an extensive range of electrode modification methods to fit multiple purposes related to analysis of different target analytes. Modification of the electrode surface can be easily achieved via physical casting on methods [51] or by incorporating a modifier into the carbon paste during fabrication for bulk modification. The composition of printing inks can be changed by addition of various substances such as metals, complexing agents, enzymes, polymers, etc [52, 53]. In the case of surface modification, deposition of films and polymers [54, 55] on the surface can introduce different properties to SPEs, making them suitable for diverse applications and can decrease detection limits [56]. The fabrication of in-house SPEs is also a popular and convenient alternative [57, 58], allowing the format of the electrodes to be adapted with respect to the requirements for the specific analyte.

Bibliography

[1] C. E. Banks and R. G. Compton, *Analyst (Cambridge, United Kingdom)* **131** (2006) 15.

[2] J. Pappis and S. L. Blum, *Journal of the American Ceramic Society* **44** (1961) 592.

[3] J. Pappis, S. Cvikevich, L. Hagen and N. Viola, *Metallurgical Society Conferences [Proceedings]* **18** (1963) 419.

[4] H. Guo, Y. Li, X. Chen, L. Nie and N. He, *Sensors* **5** (2005) 284.

[5] P. N. Bartlett, G. Denuault and M. F. B. Sousa, *Analyst (Cambridge, United Kingdom)* **125** (2000) 1135.

[6] O. D. Renedo and M. J. A. Martinez, *Analytica Chimica Acta* **589** (2007) 255.

[7] G. G. Wildgoose, P. Abiman and R. G. Compton, *Journal of Materials Chemistry* **19** (2009) 4875.

[8] W. Shen, Z. Li and Y. Liu, *Recent Patents on Chemical Engineering* **1** (2008) 27.

[9] H. Kahlert, *Journal of Solid State Electrochemistry* **12** (2008) 1255.

[10] G. G. Wildgoose, C. E. Banks, H. C. Leventis and R. G. Compton, *Microchimica Acta* **152** (2006) 187.

[11] J. C. Lennox and R. W. Murray, *Journal of Electroanalytical Chemistry and Interfacial Electrochemistry* **78** (1977) 395.

[12] R. L. McCreery, *Chemical Reviews (Washington, DC, United States)* **108** (2008) 2646.

[13] R. L. McCreery, *Electroanalytical Chemistry* **17** (1990) 221.

[14] S. Yajima, T. Satow and T. Hirai, *Journal of Nuclear Materials* **17** (1965) 116.

[15] C. E. Banks and R. G. Compton, *Analytical Sciences* **21** (2005) 1263.

[16] R. T. Kachoosangi, C. E. Banks, X. Ji and R. G. Compton, *Analytical Sciences* **23** (2007) 283.

[17] M. Lu and R. G. Compton, *Analyst (Cambridge, United Kingdom)* **139** (2014) 2397–2403.

[18] A. Sarapuu, K. Helstein, K. Vaik, D. J. Schiffrin and K. Tammeveski, *Electrochimica Acta* **55** (2010) 6376.

[19] F. Wantz, C. E. Banks and R. G. Compton, *Electroanalysis* **17** (2005) 655.

[20] C. E. Banks, T. J. Davies, G. G. Wildgoose and R. G. Compton, *Chemical Communications (Cambridge, United Kingdom)* **7** (2005) 829.

[21] R. L. McCreery, *Electroanalytical Chemistry* (1991).

[22] C. Kozlowski and P. M. A. Sherwood, *Journal of the Chemical Society, Faraday Transactions 1: Physical Chemistry in Condensed Phases* **80** (1984) 2099.

[23] R. I. R. Blyth, H. Buqa, F. P. Netzer, M. G. Ramsey, J. O. Besenhard, P. Golob and M. Winter, *Applied Surface Science* **167** (2000) 99.

[24] D. T. Fagan and T. Kuwana, *Analytical Chemistry* **61** (1989) 1017.

[25] M. A. Fryling, J. Zhao and R. L. McCreery, *Analytical Chemistry* **67** (1995) 967.

[26] S. S. Barton, G. L. Boulton and B. H. Harrison, *Carbon* **10** (1972) 395.

[27] T. Szabo, O. Berkesi, P. Forgo, K. Josepovits, Y. Sanakis, D. Petridis and I. Dekany, *Chemistry of Materials* **18** (2006) 2740–2749.

[28] R. N. Goyal, S. Chatterjee and A. R. S. Rana, *Talanta* **83** (2010) 149.

[29] K. R. Kneten and R. L. McCreery, *Analytical Chemistry* **64** (1992) 2518.

[30] T. Noda, M. Inagaki and S. Yamada, *Journal of Non-Crystalline Solids* **1** (1969) 285.

[31] S. F. Parker, S. Imberti, S. K. Callear and P. W. Albers, *Chemical Physics* **427** (2013) 44.

[32] M. Hokao, S. Hironaka, Y. Suda and Y. Yamamoto, *Wear* **237** (2000) 54.

[33] C. A. Martinez-Huitle, C. C. Jara, M. Cerro-Lopez and M. A. Quiroz, *Canadian Journal of Analytical Sciences and Spectroscopy* **54** (2009) 53.

[34] H. Gomathi and G. P. Rao, *Journal of Electroanalytical Chemistry and Interfacial Electrochemistry* **190** (1985) 85.

[35] S. Ergun and V. H. Tiensuu, *Acta Crystallographica* **12** (1959) 1050.

[36] G. M. Jenkins and K. Kawamura, *Nature (London, United Kingdom)* **231** (1971) 175.

[37] O. J. A. Schueller, S. T. Brittain, C. Marzolin and G. M. Whitesides, *Chemistry of Materials* **9** (1997) 1399.

[38] A. Burian and J. C. Dore, *Acta Physica Polonica, A* **98** (2000) 457.

[39] P. J. F. Harris, *Philosophical Magazine* **84** (2004) 3159.

[40] G. Juermann, D. J. Schiffrin and K. Tammeveski, *Electrochimica Acta* **53** (2007) 390.

[41] N. Y. Stozhko, N. A. Malakhova, M. V. Fyodorov and K. Z. Brainina, *Journal of Solid State Electrochemistry* **12** (2008) 1185.

[42] T. Nagaoka and T. Yoshino, *Analytical Chemistry* **58** (1986) 1037.

[43] S. B. Khoo and J. Zhu, *Analytica Chimica Acta* **373** (1998) 15.

[44] D. F. Untereker, J. C. Lennox, L. M. Wier, P. R. Moses and R. W. Murray, *Journal of Electroanalytical Chemistry and Interfacial Electrochemistry* **81** (1977) 309.

[45] M. Tudorache and C. Bala, *Analytical and Bioanalytical Chemistry* **388** (2007) 565.

[46] Z. Taleat, A. Khoshroo and M. Mazloum-Ardakani, *Microchimica Acta* **181** (2014) 865.

[47] M. Li, Y.-T. Li, D.-W. Li and Y.-T. Long, *Analytica Chimica Acta* **734** (2012) 31.

[48] J. P. Metters, R. O. Kadara and C. E. Banks, *Analyst (Cambridge, United Kingdom)* **136** (2011) 1067.

[49] R. O. Kadara, N. Jenkinson and C. E. Banks, *Electrochemistry Communications* **11** (2009) 1377.

[50] E. P. Randviir, D. A. C. Brownson, J. P. Metters, R. O. Kadara and C. E. Banks, *Physical Chemistry Chemical Physics* **16** (2014) 4598.

[51] O. Dominguez-Renedo, M. J. G. Gonzalez and M. J. Arcos-Martinez, *Sensors* **9** (2009) 219.

[52] J. H. Shim, J. S. Lee, G. S. Cha and H. Nam, *Bulletin of the Korean Chemical Society* **31** (2010) 1583.

[53] N. Thiyagarajan, J.-L. Chang, K. Senthilkumar and J.-M. Zen, *Electrochemistry Communications* **38** (2014) 86.

[54] K.-Y. Yao, H.-J. Chen and J.-M. Zen, *Taiwan Nongxue Huibao* **10** (2009) 364.

[55] F. Arduini, F. D. Nardo, A. Amine, L. Micheli, G. Palleschi and D. Moscone, *Electroanalysis* **24** (2012) 743.

[56] O. D. Renedo and M. J. A. Martinez, *Electrochemistry Communications* **9** (2007) 820.

[57] L. K. Fatt, K. Chuenrangsikul, P. Rijiravanich, W. Surareungchai and C. Y. Yean, *Chiang Mai Journal of Science* **39** (2012) 610.

[58] E. Kelso, J. McLean and M. F. Cardosi, *Electroanalysis* **12** (2000) 490.

Chapter 4

Experimental Methods

In this chapter, chemical reagents, apparatus and electrodes used within this thesis is detailed. Descriptions of experimental methods and apparatus specific to experiments will be described in relevant chapters.

4.1 Chemical Reagents

All chemicals were of analytical grade and were used as received without further purification. All solutions prepared with deionized water had resistivity not less than 18.2 MΩ cm at 298 K (Millipore, UHQ, Vivendi, UK). A list of chemicals and reagents is shown in Table 4.1.

4.2 Apparatus

4.2.1 Voltammetric Measurements

All voltammetric measurements were recorded using a μ-Autolab-II computer controlled potentiostat (Metrohm- Autolab BV) and operated by GPES software. A standard three-electrode configuration was used throughout consisting of a reference electrode, counter electrode and a working electrode. A typical cell assembly included a saturated calomel

reference electrode (SCE) (Hach Lange, UK), a platinum (Pt) mesh counter electrode and a carbon working electrode, as seen in Figure 4.1. Variations of the cell assembly were used and are detailed in their relevant chapters. In the case of the platinum mesh, flaming prior to the experiment ensured a clean set-up.

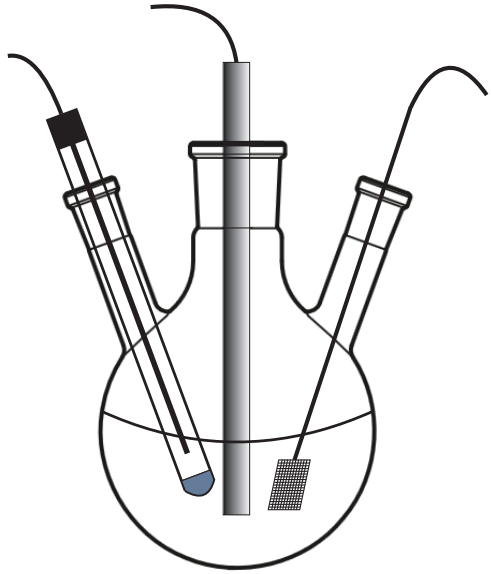


Figure 4.1: Schematic of a typical 3 electrode setup. From left to right, a reference electrode, working electrode and platinum mesh counter electrode

Where necessary and unless otherwise stated, a degassed system was established by purging solutions with inert argon or nitrogen gas (BOC, Guildford UK) prior to experiments for a minimum of 20 minutes in a seal tight environment to remove oxygen dissolved in the solutions. Since any traces of oxygen in the solution is relatively easy to reduce, its presence will contribute to the background voltammetric current and can decrease the electrochemical window of interest. It is necessary to ensure there is no reduction of oxygen as its presence can potentially alter the voltammetric behavior of solutes of interest that are reduced at more negative potentials than oxygen.

4.2.2 pH Measurements

All pH measurements were conducted using a pH213 Microprocessor pH meter (Hanna instruments, UK). Prior to the measurement of solutions, the pH meter was calibrated using Duracal buffers of pH 4.01 ± 0.01, pH 7.00 ± 0.01 and pH 10.01 ± 0.01 (Hamilton, CH). Using a 2 point calibration, the manufacturer's specifications state a working range of pH -2.0 to 16.0 at 298 K. pH measurements at elevated temperatures were made in accordance with the recommendations of the manufacturers [1].

The buffer solutions were prepared using HCl/KCl for the pH range 0.0 – 2.5, citric acid/sodium citrate for the pH range 2.5 – 5.0, monosodium phosphate/disodium phosphate for the pH range 5.0 – 9.0, sodium carbonate/bicarbonate for the pH range 9.0 – 11.0, and sodium hydroxide for the pH range 12.0 – 13.0. All solutions were made with supporting electrolyte of 100 mM KCl added to each solution. Measurement of the pH was carried out on each freshly made solution prior to experiments at their relevant temperature.

4.3 Working Electrodes

The majority of work described in the thesis used carbon based electrodes as the working electrode, in all but chapter 6. Platinum foil was the only other material used as an electrode in the work presented in this thesis. A platinum foil of thickness 12.5 μm was supplied by Goodfellow Cambridge Limited, Huntingdon and attached to a vibrating toothbrush (Oral-B, Pro-expert pulsar, Procter and Gamble, Surrey) for the easy fabrication of a vibrating electrode. Prior to use and between experiments, the platinum foil was polished using 1 μm diamond spray to ensure a clean surface.

4.3.1 Carbon Electrodes

Edge Plane Pyrolytic Graphite (EPPG) Electrodes

EPPG electrodes were made from pieces of highly ordered pyrolytic graphite (HOPG) (Le Carbone Ltd., Sussex, U. K.) of SP13 (ZYH) grade, and machined to discs 4.9 mm in diameter and 0.5 mm in length. An edge plane was achieved by orientating the disc face perpendicular to the graphite crystal surface; these were then set in custom made PTFE housing with an electrical connection made using a stainless steel core.

Renewal of the carbon surface was needed, however, before each set of standard additions to ensure a clean blank surface for the working electrode. This was simply achieved by polishing the electrode with 1.0, 0.3 and 0.05 μm alumina slurry on soft lapping pads, followed by sonication and thorough rinsing using deionised water in an ultrasonic bath to remove any adsorbed alumina particles.

Screen Printed Electrodes (SPE)

Screen printed electrodes (SPEs) (DropSens S. L. Llanera, Spain) used in the experiments consisted of a carbon working electrode, carbon counter electrode and silver reference electrode. The electrodes were all ink jet deposited onto a ceramic strip of 1 x 3 cm dimensions, with a 1 cm^2 area which encompassed the reference, counter and working electrodes; the working electrode was a disc of diameter 3.8 mm. Due to the disposable nature of screen printed electrodes, renewal of the surface is not needed.

Glassy Carbon (GC) Electrodes

The glassy carbon electrode, 3.0 mm in diameter, was purchased from CH instruments, Austin, TX, USA. The electrode was polished to a mirror finish by using an alumina slurry on soft lapping pads of decreasing grades, from 1.0 μm to 0.3 μm and finally 0.05 μm, followed by thorough sonication and rinsing using deionised water to remove any adhered alumina particles.

Bibliography

[1] HANNA instruments, *Instruction Manual : pH 213 Microprocessor-based pH Bench Meter*, Technical report, 2007.

Chemical Name	Formula/Abbreviation	Purity	Supplier
citric acid	$C_6H_8O_7$	99.7 %	BDH
deionised water	H_2O	18.2 MΩ cm	Millipore
hexaaammineruthenium (III) chloride	$[Ru(NH_3)_6]Cl_3$	98 %	Sigma Aldrich
hydrochloric acid	HCl	99.999 %	Fluka
iron (III) sulphate pentahydrate	$Fe_2(SO_4)_3.5H_2O$	97 %	Aldrich
nitric acid	HNO_3	≥99.999 %	Fluka
nitrogen (oxygen-free)	N_2	>99.998 %	BOC
potassium chloride	KCl	99 %	Sigma Aldrich
potassium hexahydroxyantimonate (V)	$KSb(OH)_6$		Fluka
potassium nitrate	KNO_3	99.5 %	Aldrich
potassium permanganate	$KMnO_4$	99.5 %	Aldrich
sodium bicarbonate	$NaHCO_3$	99.7 %	Sigma Aldrich
sodium carbonate, anhydrous	Na_2CO_3	99.9 %	BDH
sodium citrate	$Na_3C_6H_5O_7$	>99 %	Aldrich
sodium phosphate dibasic, anhydrous	Na_2HPO_4	99 %	Sigma
sodium phosphate monobasic dihydrate	$H_2NaPO_4.2H_2O$	>99 %	Sigma Aldrich
sulphuric acid	H_2SO_4	99.999 %	Aldrich
1 μm alumina powder			Buehler Ltd
0.3 μm alumina powder			Buehler Ltd
0.05 μm alumina powder			Buehler Ltd
1 μm diamond spray			Kemet Ltd, UK
araldite resin			Bostik, Stafford
silver epoxy adhesive			RS

Table 4.1: List of chemicals and reagents used throughout this thesis, including their purities and suppliers

Chapter 5

Determination of Sb(V) using Differential Pulse Anodic Stripping Voltammetry at an Unmodified Edge Plane Pyrolytic Graphite Electrode

In this chapter, antimony(V) determination at an unmodified edge plane pyrolytic graphite (EPPG) electrode is investigated using anodic stripping voltammetry (ASV). By depositing beyond the hydrogen wave, a sensitive method is established to determine pentavalent antimony at a carbon electrode in 0.25 M HCl. Interfering effects from hydrogen gas produced at the working electrode is often encountered during stripping voltammetry in acidic conditions, limiting the experiment to relatively high deposition potentials. By applying a simple conditioning procedure where the surface of the electrode is activated by depositing well below the hydrogen wave, hydrogen no longer blocks the electrode, allowing analysis of the stripping peaks. Here, using differential pulse anodic stripping voltammetry (DPASV), a bare EPPG electrode gave a detection limit of 5.8 $\pm$ 0.02 nM without the need for surface modification. This level is greatly within the EU limit for drinking water of 40 nM [1].

The work presented in this chapter has been published in *Electroanalysis*, 24, (2012), 1306-1310.

5.1 Introduction

Antimony is a naturally occurring element of significant toxicity; however its occurrence as a pollutant in the environment has become more prevalent [2] due to increasing numbers of industrial applications, including in glass making and ceramics, fabrication of fire retardants, and antimony-lead alloy formation for batteries [3, 4]. One main occurrence of antimony in water relates its use as a catalyst in the fabrication of PET bottles [5]. As such, antimony leaching occurs from bottles into juices and liquids, and fruit juices have been found to contain over 40 μg L^{-1} antimony [6], well above the European Union (EU) limit. Currently, the EU limits antimony concentration in drinking water to 5 μg L^{-1} [1], the lowest set limit, whilst the World Health Organisation (WHO) has a limit of 20 μg L^{-1} [7].

Antimony toxicity is still yet to be fully understood with respect to human health and the environment [8, 9]. At high concentrations, antimony has been seen to show toxic effects causing nausea, dizziness, vomiting and diarrhoea at large doses. Antimony has also been linked to possible carcinogenic effects and in extreme cases leads to kidney and liver damage [9–11].

Antimony predominantly exists in the trivalent and pentavalent species in the environment. Although Sb(III) is understood to be more toxic than Sb(V) [10], both forms exist in environmental samples, with antimony having a thermodynamic preference for the +V state in oxygenated waters [12, 13]. As the antimony limit guidelines are considered with respect to the total antimony concentration, it is important to analytically determine the concentration of both species.

Antimony(V) detection has been a very under-explored area electrochemically. Al-

though many spectroscopic techniques are available for antimony determination [14–17], electrochemical methods are vastly preferred for in-situ analysis owing to its simple, fast, low cost, portable and sensitive analytical procedure. The electroanalytical technique most commonly used for trace metal analysis is anodic stripping voltammetry (ASV) whereby very low limits of detection can be achieved. ASV involves cathodically pre-concentrating the element in its metallic form after reduction onto the electrode surface, followed by a stripping step whereby the metal is oxidised back into solution. Previous research has been focused on the detection of the more toxic Sb(III) form due to the perceived electroinactivity of the pentavalent species [18, 19].

As Sb(V) is only electroactive in certain conditions; highly acidic conditions are needed for its electrochemical reduction [20] however, this is not generally preferred for routine work. Prior to research based on depositing beyond the hydrogen wave [21], many previous authors reported the chemical reduction from Sb(V) to Sb(III) using reducing agents such as L-cysteine [22, 23] and sulphur dioxide [24] prior to electroanlysis. In the late 1980s, however, Jagner et al. [25] reported that electrolytic deposition at special conditions is feasible for the direct reduction of Sb(V) to Sb(0). This account used a Au-fibre working electrode and the crucial parameter of the successful reduction of Sb(V) involved an extremely concentrated supporting electrolyte (4 M HCl).

There has been little research on the trace determination of antimony(V). Here, the first account of detecting Sb in its pentavalent form on a carbon electrode is presented. To date, there has only been one other account of Sb(V) determination on an unmodified electrode by Santos et al. [26] where they have reported flow analysis on a tubular gold electrode. Otherwise, other authors have required complexing agents such as catechol and pyrogallol at hanging mercury drop electrodes (HMDE) [27]. Sensitive detection limits

have been reported in the nM region, however, due to the toxic nature of mercury, its use in analytical methodology is slowly being phased out. Carbon based electrodes can be seen to be a far more favourable and environmentally friendlier alternative.

The majority of work focused on Sb(V) detection has been performed on mercury electrodes, such as the hanging mercury drop electrode (HMDE) [28]. However, following more stringent conditions set by environmental government bodies and the toxic nature of mercury, research has been seen to migrate towards more environmentally friendly electroanalytical methods. Different complexing and chelating agents, such as catechol [27, 29], pyrogallol [30, 31] and chloranilic acid [32] have been reported at a hanging mercury drop electrode (HMDE) to give sensitive limits of detection for Sb(V).

Technique	Electrode	Modifier/ complexing agent	Sb(V) *LOD* (M)	Year	Reference
Mercury electrodes					
DP ASV	HMDE	–	5.00×10^{-08}	2008	[28]
DP ASV	HMDE	–	9.00×10^{-11}	2002	[33]
LS AdCSV	HMDE	Catechol	2.00×10^{-10}	1987	[27]
DP AdCSV	HMDE	Catechol	2.00×10^{-07}	1982	[29]
DP AdCSV	HMDE	Chloranilic acid	4.60×10^{-09}	1996	[32]
DP AdCSV	HMDE	Pyrogallol red	4.87×10^{-08}	2006	[30]
DP AdCSV	HMDE	Pyrogallol	8.20×10^{-08}	2009	[34]
DP AdCSV	HMDE	Pyrogallol	9.48×10^{-09}	2007	[31]
Carbon electrodes					
SQW CSV	EPPG	Bismuth	1.64×10^{-11}	2009	[35]
SWV ASV	EPPG	Bismuth	4.10×10^{-11}	2011	[36]
PSA	MW-CNPE	–	5.10×10^{-08}	2009	[23]
Gold electrodes					
PSA	Gold tube	–	2.60×10^{-09}	2007	[26]
DP ASV	Gold microwire	–	5.00×10^{-12}	2011	[21]
FC-CS	Gold fibre	–	2.54×10^{-09}	1987	[25]

Table 5.1: Electrochemical determination of Sb(V) using different electrodes. DP: differential pulse, ASV: anodic stripping voltammetry, CSV: cathodic stripping voltammetry, LS: linear sweep, MW-CNPE: multiwall carbon nanotube paste plectrode, PSA: potentiometric stripping analysis, SQW: squarewave, AdCSV: adsorptive cathodic stripping voltammetry, FC-CS: flow constant-current stripping

Table 5.1, adapted from reference [37] presents the literature papers regarding electro-

analytical determination of Sb(V) with respect to the electrode used and modifications where applicable. This is however not preferable as a means for a cheap, simple and rapid system due to the need for modification. Recently, Salaun et al. [21] reported a new procedure for trace antimony(V) detection involving deposition beyond the hydrogen wave. Salaun et al reported the most sensitive method for Sb(V) detection, with a detection limit of 5 pM after 60 s accumulation time on a vibrating gold microwire. Noskova et al. [38] have also used a similar method of working beyond the H_2 wave in regards to trace metal determination to obtain a 26 nM limit of detection with arsenic.

To further explore the potential of depositing beyond the hydrogen wave, an EPPG electrode was used as a substrate for antimony determination in this work. Carbon electrodes have been previously explored as possible analytical tools for trace metal detection [39, 40] and in this chapter, capabilities in this area is probed. Here, an electroanalytical method for Sb(V) detection using *unmodified* EPPG electrodes is described. This is, as far as we are aware, the first use of unmodified carbon as a low cost, simple and sensitive means for detecting antimony in its pentavalent form to a limit greatly within the 5 μg L^{-1} EU limit for antimony in drinking water.

5.2 Experimental

5.2.1 Apparatus and Reagents

A standard three-electrode configuration was used throughout; this consisted of a saturated calomel reference electrode (SCE), a platinum (Pt) mesh counter electrode and an edge plane pyrolytic graphite (EPPG) working electrode. A standard magnetic stirrer was used together within the electrochemical setup.

A 1.0 mM stock solution of Sb(V) was prepared by dissolving the appropriate quantity of $KSb(OH)_6$ in water. More diluted working solutions of Sb(V) were freshly prepared daily with deionized water to suitable concentrations. Pure HCl acid was required as standard analytical grade acid proved to contain trace contaminants which caused interferences.

5.2.2 Experimental Procedure

A 10 mL volume of 0.25 M HCl (pH 0.15) was transferred into an electrochemical cell and a degassed system was set up to remove the dissolved oxygen in solution. After assembly of the standard three electrode set up, accurate additions of Sb(V) from stock solution were made to the deoxygenated cell. The stirrer was connected and deposition was applied at a -1.80 V potential under constant stirring for 120 s. After the elapsed time, the stirrer was stopped and a 5 s equilibrium time was utilised to allow the solution to settle before making an anodic sweep with differential pulse voltammetry with scan rate 40 mV s^{-1}. Deposited Sb(V) could subsequently be stripped off by sweeping positively from -0.40 V to 0.20 V vs. SCE. Consecutive additions of Sb(V) were pipetted into the solution with no need to clean the surface of the electrode electrochemically or otherwise within each set of additions.

Renewal of the carbon surface was needed, however, before each set of standard additions to ensure a clean blank surface for the working electrode. The electrode was polished thoroughly as described in the Experimental Methods chapter. Due to the sensitive trace nature of the experiment, stringent conditions were required where all glassware were cleaned such that no contaminants were present. This was performed by soaking glassware in green acid (made by dissolving potassium permanganate in concentrated

sulphuric acid) for a minimum of 20 minutes and then thoroughly rinsing and sonicating with deionised water before use. The platinum mesh was flamed before the experiment to ensure a clean set-up.

5.3 Results and Discussions

A range of parameters were explored to optimise the differential pulse voltammetric procedure prior to the experiments. The deposition potential (E_{dep}) was varied from -0.5 V to -2.5 V and optimal peak signal corresponding to antimony stripping was found at (E_{dep} = -1.8 V giving the best stripping peak in terms of shape and size, as shown in Figure 5.1.

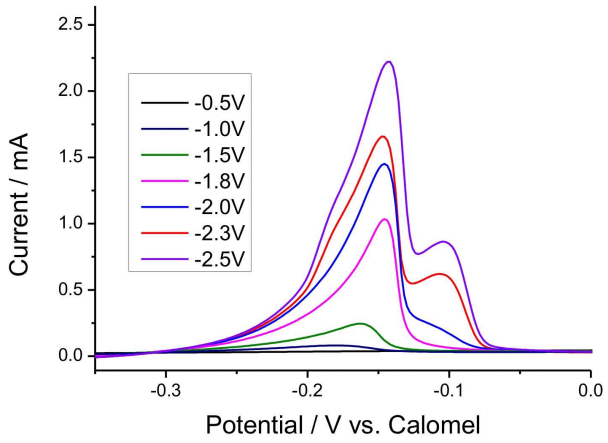


Figure 5.1: Variation of optimal peak signal at (E_{dep}) = -1.8 V with deposition potential (E_{dep}) from -0.5 V to -2.5 V. Experimental conditions: scan rate = 40 mV s^{-1}, equilibration time = 5 s, step potential = 4 mV, modulation amplitude = 40 mV, deposition time = 120 s, degassed 0.25 M HCl solution

Deposition time was also investigated between 0 s to 600 s. Though a longer accumulation time gave a larger peak due to more antimony being deposited on the surface, a 120 s deposition was chosen as the best compromise between experimental time and

peak size. Scans in normal linear sweep voltammetry (LSV) gave a signal for antimony, however more sensitive peaks were given in differential pulse. In addition, scan rates and modulation amplitudes were varied to optimise the Sb(V) stripping peaks. Our optimised parameters were: scan rate = 40 mV s^{-1}, deposition potential, E_{dep} = -1.8 V for 120 s, equilibration time = 5 s, step potential = 4 mV, modulation amplitude = 40 mV.

The surface of the EPPG did not need electrochemical activation or pre-treatment before use. After thorough polishing, as noted previously, the working electrode was held in the solution before a deposition potential was imposed upon it. It was seen during the deposition step that protons in the solution were reduced to hydrogen on the surface of the working and Pt counter electrode. Rapid evolution of hydrogen meant that no build up of the gas bubbles were seen on the electrode as it constantly streamed off the surface. Deposition could occur appropriately without the hydrogen bubbles obstructing the active surface. On the rare occasion bubbles were seen on the working electrode surface, tapping the EPPG to clear the bubbles before the sweep ensured a good voltammetric signal in the stripping scan.

Aliquots of Sb(V) were consecutively added to the electrochemical cell, and a stripping peak was produced after each addition. A defined peak was seen upon the very first addition with very high sensitivity. Figure 5.2 depicts a series of Sb(V) additions over a concentration range 10 nM to 100 nM. An inset showing the linear progression of the peak height and peak area against increasing concentration is also given. The calibration plots show high linearity with R^2 value of 0.996 and 0.993 for height and area. The limit of detection (LoD), calculated using 3 x standard deviation (3σ) divided by the slope [41], gave values of 5.8 ± 0.02 nM and 8.1 ± 0.03 nM. The plots show, however, after extrapolation there is an apparent intercept at 0.15 mA. Further experiments were thus

carried out using lower Sb(V) concentrations, but proved to have poor reproducibility.

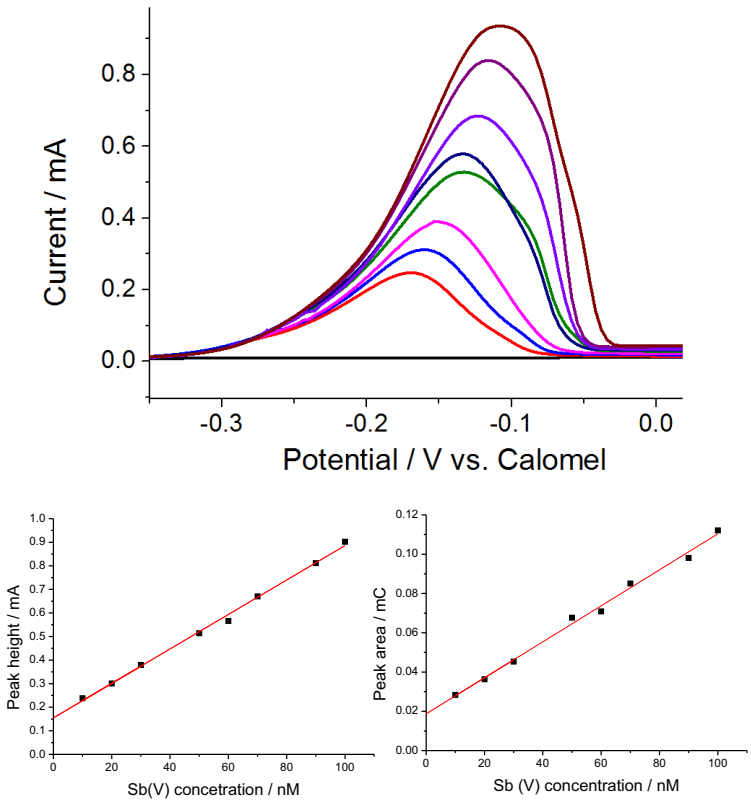


Figure 5.2: Series of Sb(V) additions over a concentration range from 10 nM to 100 nM. Insets show the linear progression of the peak height and peak area against increasing concentration

A pioneering paper by Salaun et al. [21] reported a method for sensitive trace metal analysis by working beyond the hydrogen wave on a vibrating gold microelectrode. We have applied this new methodology on a carbon electrode for the detection of Sb(V). Since solvent breakdown of 0.25 M HCl occurs at *ca.* -0.7 V, a deposition potential of -1.8 V causes hydrogen evolution to occur at the surface of the EPPG during the accumulation step. Protons from the acidic media diffuses to the electroactive surface, accepts electrons to form H atoms, and then recombination of H atoms with each other or the acid forms the evolved H_2 gas. It is likely that the very negative reduction potential ensures favourable thermodynamics and fast kinetics for Sb deposition. Salaun et al.

[21] have speculated that nascent H atoms on the surface of the electrode may catalyse the stripping of Sb(V) which enhances the peak signal. This proposed mechanism may operate since the experimental data from this work gives very high sensitivity even at low Sb(V) concentration, resulting in peaks with a large peak height. The benefits of electrodes for electroanalysis of trace metal analysis have been noted elsewhere [42].

5.4 Conclusions

Determination of Sb(V) on an EPPG electrode using anodic stripping voltammetry by depositing beyond the hydrogen wave is shown in this chapter. By taking potentials far more negative than the hydrogen wave, deposition and stripping of Sb(V) can be seen without the need for harsh acidic conditions. Sb(V) electrolysis had been explored previously by means of chelating and complexing agents with mercury electrodes, gold electrodes and carbon electrodes. However, here the first account for Sb(V) determination using an unmodified carbon based EPPG electrode is reported, suggesting a simple, low cost and sensitive method for trace analysis of this heavy metal to well within the EU limit for antimony in drinking water.

With a view for a method to aid in trace analysis of analytes, chapter 6 describes the fabrication and sensitivity enhancement of a vibrating electrode.

Bibliography

[1] Council of the European Union, *Council directive 98/83/ec*, Technical report, 1998.

[2] W. A. Maher, *Environmental Chemistry* **6** (2009) 93.

[3] J. F. J. Carlin, *U.s. geological survey, mineral commodity summaries, january 2011 - antimony*, Technical report, U.S. Geological Survey, 2011.

[4] C. A. Johnson, H. Moench, P. Wersin, P. Kugler and C. Wenger, *Journal of environmental quality* **34** (2005) 248.

[5] W. Shotyk and M. Krachler, *Environmental science & technology* **41** (2007) 1560.

[6] W. Shotyk, M. Krachler and B. Chen, *Journal of Environmental Monitoring* **8** (2006) 288.

[7] WHO, *Antimony in drinking water. background document for preparation of who guidelines for drinking water quality*, Technical report, World Health Organisation, 2003.

[8] M. Filella, P. A. Williams and N. Belzile, *Environmental Chemistry* **6** (2009) 95.

[9] C. G. Elinder and L. Friberg, *Antimony*, Handbook on the toxicology of metals (Amsterdam ; Boston : Academic Press, Amsterdam ; Boston, 2007).

[10] K. A. Winship, *Adverse Drug Reactions and Acute Poisoning Reviews* **6** (1987) 67.

[11] J. B. Adams, C. E. Holloway, F. George and D. Quig, *Biological trace element research* **110** (2006) 193.

[12] M. Filella, N. Belzile and Y.-W. Chen, *Earth-Science Reviews* **57** (2002) 125.

[13] M. Filella, N. Belzile and Y.-W. Chen, *Earth-Science Reviews* **59** (2002) 265.

[14] M. J. Nash, J. E. Maskall and S. J. Hill, *Journal of Environmental Monitoring* **2** (2000) 97.

[15] R. Miravet, E. Hernandez-Nataren, A. Sahuquillo, R. Rubio and J. F. Lopez-Sanchez, *TrAC, Trends in Analytical Chemistry* **29** (2010) 28.

[16] J. Lintschinger, O. Schramel and A. Kettrup, *Fresenius' journal of analytical chemistry* **361** (1998) 96.

[17] M. O. Andreae, J. F. Asmode, P. Foster and L. V. 't dack, *Analytical Chemistry* **53** (1981) 1766.

[18] A. Salimi, A. Korani, R. Hallaj and R. Khoshnavazi, *Electroanalysis* **20** (2008) 2509.

[19] O. D. Renedo and M. J. A. Martinez, *Electrochemistry Communications* **9** (2007) 820.

[20] T. R. Gilbert and D. N. Hume, *Analytica Chimica Acta* **65** (1973) 451.

[21] P. Salaun, K. Gibbon-Walsh and C. M. G. van den Berg, *Analytical Chemistry* **83** (2011) 3848.

[22] O. D. Renedo and M. J. A. Martinez, *Analytica Chimica Acta* **589** (2007) 255.

[23] V. S. Santos, W. de Jesus Rodrigues Santos, L. T. Kubota and C. R. T. Tarley, *Journal of pharmaceutical and biomedical analysis* **50** (2009) 151.

[24] C. Brihaye, G. Gillain and G. Duyckaerts, *Analytica Chimica Acta* **148** (1983) 51.

[25] H. Huang, D. Jagner and L. Renman, *Analytica Chimica Acta* **202** (1987) 123.

[26] J. R. Santos, J. L. F. C. Lima, M. B. Quinaz, J. A. Rodriguez and E. Barrado, *Electroanalysis* **19** (2007) 723.

[27] G. Capodaglio, C. M. G. V. den Berg and G. Scarponi, *Journal of Electroanalytical Chemistry and Interfacial Electrochemistry* **235** (1987) 275.

[28] J. Opydo, *Proceedings of ECOpole* **2** (2008) 369.

[29] C. McCrory-Joy and J. M. Rosamilia, *Analytica Chimica Acta* **142** (1982) 231.

[30] M. J. G. Gonzalez, O. D. Renedo and M. J. A. Martinez, *Electroanalysis* **18** (2006) 1159.

[31] M. J. G. Gonzalez, O. D. Renedo and M. J. A. Martinez, *Talanta* **71** (2007) 691.

[32] W. Wagner, S. Sander and G. Henze, *Fresenius' Journal of Analytical Chemistry* **354** (1996) 11.

[33] F. Quentel and M. Filella, *Analytica Chimica Acta* **452** (2002) 237.

[34] K. Zarei, M. Atabati and M. Karami, *Analytica Chimica Acta* **649** (2009) 62.

[35] P. Zong and Y. Nagaosa, *Microchimica Acta* **166** (2009) 139.

[36] P. Zong, J. Long and Y. Nagaosa, *International journal of environmental analytical chemistry* **91** (2011) 421.

[37] K. E. Toghill, M. Lu and R. G. Compton, *International Journal of Electrochemical Science* **6** (2011) 3057.

[38] G. N. Noskova, E. A. Zakharova, V. I. Chernov, A. V. Zaichko, E. E. Elesova and A. S. Kabakaev, *Analytical Methods* **3** (2011) 1130.

[39] M. Lu, K. E. Toghill, M. A. Phillips and R. G. Compton, *International Journal of Environmental Analytical Chemistry* **93** (2011) 213.

[40] S. E. W. Jones and R. G. Compton, *Current Analytical Chemistry* **4** (2008) 170.

[41] C. Brett and A. M. Oliveira-Brett, *Electroanalysis* (Oxford University Press, Oxford, 1998).

[42] C. E. Banks and R. G. Compton, *Analytical Sciences* **21** (2005) 1263.

Chapter 6

Easy Fabrication of a Vibrating Foil Electrode

Given the sensitive nature of detecting trace analytes using electrochemistry, in this chapter, a simple, rapid and cost effective fabrication of a vibrating platinum foil electrode is presented whereby significant mass transport enhancement can be seen and applied for electroanalytical work. The vibrating and stationary nature of the platinum foil electrode was characterised by cyclic voltammetry using the $Ru(NH_3)_6$ $^{2+/3+}$ redox system and a four-fold enhancement in sensitivity could be reproducibly seen. Randles - Ševčik analysis gave a diffusion coefficient, D value, of 9.4 x 10^{-6} cm^2 s^{-1} for $[Ru(NH_3)_6]^{3+}$.

The work presented in this chapter has been published in *Analytical Methods*, 4, (2012), 1932-1934.

6.1 Introduction

Electroanalytical studies using vibrating electrodes are of great interest due to their increased flux to the electrode surface [1] giving highly sensitive results. In many circumstances, vibration of the electrode is preferred over forced convection of the analyte solution (by ultrasound, hydrodynamic electrodes, etc. [2, 3]) for energy efficiency and simplicity. Such vibration offers great advantages to electrochemical processes controlled

by mass transfer by increasing the flux of active species to the electrode surface [4, 5].

Vibration techniques have been widely applied in the past; a literature review on vibrating wire electrodes by Pratt and Johnson [6] illustrates many of these cases. One of the first authors to detail vibration in electrochemistry was Harris and Lindsey [7] in 1948 where a vibrating platinum microelectrode was used. Although no experimental results were given, it was noted that reproducible results could be obtained from this method compared to the conventional hanging mercury drop electrode (HMDE) of the time. Further research by Lindsey [8] using a commercial massage vibrator as the vibrating apparatus highlighted the effect of a thinner diffusion layer at a vibrating surface compared to a stationary electrode; the result of this being a larger diffusion current. Following from this, many means of vibration for electrodes have been carried out ranging from vibrating stirrers [9] to speakers [10]. Many authors have also opted to custom design their own vibrating electrodes such as Dirscherl and Otto [11], leading to various patents on vibrating electrode instruments [8, 12]. Recently, a new voltammetric workstation (Tomanalyt LLC, Tomsk, Russia) has been designed whereby the electrodes can be vibrated within the electrochemical cell [13, 14].

In this chapter, an extremely cost effective and simple design for a vibrating electrode is presented, involving easy modification of a cheap and commercially available toothbrush and platinum foil. Fabrication of the electrode is very rapid, with scope for using different electrode materials. Cyclic voltammograms of the electrode in its stationary and vibrating states have shown a very reproducible four-fold enhancement in limiting current values that can be further applied to sensitive electroanalytical studies. As well as this, voltammetry changes from transient to steady state allowing easy analysis.

6.2 Experimental

6.2.1 Apparatus and Reagents

The cell assembly was made up of a saturated calomel reference electrode (SCE), a platinum (Pt) mesh counter electrode and a Pt film working electrode. The working electrode was fabricated using strips of platinum foil of thickness 12.5 μm supplied by Goodfellow Cambridge Limited, Huntingdon and attached to a vibrating toothbrush (Oral-B, Pro-expert pulsar, Procter and Gamble, Surrey).

A 1.0 mM solution of ruthenium(III) hexamine chloride and 100 mM potassium chloride was prepared by dissolving the appropriate quantity of $[Ru(NH_3)_6]Cl_3$ and KCl in deionised water. The platinum foil was polished using 1 μm diamond spray prior to use.

6.2.2 Experimental Procedure

Fabrication of the vibrating electrode was simply achieved by attaching thin strips of platinum foil onto a vibrating head of a toothbrush. A toothbrush was initially prepared by removing the bristles on the head. Precise measurements of the platinum foil dimensions were then noted, cut to size and carefully attached to the toothbrush. Silver epoxy was applied at the end of the platinum foil to make a connection between the film and the connecting wires. Araldite epoxy resin was applied to secure the connections before use. All connections were allowed to fully dry before use.

The platinum foil was carefully polished using diamond polish spray and a cotton bud before being thoroughly rinsed with deionised Millipore water. In order to achieve reproducible results, it was necessary to polish the electrode thoroughly and to maintain the surface conditions of the electrode as uniform as possible. A solution of 1.0 mM

ruthenium hexamine chloride with 100 mM KCl supporting electrolyte was fully degassed with argon for 20 minutes before the aforementioned three-electrode configuration was set up. The toothbrush head was completely submerged in the solution such that the platinum film was held perpendicularly within the matrix.

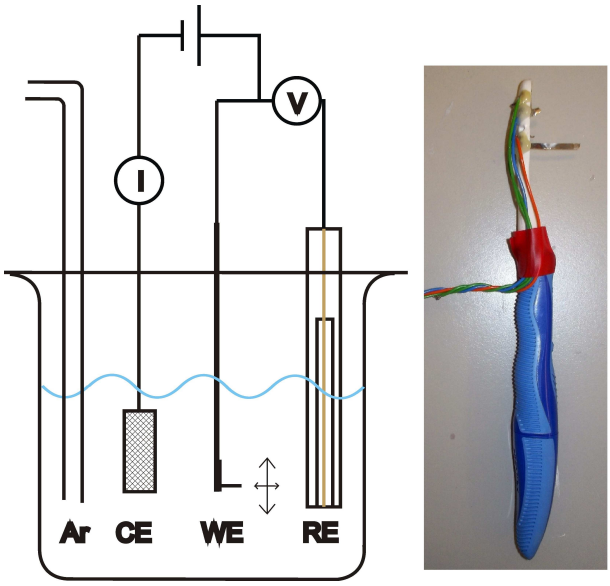


Figure 6.1: Schematic diagram of the 3-electrode setup. From left to right: argon for degassing the solution, platinum mesh counter electrode, vibrating platinum foil working electrode and a SCE reference. Inset shows a photograph of the vibrating foil electrode

A schematic diagram of the setup is shown in Figure 6.1, with a photograph of the electrode in the inset. The potential window of the platinum foil was first identified, then cyclic voltammograms were performed from +0.1 V to -0.5 V with scan rate 100 mV s^{-1}. The initial dimension of the platinum foil was 10.0 mm x 1.0 mm with thickness 12.5 μm. First, a cyclic voltammogram was taken with the electrode stationary, and then this was repeated with the electrode vibrating. After each set, the electrode was removed from the solution and decreased in length. Whilst the width of the platinum film did not change, a series of 10 lengths were taken between 10.0 mm and 1.0 mm. The

solution was purged with argon gas for 10 minutes between each set of vibrating/stationary film lengths to ensure a de-oxygenated environment to reduce the effect of dissolved oxygen in ruthenium hexamine which would interfere with the redox couple. All the experiments were conducted at 298 K. The toothbrush vibrates via a rotating motor head, causing motion of the platinum foil in both parallel and perpendicular directions. The vibrating frequency of the toothbrush was determined using a microphone attached to an oscilloscope, and a frequency of 50 ± 5 Hz was calculated.

6.3 Results and Discussions

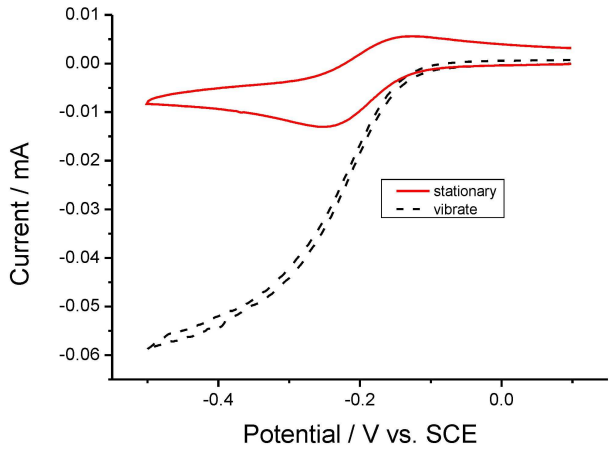


Figure 6.2: Overlay of the CV scans for the electrode whilst vibrating and stationary, for a 1 mm x 1 mm platinum foil in 1 mM $Ru(NH_3)_6$ $^{3+}$ with 100 mM KCl

A series of different platinum film lengths were investigated and their cyclic voltammograms taken whilst stationary and vibrating in a de-aerated solution of 1.0 mM ruthenium hexamine with 100 mM KCl. First, a cyclic voltammogram of the platinum length was taken in its stationary state followed by a scan with the electrode vibrating. This procedure was repeated for the different lengths of foil, with thorough degassing of the solution,

and polishing of the electrode between each set. An overlay of the two scans for a 1 mm x 1 mm piece of platinum foil is shown in Figure 6.2. A four-fold enhancement was calculated from $I_{vib}/I_{stationary}$, where the limiting current and peak current were taken respectively. Whilst stationary, the voltammogram of the electrode showed characteristic peaks corresponding to a reversible, diffusion-controlled electrode process whereas the vibrating electrode gave a sigmoidal curve with a larger limiting current.

The $Ru(NH_3)_6$ $^{2+/3+}$ redox couple is commonly used in electrochemical studies due to its chemical and electrochemical reversibility [15]. This system was chosen due to its fast electron transfer kinetics and the consequent ability to monitor rapid variations in mass transfer rates. The one electron process that occurs is: $[Ru(NH_3)_6]^{3+} + e^- \rightleftharpoons [Ru(NH_3)_6]^{2+}$.

By looking at the equation:

$$I_c = -nFAk_{red}[O]_o \tag{6.1}$$

It can be seen for a fixed electrode area, A, the reaction is controlled by the rate constant, k_{red} and the surface concentration of the reaction $[O]_o$. For systems involving fast electron transfer kinetics, such as the $Ru(NH_3)_6$ $^{2+/3+}$ redox couple, where any reactant close to the interface is immediately converted into products, it can be seen that current will be controlled by the amount of fresh reactant reaching the electrode surface from the bulk solution. As such, the rate of mass transport is important in determining the peak and limiting currents. The three forms of mass transport which can influence an electrolysis reaction are: diffusion, convection and migration.

The effects of migration in this reaction has been minimised by the presence of 100 mM

KCl supporting electrolyte. As such it can be concluded that the rate of mass transfer at the surface of the stationary electrode is controlled by diffusion through a natural convection boundary layer created by the density difference between the reactants and products at the surface of the electrode.

When the electrode is vibrated, convection plays a part in the mass transport of reactants to the electrode surface and the average current density was found to increase. Agitating the solution around the foil electrode through vibrating the electrode constantly renews the fresh reactants reaching the electrode surface, and thus reduces the diffusion layer thickness and increases mass transport. Evidence of this can be seen in Figure 6.2 as the limiting current whilst the electrode is vibrating is enhanced compared to the peak current seen whilst the electrode is stationary. There is an evident enhancement in the rate of mass transport through vibrating the foil electrode. In the stationary electrode diffusion is the rate-determining step, whereas by vibrating the electrode, convection occurs which intensifies mass transfer at the solid – liquid interface.

The limiting current for the vibrating electrode is seen to plateau as the current reaches a steady state, representing the maximum amount of fresh material transported to the electrode surface by convection. The steady state limiting current, where current is limited only by mass transport, is very useful as it can be used to give insight into the electrode kinetics.

The diffusion coefficient, D, for the set of experiments with the platinum foil stationary was calculated by plotting the peak height against the active surface area. Straight line plots for the stationary and vibrating electrodes can be seen from Figure 6.3. It was seen that the extent of enhancement of the vibrating electrode seemed to the the most pronounced with decreasing electrode lengths.

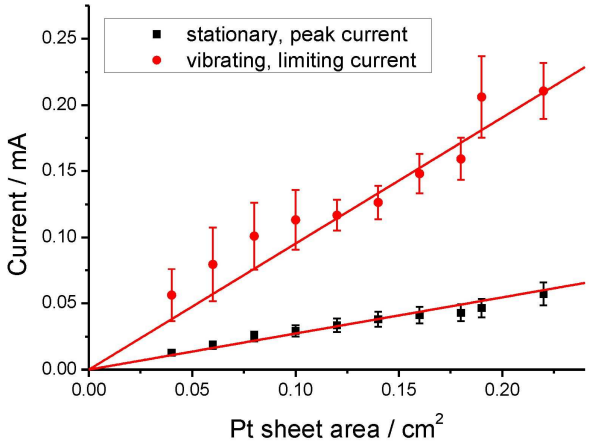


Figure 6.3: Peak height vs. active surface area for the vibrating and stationary electrodes, from which D can be calculated

The enhancement factor, $I_{vib}/I_{stationary}$, varied from 3.68 for the foil at length 10 mm, to a factor of 4.43 for the foil at its shortest length of 1 mm. It can be assumed that at longer lengths, the vibration of the foil is less pronounced towards the end of the electrode, whereas at short lengths the full effects of the vibration is felt across the electrode, resulting in increased mass transfer. From the slope of the stationary electrode, the Randles - Ševčik equation can be applied.

$$I_p = -0.446nFA[C]_{bulk}\sqrt{\frac{nF\nu D}{RT}} \tag{6.2}$$

where I_p - peak current, n – number of electrons transferred during redox, F - Faraday constant, A - electrode area, $[C]$ - concentration, v - scan rate, D - diffusion coefficient, R - gas constant, T - temperature. By substituting in all the required values and at T = 298 K, a D value of 9.4 ± 0.5 x 10^{-6} cm^2 s^{-1} was calculated for $[Ru(NH_3)_6]^{3+}$; this is comparable to the D value for ruthenium hexamine of 8.4 ± 0.03 x 10^{-6} cm^2 s^{-1} found by Wang et al. [15]. Mass transport corrected Tafel analysis for the vibrating electrodes was

linear with slopes consistent with the quasi-reversible wave observed. Figure 6.4 shows a mass transport corrected Tafel plot for the 1mm x 1mm vibrating electrode. A very linear Tafel plot is seen, with the gradient calculated to be 0.702 ± 0.01.

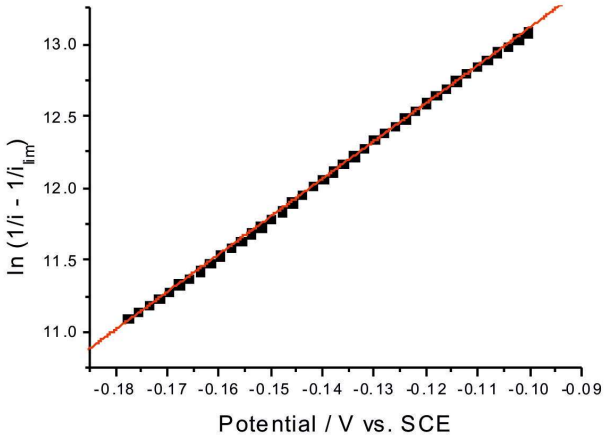


Figure 6.4: Mass transport corrected Tafel plot for 1 mm x 1mm vibrating electrode

As the lengths of the platinum foil decreased, a corresponding decrease in the peak height was seen in the stationary cyclic voltammograms. Similarly, the vibrating equivalents of the platinum lengths gave analogous behaviour and the limiting current decreased with the length of the foil, as shown in Figure 6.5.

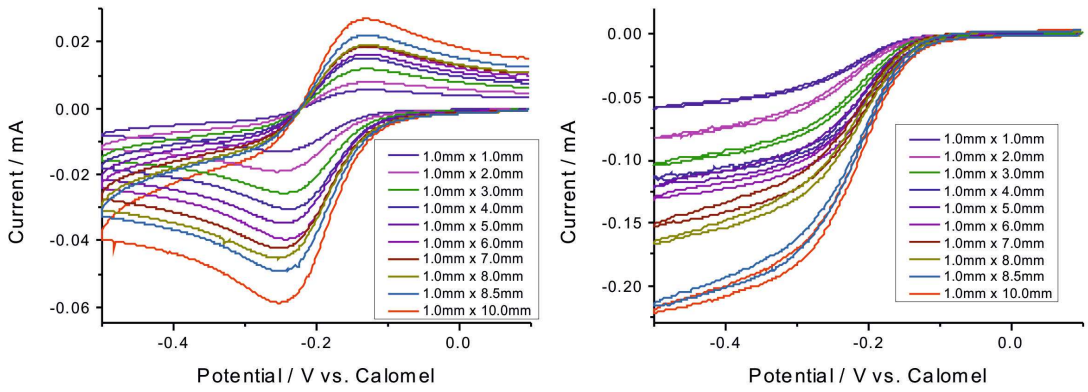


Figure 6.5: LHS: Cyclic voltammograms for stationary foil electrode, with decreasing lengths. RHS: Cyclic voltammograms for vibrating electrode, with decreasing lengths

6.4 Conclusions

It has been successfully shown that an easy and cheap fabrication of a vibrating electrode can be achieved using a toothbrush and platinum foil. A four-fold current enhancement was seen which can be applied to sensitive electroanalytical work. As well as this, a change in voltammetry shows a conversion from a transient to a steady state, allowing simple analysis. By vibrating the electrode, convection becomes the dominant mass transport process over diffusion in a stationary electrode and this results in a thinner diffusion layer which leads to enhanced mass transport to the electrode surface. Though rotating disk electrodes have been traditionally used to incorporate convection, the vibrating foil electrode presented here gives an alternative fabrication method whereby the electrode can move in both parallel and perpendicular directions. In the interest of detecting trace analytes, this method can be easily applied and incorporated into a setup.

Aside from detecting toxic heavy metal ions in the environment, iron is also of great interest and widely studied. A review of iron determination using electrochemical methods is covered in the next chapter to highlight some important methods of detection.

Bibliography

[1] R. G. Compton and C. E. Banks, *Understanding Voltammetry* (Imperial College Press, London, 2011), 2nd ed. edition.

[2] A. D. Clegg, N. V. Rees, O. V. Klymenko, B. A. Coles and R. G. Compton, *ChemPhysChem* **5** (2004) 1234.

[3] M. Thompson, O. V. Klymenko and R. G. Compton, *Journal of Electroanalytical Chemistry* **575** (2005) 329.

[4] A. H. Fakeeha, F. A. A. Aleem and A. I. Inamah, *Proceedings - Electrochemical Society* **97** (1998) 17.

[5] H. Gomaa, A. M. A. Taweel and J. Landau, *Chemical Engineering Journal (Amsterdam, Netherlands)* **97** (2004) 141.

[6] K. W. P. Jr. and D. C. Johnson, *Electrochimica Acta* **27** (1982) 1013.

[7] E. D. Harris and A. J. Lindsey, *Nature* **162** (1948) 413.

[8] A. J. Lindsey, *Journal of Physical Chemistry* **56** (1952) 439.

[9] S. Rosenberg, J. C. Perrone and P. L. Kirk, *Analytical Chemistry* **22** (1950) 1186.

[10] J. J. Podesta, G. F. Paus and A. J. Arvia, *Electrochimica Acta* **19** (1974) 583.

[11] W. Dirscherl and K. Otto, *Chemie Ingenieur Technik* **26** (1954) 321.

[12] D. A. Petrov, I. P. Shentov and V. V. Genevski, *Method and installation for electrolysis of nonferrous metals.*, 1976.

[13] G. N. Noskova, E. A. Zakharova, V. I. Chernov, A. V. Zaichko, E. E. Elesova and A. S. Kabakaev, *Analytical Methods* **3** (2011) 1130.

[14] *www.tomanalyt.ru*.

[15] Y. Wang, J. G. Limon-Petersen and R. G. Compton, *Journal of Electroanalytical Chemistry* **652** (2011) 13.

Chapter 7

Determination of Iron: Electrochemical Methods

A common analyte of interest is iron. Iron is an abundant element in the environment which plays an important role in environmental and biological systems. In particular, its essential function in photosynthesis has been seen as a limiting factor for phytoplanktons in ocean waters. Thus, sensitive speciation and determination of iron is of major interest, and many techniques have been established for analytical purposes. Electrochemical methods have been commonly explored due to their inexpensive, simple and rapid nature, with adsorptive stripping voltammetry (AdSV) being widely used due to its ability to complex and preconcentrate iron ions for ultrasensitive detection. This chapter aims to summarise and present a review of recent determinations of trace iron using electrochemical methods.

The work presented in this chapter has been published in *Electroanalysis*, 24, (2012), 1693-1702.

7.1 Introduction

Iron is one of the most common elements in the Earth's crust and exists naturally in the environment in mineral species, rock, groundwater and seawater [1]. It plays an

important role in environmental, industrial, human and biological systems [2], and as such, it is of key interest for analytical study. Iron determination in seawater is of major interest due to its importance in oceanic biogeochemistry [3–6]. In waters, iron uptake is influenced by its oxidation state and complexation by ligands and as a consequence, has been found to be a limiting growth nutrient for phytoplankton [3, 7]. This imposes important implications for air-sea exchange of carbon dioxide which could be a cause of concern for marine life. Its biological activity is often monitored as it is one of the key trace elements for living organisms and is seen to play an essential part in photosynthesis, acting as an enzyme cofactor in plants [8]. Redox reactions are reliant on iron-containing enzymes whereby electron transport is facilitated by oxidation state change of the metal. Iron is an essential metal for life and plays several key roles within humans [9]. It is found in bulk in haemoglobin in the red blood cells where it complexes to molecular oxygen and transports this around the body [10]. As a carrier of oxygen to the cells, deficiency of iron in the body can interfere with vital functions and lead to lethargy, fatigue and anaemia [11].

Iron exists in many oxidation states ranging from -II to +VI [12], however it is most commonly seen as ferrous (+II) and ferric (+III) ions in the environment. Thermodynamic properties of the iron species vary greatly. Fe(II) is a soluble species in water, however it is rapidly oxidised in oxygen rich environments. On the other hand, Fe(III) forms stronger complexes and is thermodynamically stable in water albeit of low solubility [13], but photo-reduction of the species converts it to Fe(II) [14]. In seawater, natural Fe(III) chelators exist and some believe up to 99% of iron in waters is found complexed to organic ligands and thus its concentration is low except when extremely stable complexes are formed [15]; concentration of iron ranging from 0.1 nM to 10 nM [16, 17] has been

suggested. It has also been reported that the concentration of dissolved iron in freshwater is greater than that of seawater [17] due to the proximity to terrestrial and continental shelf sources. Soluble iron species in natural waters can vary from 10^{-6} M for river water, to 10^{-9} M for coastal sea water and to 10^{-11} M for ocean water [18]. The World Health Organisation (WHO) does not issue a health based guideline value for iron [19], however permissible values in drinking water ranges from 0.3 – 3 mg L^{-1}, as levels greater than this causes water to become discoloured and taste metallic.

The abundance of iron and its variable oxidation states in the environment calls for their accurate determination and quantification. Many analytical methods have been developed to detect and quantify iron; these include voltammetry [20], flow injection analysis [17], chromatography, chemiluminescence [21], spectrophotometry [22] and spectrofluorescence [23]. Spectrophotometric methods [17, 24, 25] have been widely used, however, these are relatively expensive for use in ultra trace determination of metal ions and can suffer from interferences. The size and weight of the instruments also restricts their use to land based experiments.

Electrochemical methods such as stripping voltammetry have been favoured due to their inexpensive, simple and rapid nature [26, 27]. Anodic and cathodic stripping voltammetry, in particular, have shown many benefits such as good selectivity and highly sensitive determination [28]. As well as this, square wave voltammetry and differential pulse voltammetry are commonly utilized for ultra sensitive detection. Direct reduction of Fe(III) to elemental metal occurs at around -1.5 V vs. SCE [29], however it cannot be analytically employed in acidic solutions as the signal for hydrogen reduction coincides with that of the voltammetric signal for iron . In addition, iron also has extreme redox potentials and due to the low solubility of iron in mercury for polarographic methods

[30–32], voltammetric stripping of iron via the metal in its elemental form is limited. As a result of this, trace iron is a metal that cannot be quantified by conventional ASV.

Determining dissolved iron concentration in waters may be difficult without preconcentration, and as such, complexation can be carried out prior to sample determination. A practical method for such determination of low levels of iron is cathodic stripping voltammetry (CSV). In ocean waters, when iron becomes complexed with organic ligands, concentration of iron is deduced by taking advantage of ligand competition between natural ligand present in the medium and the added ligand used for voltammetric detection [33–35]. Concentration of the labile iron can be calculated from a linear plot made from : $[Fe^{3+}]/[FeL]=[Fe^{3+}]/C_L+1/(K_{FeL}C_L)$ where [FeL] is the concentration of iron complexed by the natural ligand, L, C_L is the total concentration of L, and $K_{FeL}C_L$ is the conditional stability constant of the complex [33].

Specific adsorption of a complex of the metal ion with the chelator occurs first at the electrode surface, followed by reductive stripping to Fe(II). The reduction current is then measured to give the concentration of the adsorbed metal ion. Without chelation, it may be difficult to accurately determine Fe^{2+} and Fe^{3+} concentrations due to the reversibility of the $Fe^{2+/3+}$ couple at a bare electrode. One main advantage of CSV includes the ability to determine the chemical speciation of iron; it is important to determine the speciation of iron as well as its concentration in waters. Pehkonen [12] noted that whilst iron may be the limiting nutrient for phytoplankton growth, Fe(II) is probably the preferred nutrient. A common procedure for iron speciation involved first complexing Fe(II) with a chelating agent then determining its concentration. Following from this, Fe(III) is reduced to Fe(II) from which the total iron concentration is found, and then by subtraction of Fe(II) from the total iron, concentrations of each species can be calculated [36, 37]. Being a long and

complicated approach to speciation of iron, more modern techniques for simultaneous determination of Fe(II) and Fe(III) have been devised [38, 39].

At subnanomolar levels of iron, sensitivity of metal ions by adsorptive stripping voltammetry can be seen to be improved by their complexation or chelation with specific ligands. This technique employs a preconcentration step before voltammetric measurements, which allows highly sensitive measurements of metal ions to be made. Chelating reagents for iron determination include catechol [40], 1-nitroso-2-naphthol (NN) [18], solochrome violet RS [41], cupferron [42], 2-(2-thiazolylazo)-p-cresol (TAC) [43] and 1,2-cyclohexanedione dioxime [44]. The use of chelates, however, changes the reduction potential of the complex with respect to the iron. Catalytic enhancement with adsorptive stripping voltammetry is another technique for decreasing limits of detection [44–47]. Addition of an oxidant can catalytically enhance the reoxidation of Fe(II) formed during the stripping step leading to an increase in peak current. Catalytic behaviour has been observed in the presence of oxidizing agents such as H_2O_2, BrO_3^-, ClO_2^- and NO_2^-, resulting in very high sensitivity [33, 46].

Traditionally, the most sensitive working electrode for trace metal detection had been the hanging mercury drop electrode [48]; however, nowadays analytical methods involving mercury electrodes are avoided. Due to the drawbacks of mercury toxicity [49, 50], development for mercury-free electrodes has been of obvious interest and one of the main materials for electrode design is carbon. Carbon electrodes such as carbon paste (CPE), glassy carbon (GCE), edge plane pyrolytic graphite (EPPG) [51–53] are analytically useful materials and avoid the toxic complications arising from mercury. Under optimised conditions, it can provide selective determination with minimum interferences. Diamond paste electrodes have also shown to be a very promising material for iron detection. This

new technique was investigated by Stefan et al. [20], giving the most sensitive voltammetric determination of iron to date with a limit of detection of 0.1 pM. Many methods involving chemical modification of the electrode surface have also been explored; this will be covered later in the text.

In this chapter, recent (post-millennium) publications for sensitive iron determination are reviewed to provide a timely and much needed update of the field, which has developed significantly since the landmark reviews of Pehkonen [12] and Achterberg [54] in 1995 and 2001, respectively. Focus will be directed towards electrochemical methods for detection. A range of methodologies is summarised and a collection of tables with limits of detection and analytical method for each electrode material is included. Tables 7.1, 7.2 and 7.3 are provided in the text, reviewing iron analyses using the different electrodes.

7.2 Electrochemical Methods

Many different electrochemical methodologies for Fe(II) and Fe(III) detection have been reported and recent voltammetric determinations are reviewed here. The most common method used has been adsorptive cathodic stripping voltammetry (AdCSV). In this method, ligands are used to complex with iron and this adsorbs onto the surface of the working electrode. By holding the electrode at a specific potential, the complex is preconcentrated prior to reductive stripping of the complex back into solution, allowing a very low detection limit to be achieved; $Fe^{n+}_{(aq)} + L_{(aq)} \rightarrow FeL_{(ads)}$, $FeL_{(ads)} + ne^{-} \rightarrow Fe^{n+}_{(aq)} + L_{(aq)}$. Further lowering of detection limits by extending the deposition time for adsorption and using catalytic oxidants has also been reported. Major advantages of AdCSV include low cost, compact and portable instrumentation and good sensitivity which is useful for

on board detection.

A variety of electrode materials have been used, and in the following, three main materials; mercury, platinum and carbon, have been detailed. The sections detail all the different voltammetric methods used with the different electrode materials.

7.2.1 Mercury Electrodes

Mercury based electrodes such as hanging mercury drop electrodes (HMDE) and mercury film electrodes (MFE) have been commonly used for analytical stripping analysis owing to their high resistivity, large hydrogen overpotential and reproducibility [27, 48, 55]. Sensitive detection of iron has been achieved with many authors reporting detection limits in the nanomolar [18, 40], and even picomolar range [35, 45]. Whilst the majority of iron determination in the 20^{th} century was performed using mercury electrodes, mercury toxicity concerns [50, 56] have led to the use of mercury dwindling in recent years, and research has turned towards alternative electrodes with reports of iron determination using mercury based electrodes becoming rare.

One of the earliest voltammetric studies of iron on a mercury electrode was carried out by Brainina and Roizenblat [57] in 1963 using cathodic stripping voltammetry (CSV) at a mercury drop electrode (MDE), giving a 10 μM detection limit. Many followed, including Berge and Drescher [58] who looked into exchange reactions for the determination of iron. Here, iron displacing lead from lead-EDTA complex was determined by anodic stripping voltammetry down to a concentration of 0.4 nM at a HMDE. The most sensitive detection of iron, pre-2000, was reported by Gledhill and Van den Berg [33]. These authors used catalytic cathodic stripping voltammetry (CCSV) to take advantage of ligand competition between the NN (1-nitroso-2-napthol) ligand and natural ligands present in seawater, in

the presence of H_2O_2. The dissolved Fe(II) is oxidised to Fe(III) in the presence of the oxidising agent, and Fe(III) forms a complex with the ligand which subsequently adsorbs onto the HMDE electrode during the deposition step. During the voltammetric scan, the Fe(III) complex is reduced to Fe(II), but is then reoxidised by H_2O_2. The reoxidised Fe(III) contributes again to the reduction current, greatly enhancing the sensitivity of the stripping method. Whilst a very sensitive detection limit of 0.8 pM was achieved, the authors also used this technique to investigate the organic speciation of iron in seawater. Fe(II) was first masked with 2-2-dipyridyl so that Fe(III) could be determined; the Fe(II) concentration could then be calculated by subtraction.

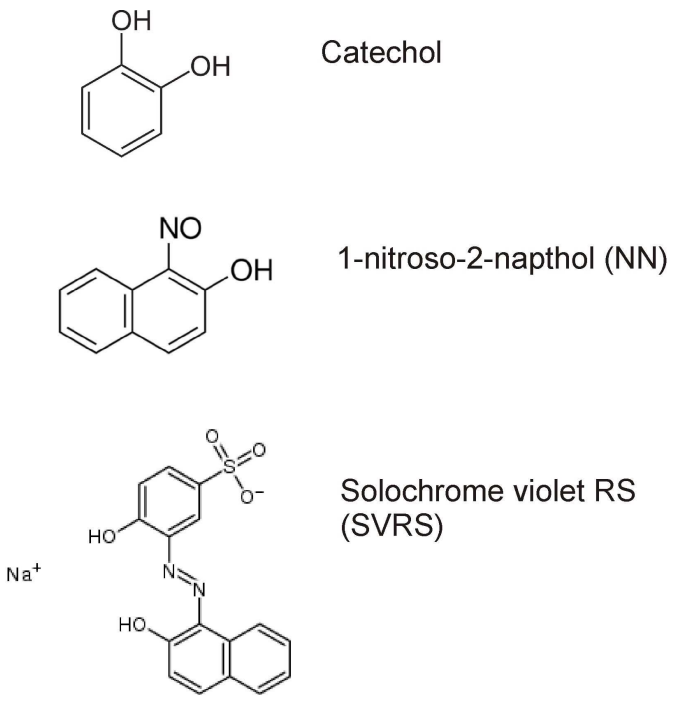


Figure 7.1: Ligand structures

It can be seen that use of mercury electrodes sometimes eliminates the need for surface modification for analytical study, however, in most cases, a complexing agent is

required for successful stripping voltammetry by adsorptive cathodic stripping voltammetry (AdCSV). Some commonly used complexing agents for AdCSV include catechol [40], 1-nitroso-2-napthol (NN) [59], and solochrome violet [41]. The structures of these ligands are shown in Figure 7.1.

Van den Berg and Huang [40] complexed iron with catechol and used cyclic voltammetry to characterise the potential of the catechol-Fe(III) complex. Catechol is quite easily oxidized and can thus act as a reducing agent in some cases; as well as this, the Fe(III) oxidation state is stabilized as a result of complexation by catechol ions. This direct determination of dissolved iron was applied to seawater and a detection limit of 0.6 nM was achieved. However, despite being a sensitive analytical method, the technique was not able to determine Fe(III) and Fe(II) simultaneously and speciation of iron could not be distinguished.

A similar complex-based adsorptive approach was performed by Wang and Mahmoud [41], with solochrome violet RS (SVRS) as the complexing agent for Fe(III). Iron was chelated with SVRS and adsorbed onto a HMDE before reductive stripping of the species was used to determine sensitive detection of iron. The method relies on effective interfacial accumulation of the Fe(III)/ SVRS chelate onto the mercury electrode. Although the technique offers similar detectability as the catechol based adsorptive approach, Wang and Mahmoud report shorter preconcentration times, extended linear range, and less interferences from iron(II), copper and lead to give a LoD of 0.7 nM. Another frequently used complexing agent is 1-nitroso-2-napthol (NN), most commonly taken advantaged of by Van den Berg et al. [18, 33, 60] to complex Fe(III). In 1991, Van den Berg and Mentasti [18] reported a sensitive method to determine trace levels of iron in seawater using adsorptive deposition of the iron complex on the mercury drop electrode (MDE).

Although a sensitive detection of 0.2 nM Fe could be seen, this required a 10 minute deposition time of the iron complex onto the electrode. NN as a complexing ligand yielded highly sensitive results towards Fe(III); the authors attributed this to the strong complexing ability with Fe(III) because they contain π-orbital electrons which apparently improves adsorption of the complexes on the mercury drop [61]. The analytical method described looks exclusively at the concentration of Fe(III) as oxidation of Fe(II) to Fe(III) is performed at the electrode surface before subsequent complexation and reduction.

Many more authors have reported a range of different voltammetric determination of iron at mercury electrodes, a collection of these have been included Table 7.1.

Post-millennium, the most sensitive account of iron determination was reported by Obata and Van den Berg [45] who were able to detect picomolar levels of iron in seawater using catalytic cathodic stripping voltammetry. Adsorptive accumulation of the iron complex, Fe(III)-2,3-dihydroxonaphthalene (DHN), onto a static mercury drop electrode in the presence of bromate ions was followed by cathodic stripping of the species. The reductive current was catalytically enhanced by the oxidizing agent, BrO_3^-, and after 60 s adsorption time, gave a detection limit of 13 pM. The authors also claim to achieve even lower limits of detection by extending the adsorption time. Obata and Van den Berg used several ligands, and evaluated their use for the detection of iron. It was seen that the Fe(III)-2,3-dihydroxonaphthalene (DHN) complex gave the highest sensitivity, suggesting greater stability of the complex. The new catalytic method gave very sensitive results, which was subsequently applied to iron determination in the North Atlantic Ocean. Following on, in 2006, Van den Berg [62] reported the chemical speciation of iron in seawater by cathodic stripping voltammetry using 2,3-dihydroxynaphthalene (DHN) as an adsorptive and competing ligand.

In 2000, Croot and Johnsson [43] reported sensitive determination of iron and its speciation by cathodic stripping voltammetry in seawater using competing ligand 2-(2-thiazolylazo)-p-cresol (TAC). A detection limit of 0.1 nM using sensitive competitive ligand exchange-adsorptive cathodic stripping voltammetry (CLE-ACSV) with an iron-TAC complex could be seen. Nagai et al. used cathodic stripping voltammetry with NN to determine the total dissolved iron concentration and its speciation in freshwater. Determination of Fe(III) complexation by natural organic ligands was determined by the competitive ligand equilibration method. A detection limit of 1.8 nM was achieved.

Ghoneim et al. [63] carried out the simultaneous determination of iron with 10 other elements (Cd, Pb, Cu, Sb, Bi, Se, Zn, Mn, Ni and Co) in water by adapting the conditions of the sample to optimise the detection of each element. Differential pulse anodic stripping voltammetry (DPASV) with a hanging mercury drop electrode (HMDE) was used for direct simultaneous determination of the metal elements. An ordered set of procedures was used involving varied pHs to detect each of the elements in turn; iron was detected last after 2-(5-bromo-2-pyridylazo)-5-diethlyaminophenol (5-Br-PADAP) was added to solution and determined by DPAdSV. 5-Br-PADAP was needed as a complexing agent for iron and a preconcentration time applied before a detection limit of 0.39 nM was determined. Witter et al. [64] measured the total iron concentration by cathodic stripping square wave voltammetry (CSSWV) to give a detection limit, after an 8 minute deposition period, of 0.15 nM. The authors employed a competitive ligand exchange stripping (CLECSV) technique for the speciation of iron by establishing competition between the added ligand (NN) and the natural organic ligands present for the complexation of added Fe(III).

Mikkelsen and Schroder [65] monitored Fe(II) using a dental amalgam sensor electrode using differential pulse anodic stripping voltammetry to detect iron in the nanomolar

region. The authors present solid amalgam electrodes as a non toxic material with unique sensitivity for bivalent iron. Detection limits for 180 s preconcentration gave a value of 9.0 nM for Fe(II). Mikkelsen et al. [66] presented a new method for the determination of iron in estuarine and coastal seawater based on differential pulse anodic stripping voltammetry (DPASV) at a rotating Ag-alloy disk electrode. The Ag-alloyed mercury electrode allowed very sensitive detection to be carried out, with a limit of detection of 0.3 nM for iron, and as well as this, iron speciation could be carried out by using chelating agents such as EDTA to mask the electrochemically labile species.

In 2005, Stozhko et al. [67] determined iron in natural and drinking waters by stripping voltammetry using a thick film graphite containing electrode modified with calomel. Addition of pyrocatechol allowed an iron complex to be formed for preconcentration at the electrode, and a sensitive detection of 0.36 nM Fe(III) was achieved. In the course of analysis, a very thin droplet-like mercury coating is formed, but despite this, the electrode can be considered safe because after analysis, the thin mercury layer can be easily and completely converted back to calomel. The authors report a non-toxic procedure for determining trace amount of Fe(III) in natural and drinking waters.

Another report using catechol, together with dimethylglyoxime (DMG), for iron complexation was carried out by Echeandia [68] in 2011. Adsorptive cathodic stripping voltammetry with the mixed ligands was performed at a HMDE and a detection limit of 1.29 nM iron could be determined. This procedure is suitable for the direct simultaneous detection of five metals, Co, Cu, Fe, Ni and V, in sediment pore waters.

Technique	Electrode	Modifier/Complexing agent (if any)	Speciation	*LoD*(M)	Year	Reference
CSV	MDE	N/A	Fe(II)	1.0×10^{-07}	1963	[57]
ASV	HMDE	Pb-EDTA	Fe(III)	4.0×10^{-08}	1967	[58]
CV/SV	HMDE	TEA	Fe(III)	1.0×10^{-06}	1980	[69]
Indirect Polarography	MDE	5-ASA	Fe(III)	3.6×10^{-08}	1981	[70]
DPAdCSV	HMDE	ANSA, Catechol	Fe(III)	6.0×10^{-10}	1984	[40]
DPSV	HMDE	Catechol	Fe(III)	1.8×10^{-09}	1986	[71]
CSV	HMDE	Catechol	Fe(III)	1.0×10^{-09}	1986	[72]
AdCSV	HMDE	SVRS	Fe(III)	7.0×10^{-10}	1987	[41]
DPP	MDE	N/A	Fe(II)	1.0×10^{-07}	1988	[73]
DPCSV	HMDE	TEA, Bromate ions	Fe(III)	7.2×10^{-08}	1989	[74]
AdSV	HMDE	SVRS	Fe(III)	$_{Fe(III)}$ 2.7×10^{-05} $_{Fe(tot)}$ 4.1×10^{-05}	1989	[36]
AdCSV	MDE	NN	Fe(III)	2.0×10^{-10}	1991	[18]
PSA/ASV	HMDE	5-Br-PADAP	Fe(III)	2.0×10^{-09}	1991	[75]
AdCSV	MDE	NN	Fe	6.1×10^{-10}	1992	[60]
AdCSV	MDE	2,2-Thiazolylazo-4-methylphenol	Fe(III)	1.8×10^{-09}	1992	[76]
DPV	HMDE	PBA	Fe(III)	1.8×10^{-07}	1992	[77]
Catalytic CSV	HMDE	NN	Fe(III)	8.0×10^{-11}	1994	[33]
CLE/CSV	HMDE	NN	Fe(III)	4.5×10^{-10}	1994	[78]
DPAdSV	HMDE	SVRS	Fe(III)	9.0×10^{-09}	1994	[79]
DPP	DME	DCDT	Fe	9.0×10^{-08}	1994	[80]
CLE-AdCSV	MDE	SA	Fe(III)	7.0×10^{-14}	1995	[35]
AdCSV	HMDE	NN	Fe(III)	3.6×10^{-09}	1995	[81]
DPV/ACV	HMDE	N/A	Fe	1.0×10^{-09}	1996	[82]
DPV/DPP	DME/HME	B-T	Fe(III)	2.0×10^{-07}	1996	[83]
Catalytic AdCSV	HMDE	Iron-thiocyanate nitric oxide	Fe(II)	7.1×10^{-10}	1996	[84]
AdCSV	MDE	Iron acetate	Fe(III)	6.0×10^{-10}	1997	[85]
AdCSV	HMDE	Cupperon	Fe(III)	3.6×10^{-09}	1997	[42]
Photochemical voltammetry	DME/HME	BG	Fe(III)	5.4×10^{-08}	1997	[86]
Catalytic CSV	HMDE	NN	Fe(tot)	4.0×10^{-10}	1998	[87]
Catalytic CSV	MDE	NN	Fe(II)	8.0×10^{-10}	1998	[46]
AdSV	HMDE	Catechol, Quartz and Silica glass	Fe	3.9×10^{-08}	1999	[88]
CLE-ACSV	MDE	TAC	Fe(tot)	1.0×10^{-10}	2000	[43]
DPAdSV	HMDE	5-Br-PADAP	Fe	3.9×10^{-10}	2000	[63]
DPP	DM/HMDE	Tri-BAP	Fe(III)	1.5×10^{-06}	2000	[89]
CLE-SWV	MDE	NN	Fe(III)	1.3×10^{-09}	2000	[64]
CSV	MDE	DHN	Fe(III)	1.3×10^{-11}	2001	[45]
DPASV	Dental amalgam electrode	Ammonium oxalate	Fe(II)	9.0×10^{-09}	2003	[65]
DPCSV	HMDE	NN	Fe(III)	1.8×10^{-09}	2004	[90]
ASV	TFGME	Calomel, Pyrocatechol	Fe(II)+Fe(III)	3.6×10^{-10}	2005	[67]
CSV	MDE	DHN	Fe(II)+Fe(III)	1.1×10^{-09}	2006	[62]
AdCSV	HMDE	SVRS	Fe(III)	3.2×10^{-08}	2008	[91]
AdCSV	HMDE	DMG, Catechol	Fe	1.3×10^{-09}	2011	[68]
CLE/CSV	HMDE	Humic substances SA, DHN	Fe(II)+Fe(III)	NR	2011	[92]

Table 7.1: Iron analyses using mercury electrodes. **Technique**: ASV, Anodic Stripping Voltammetry; CSV, Cathodic Stripping Voltammetry; AdCSV, Adsorptive Cathodic Stripping Voltammetry; CV, Cyclic Voltammetry; PSA, Potentiometric Stripping Analysis; DPP, Differential Pulse Polarography; CLE, Competitive Ligand Exchange; DPV, Differential Pulse Voltammetry; SWV, Square Wave Voltammetry. Electrode: MDE, Mercury Drop Electrode; HMDE, Hanging Mercury Drop **Electrode**; DME, Drop Mercury Electrode; HME, Hanging Mercury Electrode; TFGME, Thick Film Graphite Modified Electrode. **Modifier/complexing agent**: ANSA, 1-amino-2-naphthol-4-sulfonic acid; SVRS, Solochrome Violet RS; TEA, Triethanolamine; 5-ASA, 5-aminosalicylic acid; NN, 1-nitroso-2-naphthol; B-T, Bis-(2-hydroxymethyl)imino-tris(hydroxymethy)methane; BG, Brilliant Green (triphenylmethane dye); PBA, N-phenylbenzohydroxamic acid; 5-Br-PADAP, 2-(5-bromo-2-pyridylazo)-5-diethlyaminophenol; DCDT, 5,5-dimethylcyclohexan-1,2,3-trione 1,2-dioxime 3-thiosemicarbazone; TAC, 2-(2-thiazolylazo)-p-cresol; Tri-BAP, tributylammonium perchlorate; DMG, dimethylglyoxime; DHN, 2,3-dihydroxynaphthalene; SA, salicylaldoxime. **Other**: N/A, not applicable, NR, not reported

7.2.2 Platinum Electrodes

Platinum was not widely used analytically in the 20^{th} century, however, modern analytical research using it as an electrode material has recently become more prevalent. In 1972, Young and Laitinen [93] reported the first account of voltammetric determination of iron at a platinum electrode. Cathodic stripping of iron had previously been investigated by Brainina [57, 94] but at a HMDE, a low limit of detection was achieved with a value of 70 μM for ferrous ions. Not long after, Cox and Majda [95] looked into the detection of Fe(III) and Fe(II) using a adenosine-5-monophosphate modified platinum electrode. It was found using cathodic stripping voltammetry, that a nonlabile complex with Fe(III) can be readily plated onto platinum, and subsequent reduction to the iron (II) complex gives the stripping peak.

Two decades later, the determination of iron on platinum electrodes was revisited by several authors. Strycker et al. [96] looked into the electrochemical behaviour of iron in molten enamel using a rotating platinum disc electrode. Initial experiments at a platinum disc electrode characterised by cyclic and square wave voltammetry showed that due to a slow chemical equilibration between Fe(II) and Fe(III) in homogeneous solution, it was not possible to calculate the analytical concentration of Fe(III). However, further investigation with rotating disc chronoamperometry was carried out, and the Fe(II) and Fe(III) equilibrium concentrations could successfully be determined. The next account of iron stripping from a platinum electrode by Barbosa et al. [97] involved the voltammetric dissolution of an iron-zinc alloy film. Here, a Fe-Zn alloy film was deposited on platinum. It was seen that only one anodic stripping peak was produced, suggesting that Fe and Zn in the film dissolved simultaneously; iron as Fe(III) and zinc as Zn(II), which gives great

insight to its kinetic studies.

Subsequent determination of iron were all performed at a rotating platinum electrode the increase in mass transport leads one to believe that more sensitive limits of detection may be achieved. This is not the case however, as Jin and Botte [38] and Scheers et al. [98] in 2009 and 2010, respectively, were not able to determine iron to low concentrations, despite this methodology.

Jin and Botte [38] managed to achieve a limit of detection of no lower than 0.02 mM. Here, the authors simultaneously detected Fe(II) and Fe(III) at a rotating disk electrode using a steady state polarization technique. The technique, called Electrochemical Measurement of Multivalent Cations Concentration (EM2C2) is based upon the electrochemical properties of the cations in solution, and can suitably determine the concentrations of Fe(II) and Fe(III) ions simultaneously. The EM2C2 method is based on the reduction/oxidation reaction of Fe(III)/ Fe(II) : $Fe^{3+} + e^{-} \leftrightarrow Fe^{2+}$. A potentiostat is used to apply a potential wave change between the working and reference electrode, and the corresponding currents between the working and counter electrode are recorded. The experimental results are then plotted as a graph of current against potential, and with a rotating Pt working electrode, a sigmoidal wave is produced as expected for a rotating disk electrode, and can be described by the Levich equation, $i_L = 0.620nFAD^{2/3}\omega^{1/2}\nu^{-1/6}C$. The concentrations of Fe(II) and Fe(III) can consequently be predicted using the analytical signals and the equations derived. At a rotation speed of 1000 rpm, the *LoD* value is 0.1 mM, however by increasing the rotation speed to a maximum limiting value of 3000 rpm, the *LoD* value decreases to 0.02 mM. Despite the lower sensitivity using EM2C2, the authors suggest it a promising beginning for determining the concentration of other multivalent cations such as As(III)/As(V), Cr(VI)/Cr(III) and Sb(III)/Sb(V).

Scheers et al. [98] determined Fe(II) and Fe(III) concentrations in aqueous solutions containing food chelators by differential pulse anodic stripping voltammetry (DPASV). By simulating the environment of the human duodenum, the net complexation of Fe^{2+} and Fe^{3+} with organic acids was determined and using a platinum rotating disc electrode, a detection limit of 0.13 μM for Fe(II) and 0.26 μM for Fe(III) was given. A Pt-silver alloy electrode was used by Diao and Sumi [99] to measure Fe^{2+}, however with linear sweep voltammetry, a limit of detection can only be reported to a value of 1.2 mM with iron sulfides in suspension.

It can be seen that a number of platinum electrodes have been used for the detection of iron with fairly low limits of detection. Though fairly expensive, platinum is environmentally friendly and can be used in the most cases, unmodified. Table 7.2 gives a summary of iron analyses using platinum electrodes.

Technique	**Electrode**	**Modifier/Complexing agent (if any)**	**Speciation**	***LoD*(M)**	**Year**	**Reference**
CSV	Pt ring-disk	1,10-Phrenanthroline	Fe(II)	7.0×10^{-07}	1972	[93]
CSV	Pt wire	Adenosine-5-monophosphate	Fe(II)+Fe(III)	1.0×10^{-08}	1980	[95]
SWV	Pt disk	N/A	Fe(III)	NR	2004	[96]
DPASV	Rotating Ag-alloy disk	N/A	Fe(II)	3.0×10^{-10}	2005	[66]
ASV	Pt disk	Fx10-Zn alloy film	Fe(III)	NR	2005	[97]
EM2C2	Pt-RDE	N/A	Fe(II)+Fe(III)	2.0×10^{-05}	2009	[38]
DPASV	Pt-RDE	Food chelators (lactate, phytate)	Fe(II)+Fe(III)	1.3×10^{-05}	2010	[98]
CSV	Pt-Ag twin electrode	Silver sulfide	Fe(II)	1.2×10^{-03}	2010	[99]

Table 7.2: Iron analyses using platinum electrodes. CSV, Cathodic Stripping Voltammetry; SWV, Square Wave Voltammetry; DP, Differential Pulse; ASV, Anodic Stripping Voltammetry; EM2C2, Electrochemical Measurement of Multivalent Cations Concentration; RDE, Rotating Disk Electrode; NR, not reported; N/A, not applicable

7.2.3 Carbon Electrodes

Carbon is an ideal replacement material for mercury as it possesses properties that lend itself adequately for analytical study [51–53, 100]. Carbon is also widely used due to its cheap and disposable nature. Some popular carbon electrodes used for the determination of iron are carbon paste electrodes [101, 102] and glassy carbon electrodes [39, 103], with the active surface being modified in some instances. A list of iron determinations using carbon electrodes, together with their limits of detection is given in Table 7.3.

Technique	**Electrode**	**Modifier/Complexing agent (if any)**	**Speciation**	***LoD*(M)**	**Year**	**Reference**
ASV	Rotating GCE	Pb film, Bi-EDTA	Fe(III)	9.0×10^{-09}	1970	[104]
CSV	Rotating GCE	N/A	Fe(III)	1.0×10^{-05}	1976	[30]
ASV	GCE	Hg plated in situ, EDTA	Fe(III)	1.0×10^{-07}	1980	[105]
FIA	GCE	N/A	Fe(II)+Fe(III)	1.0×10^{-06}	1980	[106]
AdCSV	Carbon fibre	Solochrome violet	Fe(III)	1.8×10^{-08}	1988	[107]
DPCSV	CPE	Montmorillonite clay	Fe(III)	3.6×10^{-06}	1989	[102]
DPASV	CPE	Nafion, 1,10-phenanthroline	Fe(II)	3.0×10^{-08}	1990	[108]
DPASV	CPE	2,2-bipyridyl, Nafion	Fe(II)	1.0×10^{-08}	1991	[101]
CSV	GCE	Nafion, BP	Fe(III)	8.9×10^{-10}	1995	[109]
DPCSV	CPE	AIPA	Fe(II)	3.0×10^{-07}	1998	[110]
DPASV	GCE	Pyrophosphates	Fe(II)	2.7×10^{-08}	1998	[39]
			Fe(III)	2.4×10^{-08}	1998	
MSWV-DD	GCE	Nafion	Fe(II)+Fe(III)	1.5×10^{-06}	2001	[111]
CSV	GCE	Chitosan, oxalates	Fe(tot)	1.8×10^{-07}	2001	[103]
LSV/DPV	CPE	Graphite/polyester composite, Na_2EDTA	Fe(II)+Fe(III)	NR	2001	[112]
IEV	GCE	Nafion, Tosflex	Fe(II)+Fe(III)	1.0×10^{-07}	2002	[113]
DPASV	Diamond paste electrode	N/A	Fe(III)	1.0×10^{-13}	2003	[20]
CV	CPE	N/A	Fe powder	NR	2005	[114]
SWAdSV	GCE	Bismuth coated PAN	Fe(III)	1.8×10^{-09}	2008	[115]
SW-AdCSV	CPE	5-Br-PADAP	Fe(III)	1.7×10^{-09}	2010	[29]
DPASV	CPE	DTDA and Au NPs	Fe(II)	5.0×10^{-11}	2011	[116]
FIA	GCE	MWCNTs, Pt NPs	Fe(III)	3.0×10^{-09}	2012	[117]

Table 7.3: Iron analyses using carbon electrodes. **Method**: ASV, Anodic Stripping Voltammetry; CSV, Cathodic Stripping Voltammetry; FIA, Flow Injection Analysis; AdCSV, Adsorptive Cathodic Stripping Voltammetry; DPV, Differential Pulse Voltammetry; IEV, Ion-Exchange Voltammetry; MSWV-DD, Double Differential Multiple Square Wave Voltammetry; LSV, Linear Sweep Voltammetry; CV, Cyclic Voltammetry; SW, Square Wave; FIA, Flow Injection Analysis. **Electrode**: GCE, Glassy Carbon Electrode; CPE, Carbon Paste Electrode; MWCNTs, Multiwall Carbon Nanotubes. **Modifier/complexing agent**: AIPA, 2-aminoisophthalic acid; 5-Br-PADAP, 2-(5-bromo-2-pyridylazo)-5-diethlyaminophenol; DTDA, dithiodianiline; NPs, nanoparticles; Bi-EDTA, bismuth ethylenediaminetetraacetic acid; BP, aa-bipyridine; PAN, 1-(2-piridylazo)-2-naphthol. **Other**: N/A, not applicable; NR, not reported

Carbon electrodes were used by many authors pre-2000. Despite being one of the earliest accounts of iron determination at a carbon electrode, Florence [104] was able to achieve one of the lowest limits of detection of the time at a rotating glassy carbon electrode. Since iron could not be determined directly by anodic stripping voltammetry, a rotating glassy carbon electrode with a thin mercury film deposited in situ was used to investigate Fe^{3+}. Here, a chemical exchange reaction between ferric ion and bismuth-EDTA was used to successfully determine iron to a limit of 9 nM. Other accounts of iron determination were in between the region of 0.1 μM and 0.1 nM. Stulikova and Vydra [31] have been the only other authors to report voltammetry of iron at a rotating carbon electrode. In this case, Fe(III) was detected at a glassy carbon rotating disk electrode. After de-aeration with nitrogen, a limit of detection of 0.1 μM could be achieved in acidic media by cathodically scanning to a lower potential.

One of the most sensitive limits of detection was reported by Yang et al. [109] in 1995 at a glassy carbon electrode by modifying the surface with Nafion for the cathodic stripping determination of Fe(III). The authors realised a Nafion coated electrode facilitated the preconcentration of the iron complex. Nafion has been proved to be an ideal polymer for chemically modified electrodes as it is very chemically inert, non-electroactive, hydrophilic, thermally stable and insoluble in water. Here, Yang et al. described the cathodic stripping voltammetry of iron based on the preconcentration of Fe(III)-$\alpha\alpha$-bipyridine (BP) complex on the Nafion modified electrode. Optimum concentration of the complexing agent was determined, and with a 2 minute preconcentration time, Fe(III) was detected to a limit of 0.89 nM. Application of this technique was successfully used to determine iron concentrations in fountain water and longan fruit. Differential pulse voltammetry (DPV) was applied by many authors as a means for sensitive detection of iron, with limits of

detection ranging from 0.3 μM [110], by complexing iron(II) with 5-aminoisophthalic acid (AIPA), to 10 nM [101] by modifying carbon paste electrodes with 1,10-phrenanthroline and Nafion.

In the 21^{st} century, limits of detection of iron using carbon electrodes were seen to be several orders of magnitude lower than that reported previously. The most sensitive detection of iron was reported by Stefan et al. [20] using a new electrode design based on diamond paste. Differential pulse anodic stripping voltammetry was used to detect Fe(III) to a limit of 0.1 pM using natural diamond powder cast with paraffin oil. The superiority of the monocrystalline diamond as an electrode material was seen over carbon allotrope based electrodes such as glassy carbon electrodes. Here, lower background currents and noise signals were seen, there was a wide electrochemical potential window, it was electrochemically stable and there was very low capacitance. The electrode looks to be a promising new material for sensitive detection, especially since no modification of the surface is needed, and no complexing agents were required for the detection of Fe(III).

Many authors have used glassy carbon electrodes, however the surface is generally modified for detection of Fe(III). In 2001, Ugo et al. [111] used Nafion coated glassy carbon electodes (NCE) for preconcentrating and detecting Fe^{2+} and Fe^{3+} cations from aqueous solutions. The authors realised, like Yang et al. [109], that Nafion proved to be a good electrode modifier for preconcentrating iron complexes. First, using cyclic voltammetry, the ion-exchange voltammetric (IEV) determination of iron, which takes advantage of the preconcentration capability and selectivity of thin films, could be determined in the μM range. However, lower detection limits could be achieved by combination of the Nafion coated electrodes with multiple square wave voltammetry (MSWV), giving a detection limit of 2.5 nM. Although voltammetric measurements at the NCE give only the overall

iron concentration, open circuit potential measurements performed before starting the voltammetric scan can determine speciation of iron.

More voltammetric iron determination at glassy carbon electrodes were reported by Lu et al. [103], Ugo et al. [113] and Segura et al. [115]. All three accounts involved the modification of the electrode surface; this included chitosan, ionomers such as Nafion and 1-(2-piridylazo)-2-naphthol (PAN) respectively. The authors noticed the enhanced ability to increase the preconcentration of iron complexes onto a modified carbon electrode surface, to give lower limits of detection. Lu et al. [103] were able to detect total iron concentration to a limit of 0.18 μM using cathodic stripping voltammetry and took advantage of the instability of $Fe(C_2O_4)_3^{3-}$ to light and the reductive effects of $C_2O_4^{2-}$. It was found that using $C_2O_4^{2-}$ as a complexing agent and reductant, there was no reductive stripping signal for iron on a bare unmodified glassy carbon electrode. However, sensitivity of the electrode was vastly enhanced with a chitosan modified glassy carbon electrode (CMGCE), indicating obvious adsorptive behaviour. Previous authors have demonstrated the ability for iron ions to be preconcentrated by Nafion, however, since both Fe(II) and Fe(III) species are equally preconcentrated, redox speciation to distinguish between the two oxidation states is very difficult. Ugo et al. [113] used ionomer coated glassy carbon electrodes to combine potentiometric and voltammetric measurements with anion exchanger Tosflex and cation exchanger Nafion. This method allowed for the determination and speciation of iron ions at trace concentration levels. Segura et al. [115], like previous authors, also combined the use of a complexing agent and subsequently preconcentrates the iron complex onto a modified carbon surface. Here, a complex of iron with PAN is adsorbed onto a bismuth coated glassy carbon electrode (BiFE). The authors use square wave adsorptive stripping voltammetry (SWAdSV) and an adsorption time of 60 s

to obtain a limit of detection of 1.79 nM for Fe(III); it was also noted that more sensitive results could be achieved using longer adsorption times.

The most recent paper regarding iron detection on a glassy carbon electrode was by Anguiano et al. in 2012 [117]. Modification of GCEs with Multiwall Carbon Nanotubes (MWCNTs) in the presence of Pt nanoparticles was presented as an effective electrocatalytic material for metallic pollutants detection. The GCE modified with CNTs have been claimed to show better performance than conventional carbon electrodes. The use of Pt nanoparticles helps to facilitate the electron transfer and electrocatalytic properties. The constructed electrodes were incorporated as amperometric detectors of ionic iron electroreduction using the Flow Injection Amperometric (FIA) technique in aqueous solution, exhibiting a detection limit of 3 nM. Application of this has been used on samples of polluted soil in Guanajuato, Mexico.

The other carbon electrode regularly used for iron detection is the carbon paste electrode (CPE). Carbon paste electrodes are well known materials for analytical purposes. Its simple fabrication and its ability to be easily modified is often utilized for important selectivity towards target species. In the detection and speciation of iron, many authors chose to modify the CPE or use complexing agents such that preconcentration of iron occurs better to get a more sensitive limit of detection. A recent publication by Gholivand et al. [116] employed a differential pulse anodic stripping voltammetric procedure for the determination of Fe(II) at a carbon paste electrode modified with dithiodianiline (DTDA) and gold nanoparticles. Though a complexing agent was not used, the accumulation of Fe(II) at the surface of the modified electrode was based on the complex formation between the metal ion and the modifier, DTDA. After preconcentration, an anodic stripping peak was given where a detection limit of 0.05 nM could be calculated.

Ghoneim [29] found that by complexing Fe(III) with 2-(5-bromo-2-pyridylazo) -5-diethylaminophenyl (5-Br-PADAP), iron could be accurately detected using square wave adsorptive cathodic stripping voltammetry at a CPE. Without need for surface modification of the electrode, this technique was used to simultaneously detect Mn(II), Cu(II) and Fe(III) in tap, bottled and ground water to a detection limit of 1.67 nM.

Kladekova et al. [114] reported the anodic dissolution of iron at a paraffin impregnated graphite electrode by linear and cyclic voltammetry. Voltammetric analysis was carried out on the oxidation of iron powder and although the quantification of iron was not determined, it was seen that the pH values of the electrolyte solution as well as particle size fraction significantly influence the course of the dissolution of iron powder. Electrochemical determination of the Fe(II)/(III) ratio in ceramic materials using carbon paste and composite electrodes was carried out by Domenech-Carbo et al. [118]. Carbon paste electrodes were fabricated by mixing graphite powder with a polyester modifier and voltammetry on clay samples were carried out. This technique, based on micro sample attachment to graphite/polyester composite electrodes, describes the electrochemistry of iron in terms of reductive dissolution processes of Fe(III) and oxidative dissolution processes of Fe(II).

7.3 Conclusions

From this collection of recent reports on iron determination, it can be seen that analytical studies in this field is active. Many sensitive voltammetric methods have been used, with limits of detection as low as 13 pM in some cases [45]. This is greatly within the WHO [19] guideline for iron concentration, where an acceptable level in fresh water is

quoted at 0.3 - 3 mg L^{-1}. Although iron in drinking water is not a health concern, concentrations above 0.3 mg L^{-1} can cause food and water to become discoloured and taste metallic. The development of sensitive determination allows for important insight into the biogeochemistry of iron in waters, and further speciation of iron ions can be made. A collection of tables summarising the voltammetric technique and electrode material is included within the text, giving the detection limit in each account. With nontoxic electroanalytical methods being at the forefront of analytical research, there looks to still be a wide scope for carbon as an electrode material for iron determination, with only glassy carbon electrodes and carbon paste electrodes dominating the field presently. Building on the use of previously discussed methods such as adsorptive stripping analysis, coupled with oxidative catalysts and complexing agents, further advancement in the field of iron determination and speciation can be hoped to be made.

In the next chapter, determination of iron in a real sample of drinking water using electroanalytical methods is investigated.

Bibliography

[1] S. R. Taylor and S. M. McLennan 312.

[2] P. T. Lieu, M. Heiskala, P. A. Peterson and Y. Yang, *Molecular aspects of medicine* **22** (2001) 1.

[3] J. H. Martin and S. E. Fitzwater, *Nature* **331** (1988) 341.

[4] J. P. Riley and R. Chester 466.

[5] S. J. Ussher, E. P. Achterberg and P. J. Worsfold, *Environmental Chemistry* **1** (2004) 67.

[6] W. M. Landing and K. W. Bruland, *Geochimica et Cosmochimica Acta* **51** (1987) 29.

[7] P. N. Sedwick, G. R. DiTullio, D. A. Hutchins, P. W. Boyd, F. B. Griffiths, A. C. Crossley, T. W. Trull and B. Queguiner, *Geophysical Research Letters* **26** (1999) 2865.

[8] J.-F. Briat, *Advances in Botanical Research* **46** (2008) 137.

[9] N. C. Andrews, *Blood* **112** (2008) 219.

[10] P. Ponka, *Journal of Trace Elements in Experimental Medicine* **13** (2000) 73.

[11] L. Garby, *Acta Medica Scandinavica, Supplementum* **445** (1966) 264.

[12] S. Pehkonen, *Analyst* **120** (1995) 2655.

[13] X. Liu and F. J. Millero, *Marine Chemistry* **77** (2002) 43.

[14] W. L. Miller and D. Kester, *Journal of Marine Research* **52** (1994) 325.

[15] D. R. Turner, M. Whitfield and A. G. Dickson, *Geochimica et Cosmochimica Acta* **45** (1981) 855.

[16] M. L. Wells, *Journal of Marine Biology & Oceanography* **6** (1991) 463.

[17] V. A. Elrod, K. S. Johnson and K. H. Coale, *Analytical Chemistry* **63** (1991) 893.

[18] C. M. G. V. den Berg, M. Nimmo, O. Abollino and E. Mentasti, *Electroanalysis* **3** (1991) 477.

[19] W. H. Organisation, *Guidelines for drinking-water quality*, volume 2 (1996), 2nd edition.

[20] R.-I. Stefan, S. G. Bairu and J. F. van Staden, *Instrumentation Science Technology* **31** (2003) 411.

[21] A. R. Bowie, E. P. Achterberg, R. F. C. Mantoura and P. J. Worsfold, *Analytica Chimica Acta* **361** (1998) 189.

[22] M. Grotti, F. Soggia, F. Ardini and R. Frache, *Journal of Analytical Atomic Spectrometry* **24** (2009) 522.

[23] K.-W. Cha and K.-W. Park, *Talanta* **46** (1998) 1567.

[24] S. Blain and P. Treguer, *Analytica Chimica Acta* **308** (1995) 425.

[25] L. V. Mulaudzi, J. F. van Staden and R. I. Stefan, *Analytica Chimica Acta* **467** (2002) 35.

[26] R. G. Compton and C. E. Banks, *Understanding Voltammetry* (Imperial College Press, London, 2011), 2nd ed. edition.

[27] J. Wang, *Analytical electrochemistry* (Wiley-VCH, New York, 2000), 2nd edition.

[28] T. Miwa, *The Journal of Materials Science* **33** (1994) 374.

[29] E. M. Ghoneim, *Talanta* **82** (2010) 646.

[30] F. Vydra, *Electrochemical Stripping Analysis* (Halsted Press, 1976).

[31] M. Stulikova and F. Vydra, *Journal of Electroanalytical Chemistry and Interfacial Electrochemistry* **38** (1972) 349.

[32] M. Stulikova and F. Vydra, *Journal of Electroanalytical Chemistry and Interfacial Electrochemistry* **39** (1972) 229.

[33] M. Gledhill and C. M. G. V. den Berg, *Marine Chemistry* **47** (1994) 41.

[34] M. Boye, C. M. G. V. den Berg, J. T. M. D. Jong, H. Leach, P. Croot and H. J. W. D. Baar, *Deep-Sea Research, Part I: Oceanographic Research Papers* **48** (2001) 1477.

[35] E. L. Rue and K. W. Bruland, *Marine Chemistry* **50** (1995) 117.

[36] J. Wang and S. Mannino, *Analyst (Cambridge, United Kingdom)* **114** (1989) 643.

[37] R. Kuroda, T. Nara and K. Oguma, *Analyst* **113** (1988) 1557.

[38] X. Jin and G. G. Botte, *Journal of Applied Electrochemistry* **39** (2009) 1709.

[39] J. F. van Staden and M. C. Matoetoe, *Analytica Chimica Acta* **376** (1998) 325.

[40] C. M. G. V. den Berg and Z. Q. Huang, *Journal of Electroanalytical Chemistry and Interfacial Electrochemistry* **177** (1984) 269.

[41] J. Wang and J. Mahmoud, *Fresenius' Zeitschrift fuer Analytische Chemie* **327** (1987) 789.

[42] J. Wang, J. Lu, D. Luo, J. Wang and B. Tian, *Electroanalysis* **9** (1997) 1247.

[43] P. L. Croot and M. Johansson, *Electroanalysis* **12** (2000) 565.

[44] A. Bobrowski and A. Krolicka, *Electroanalysis* **15** (2003) 591.

[45] H. Obata and C. M. G. van den Berg, *Analytical Chemistry* **73** (2001) 2522.

[46] A. P. Aldrich and C. M. G. V. den Berg, *Electroanalysis* **10** (1998) 369.

[47] J. Lu, J. Wang and C. Yarnitzky, *Electroanalysis* **7** (1995) 79.

[48] A. Economou and P. R. Fielden, *Analyst* **128** (2003) 205.

[49] R. F. Palmer, S. Blanchard, Z. Stein, D. Mandell and C. Miller, *Health place* **12** (2006) 203.

[50] F. Zahir, R., F. Zahir, S. J. Rizwi, S. K. Haq and R. H. Khan, *Environmental toxicology and pharmacology* **20** 351.

[51] S. E. W. Jones and R. G. Compton, *Current Analytical Chemistry* **4** (2008) 170.

[52] K. Kalcher, I. Svancara, R. Metelka, K. Vytras and A. Walcarius, *Section Title: Inorganic Analytical Chemistry*, volume 4, 283–429 (2006).

[53] C. E. Banks and R. G. Compton, *Analytical Sciences* **21** (2005) 1263.

[54] E. P. Achterberg, T. W. Holland, A. R. Bowie, R. F. C. Mantoura and P. J. Worsfold, *Analytica Chimica Acta* **442** (2001) 1.

[55] J. Wang, *Section Title: Inorganic Analytical Chemistry*, volume 3, 125 (2003).

[56] J. F. Risher, *Elemental mercury and inorganic mercury compounds: human health aspects*, Technical report, World Health Organisation, 2003.

[57] K. Z. Brainina and E. M. Roizenblat, *Zhurnal Analiticheskoi Khimii* **18** (1963) 1362.

[58] H. Berge and A. Drescher, *Fresenius' Zeitschrift fuer Analytische Chemie* **231** (1967) 11.

[59] J. Wu and G. W. I. Luther, *Marine Chemistry* **50** (1995) 159.

[60] K. Yokoi and C. M. G. V. den Berg, *Electroanalysis* **4** (1992) 65.

[61] C. M. G. V. den Berg, *Analyst* **114** (1989) 1527.

[62] C. M. G. van den Berg, *Analytical Chemistry* **78** (2006) 156.

[63] M. M. Ghoneim, A. M. Hassanein, E. Hammam and A. M. Beltagi, *Fresenius' journal of analytical chemistry* **367** (2000) 378.

[64] A. E. Witter, B. L. Lewis and G. W. L. III, *Deep-Sea Research, Part II: Topical Studies in Oceanography* **47** (2000) 1517.

[65] O. Mikkelsen and K. H. Schroder, *Electroanalysis* **16** (2004) 386.

[66] O. Mikkelsen, C. M. G. van den Berg and K. H. Schoeder, *Electroanalysis* **18** (2006) 35.

[67] N. Y. Stozhko, O. V. Inzhevatova and L. I. Kolyadina, *Journal of Analytical Chemistry* **60** (2005) 668.

[68] J. Santos-Echeandia, *Talanta* **85** (2011) 506.

[69] E. Bednarkiewicz and Z. Kublik, *Journal of Electroanalytical Chemistry and Interfacial Electrochemistry* **106** (1980) 61.

[70] T. Nomura, *Journal of Electroanalytical Chemistry and Interfacial Electrochemistry* **124** (1981) 213.

[71] K. Torrance and C. Gatford, *Analyst* **111** (1986) 359.

[72] C. M. G. V. den Berg, *Science of the Total Environment* **49** (1986) 89.

[73] W. Davison, J. Buffle and R. Devitre, *Pure and Applied Chemistry* **60** (1988) 1535.

[74] J. Golimowski, *Analytical Letters* **22** (1989) 481.

[75] W. Jin and J. Wang, *Analytica Chimica Acta* **245** (1991) 77.

[76] P. A. M. Farias, A. Kohara and S. L. G. Ferreira, *Analytical Letters* **25** (1992) 1929.

[77] Y. Nagaosa and A. M. Bond, *Electroanalysis* **4** (1992) 581.

[78] J. Wu and G. W. I. Luther, *Limnology and Oceanography* **39** (1994) 1119.

[79] R. Naumann, W. Schmidt and H. G, *Fresenius' journal of analytical chemistry* **349** (1994) 643.

[80] M. E. V. Diaz, J. C. J. Sanchez, M. C. Mochon and A. G. Perez, *Analyst (Cambridge, United Kingdom)* **119** (1994) 1571.

[81] O. Abollino, M. Aceto, G. Sacchero, C. Sarzanini and E. Mentasti, *Analytica Chimica Acta* **305** (1995) 200.

[82] C. Locatelli, *Talanta* **43** (1996) 45.

[83] J. Zarebski, *Fresenius' journal of analytical chemistry* **356** (1996) 299.

[84] Z. Gao and K. S. Siow, *Talanta* **43** (1996) 727.

[85] N. A. El-Maali, Y. M. Temerk and M. S.-A. El-Aziz, *Analytica Chimica Acta* **353** (1997) 313.

[86] Z. Jiang, X. Liu, M. Zhao and W. Mo, *Analytica Chimica Acta* **354** (1997) 359.

[87] M. Gledhill, C. M. G. van den Berg, R. F. Nolting and K. R. Timmermans, *Marine Chemistry* **59** (1998) 283.

[88] M. Gawrys and J. Golimowski, *Electroanalysis* **11** (1999) 1318.

[89] M. H. Pournaghi-Azar and B. M. Fatemi, *Microchemical Journal* **65** (2000) 199.

[90] T. Nagai, A. Imai, K. Matsushige, K. Yokoi and T. Fukushima, *Limnology* **5** (2004) 87.

[91] P. C. Nascimento, L. D. Del-Fabro, D. Bohrer, L. M. de Carvalho, M. B. Rosa and S. M. Noremberg, *Electroanalysis* **20** (2008) 1078.

[92] L. M. Laglera, G. Battaglia and C. M. G. van den Berg, *Marine Chemistry* **127** (2011) 134.

[93] C. C. Young and H. A. Laitinen, *Analytical Chemistry* **44** (1972) 457.

[94] K. Z. Brainina, E. M. Roizenblat, V. B. Belyavskaya, N. K. Kiva and T. I. Fomicheva, *Zavodskaya Laboratoriya* **33** (1967) 274.

[95] J. A. Cox and M. Majda, *Analytica Chimica Acta* **118** (1980) 271.

[96] J. D. Strycker, P. Westbroek and E. Temmerman, *Journal of Electroanalytical Chemistry* **565** (2004) 149.

[97] L. L. Barbosa, G. A. O. Brito, M. C. Lopez, R. L. Broggi and I. A. Carlos, *Electrochimica Acta* **50** (2005) 4710.

[98] N. Scheers, T. Andlid, M. Alminger and A.-S. Sandberg, *Electroanalysis* **22** (2010) 1090.

[99] X. Diao and K. Sumi, *Analytical Sciences* **26** (2010) 681.

[100] N. Y. Stozhko, N. A. Malakhova, M. V. Fyodorov and K. Z. Brainina, *Journal of Solid State Electrochemistry* **12** (2008) 1185.

[101] Z. Gao, P. Li and Z. Zhao, *Talanta* **38** (1991) 1177.

[102] J. Wang and T. Martinez, *Electroanalysis* **1** (1989) 167.

[103] G. Lu, X. Yao, X. Wu and T. Zhan, *Microchemical Journal* **69** (2001) 81.

[104] T. M. Florence, *Journal of Electroanalytical Chemistry and Interfacial Electrochemistry* **26** (1970) 293.

[105] K. Ogura and Y. Miwa, *Journal of Electroanalytical Chemistry and Interfacial Electrochemistry* **111** (1980) 253.

[106] J. W. Dieker and W. E. V. der Linden, *Analytica Chimica Acta* **114** (1980) 267.

[107] C. Hua, D. Jagner and L. Renman, *Talanta* **35** (1988) 597.

[108] Z. Gao, P. Li, G. Wang and Z. Zhao, *Analytica Chimica Acta* **241** (1990) 137.

[109] S. Yang, L. Du and B. Ye, *Microchemical Journal* **52** (1995) 216.

[110] A. Komersova, M. Bartos, K. Kalcher and K. Vytras, *Journal of pharmaceutical and biomedical analysis* **16** (1998) 1373.

[111] P. Ugo, L. M. Moretto, D. Rudello, E. Birriel and J. Chevalet, *Electroanalysis* **13** (2001) 661.

[112] A. Domenech-Carbo, M. T. Domenech-Carbo, J. V. Gimeno-Adelantado, F. Bosch-Reig, M. C. Sauri-Peris and S. Sanchez-Ramos, *Analyst (Cambridge, United Kingdom)* **126** (2001) 1764.

[113] P. Ugo, L. M. Moretto, A. D. Boni, P. Scopece and G. A. Mazzocchin, *Analytica Chimica Acta* **474** (2002) 147.

[114] D. Kladekova, M. Galova and L. Pikna, *Particulate Science and Technology* **23** (2005) 189.

[115] R. Segura, M. I. Toral and V. Arancibia, *Talanta* **75** (2008) 973.

[116] M. B. Gholivand, B. Geravandi and M. H. Parvin, *Electroanalysis* **23** (2011) 1345.

[117] D. I. Anguiano, M. G. Garcia, C. Ruiz, J. Torres, I. Alonso-Lemus, L. Alvarez-Contreras, Y. Verde-Gomez and E. Bustos, *International Journal of Electrochemistry* **739408** (2012) 6.

[118] A. Domenech-Carbo, S. Sanchez-Ramosa, M. T. Domenech-Carbo, J. V. Gimeno-Adelantado, F. Bosch-Reig, D. J. Yusa-Marco and M. C. Sauri-Peris, *Electroanalysis* **14** (2002) 685.

Chapter 8

Voltammetric Determination of Iron(III) in Water

In this chapter, a square wave voltammetric procedure is developed for the determination of trace amounts of Fe(III) at an unmodified edge plane pyrolytic graphite (EPPG) electrode and a screen printed electrode (SPE). This simple procedure was applied to real samples of commercial bottled mineral water. Sensitive results in the micromolar region were achieved without modification of the electrode. Using the WHO guideline limits for the Fe(III) concentration in drinking water, recovery percentages at an EPPG gave 103 % and 107 %, and 98.6 % and 95.0 % at a SPE for the 5.36 μM (0.3 mg L^{-1}) and 53.6 μM (3.0 mg L^{-1}) additions of Fe(III), respectively.

The work presented in this chapter has been published in *Electroanalysis*, 25, (2013), 1123-1129.

8.1 Introduction

The existence of iron in the environment is abundant. Its oxidation states range from -II to +VI [1], however it is overwhelmingly most commonly seen as ferrous (+II) and ferric (+III) ions in the environment. Many analytical methods have been developed to detect and quantify iron as detailed in the review [2]. Anodic and cathodic stripping

voltammetry have shown good selectivity and is highly favoured due to their inexpensive, simple and rapid nature [3]. In addition to this, square wave voltammetry and differential pulse voltammetry are commonly utilized for ultra sensitive detection.

In the interest of developing mercury-free electrodes to avoid the drawbacks of mercury toxicity [4, 5], carbon electrodes have repeatedly been targeted as an electrode material. Carbon is an ideal replacement material for mercury as it possesses properties that lend itself adequately for analytical studies [6–9]. Carbon is also widely used due to its cheap and disposable nature. In the past, many methods involve chemical modification of the electrode surface, however such modifications may often complicate the process and can be costly. The procedure described within this chapter involves the use of an unmodified EPPG electrode and cheap and disposable screen printed electrodes (SPEs) for the detection of Fe(III). Previously, Stefan et al [10] have used diamond paste electrodes to give extremely sensitive voltammetric determination of iron with a limit of detection of 13 pM, however this is far below the WHO guideline recommendation of 0.3 mg L^{-1} – 3.0 mg L^{-1} in drinking waters. Here, a simple and cheap square wave voltammetric procedure is shown and applied on commercially bottled water samples, highlighting the possible application of these unmodified carbon electrodes for trace iron detection.

8.2 Experimental

8.2.1 Apparatus and Reagents

A standard three-electrode configuration was used throughout which included a platinum (Pt) mesh counter electrode and a silver – silver chloride in saturated KCl reference electrode (Ag/AgCl) (Radiometer, UK). The working electrode in the two cases investigated

was an edge plane pyrolytic graphite (EPPG) electrode and a screen print electrode (SPE). Details of the carbon electrodes used are described in the Experimental Methods chapter.

A 1 mM stock solution of Fe(III) was freshly prepared daily by dissolving the appropriate quantity of $Fe_2(SO_4)_3.5H_2O$ in deionised water. Pure HNO_3 acid was used to eliminate the presence of trace contaminants in the solution.

KNO_3 provided ionic support for the electrolyte solution. The test water sample for real data analysis was supermarket purchased Buxton still natural mineral water from the Peak District of the UK. Analytical data from the bottle does not state the amount of iron present, however a range of other ions such as calcium, magnesium, potassium, sodium is included, along with the pH at source, specified at 7.4.

8.2.2 Experimental Procedure

A 10 mL volume of 0.01 M HNO_3 and 0.1 M KNO_3 (pH 2.08) was transferred into an electrochemical cell and a degassed system was set up after purging with nitrogen for a minimum of 20 minutes to remove the dissolved oxygen in solution. Where the working electrode used was an EPPG, a standard three electrode configuration was set up before accurate additions of Fe(III) from stock solution were made to the deoxygenated cell. Cathodic linear sweep measurements were performed, however after a series of optimisation experiments, it was noted that more sensitive results could be achieved using square wave voltammetry.

Consecutive additions of Fe(III) were pipetted into the solution with no need to clean the surface of the EPPG electrode electrochemically or otherwise within each set of additions. Renewal of the carbon surface was required, however, before each set of standard additions to ensure a clean blank surface of the working electrode. This was simply

achieved by polishing the electrode with 1.0 μm alumina slurry on soft lapping pads, followed by sonication and thorough rinsing using deionised water. The sensitive trace nature of the experiment required stringent conditions where all glassware were cleaned such that no contaminants were present. This was performed in green acid (made by dissolving potassium permanganate in concentrated sulphuric acid) whereby glassware were soaked for a minimum of 20 minutes and then thoroughly rinsed and sonicated with deionised water before use. The platinum mesh was flamed before the experiment to ensure a clean set-up.

For the screen printed electrodes, similar additions of Fe(III) were made to the cell, however, a small aliquot of solution was pipetted from the pot and onto the electrode surface. No polishing was needed for the SPEs before use, though repeated scans were seen to optimise the iron signal.

8.3 Results and Discussions

8.3.1 Optimisation of the EPPG Electrode

A range of parameters was explored to optimise the square wave procedure prior to the experiments. The optimal peak signal corresponding to iron was found at E_p = 0.58 V. Scans in normal linear sweep voltammetry (LSV) gave a reduction signal for iron, however more sensitive peaks were given in square wave voltammetry. In addition, scan rates and modulation amplitudes were varied to optimise the Fe(III) reduction peaks. Initial experiments also showed the presence of an active quinone group at 0.35 V on the surface of the carbon EPPG electrode which increased in peak height upon consecutive scans in the potential range +1.3 V to -0.25 V. This peak could be seen to stabilise after

10 repeated cycles, so this step was incorporated within the procedure prior to Fe(III) additions.

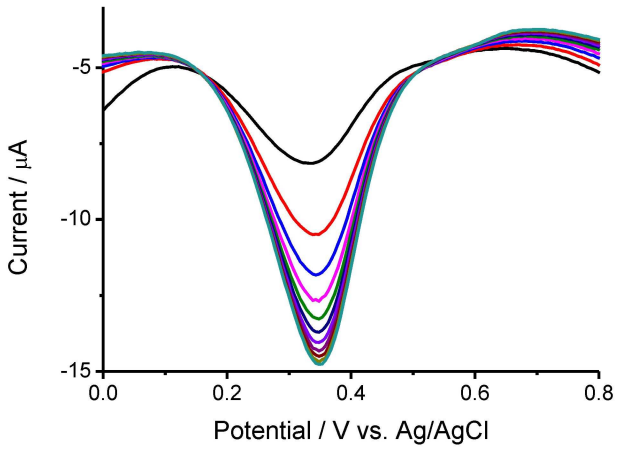


Figure 8.1: Stabilisation of the surface quinone peak by repeated cycling on a EPPG electrode in 0.01 M HNO_3 and 0.1 M KNO_3

Figure 8.1 shows the quinone peak stabilising after repeated cycling in a blank solution of 0.01 M HNO_3 and 0.1 M KNO_3. The effect of pH was also investigated between pH 1.08 and 3.09, and it could be seen that the quinone reduction peak shifted to lower potentials with increasing pH; the electrolyte solution had a measured pH value of 2.08. The optimised square wave parameters for the EPPG electrode were: frequency – 10 Hz, scanning from +1.3 V $\rightarrow$ 0.25 V, step potential – 5 mV, amplitude – 20 mV, equilibrium threshold – 0.05 A. Similar parameters were used for the SPE, however the scan was from +0.5 $\rightarrow$ -0.5 V.

8.3.2 Fe(III) Analysis on EPPG Electrode

The surface of the EPPG did not need electrochemical activation or pretreatment before use. After thorough polishing, as noted above, the electrode was placed in a degassed cell

and fifteen aliquots of 1 μM Fe(III) were consecutively added to the electrochemical cell containing 0.01 M HNO_3 and 0.1 M KNO_3, and a reduction peak was recorded after each addition, representing the reaction $Fe^{3+} + e^- \rightarrow Fe^{2+}$. A defined peak was seen upon the very first addition with high sensitivity. Figure 8.2 depicts a voltammetric graph showing 15 consecutive additions of Fe(III).

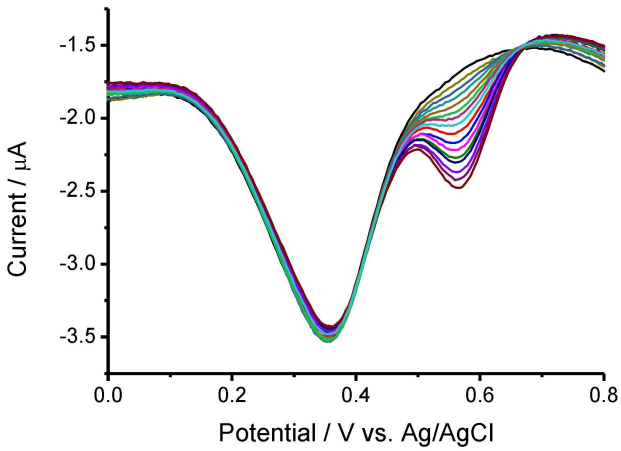


Figure 8.2: Voltammetric graph showing 15 consecutive 1 μM additions of Fe(III) on EPPG in 0.01 M HNO_3 and 0.1 M KNO_3 and its subsequent reduction

After background subtraction, the influence of the quinone group can be removed, and a clear Fe(III) peak can be seen to increase with increasing Fe(III) concentration as seen in Figure 8.3. An inset showing the linear progression of the peak height against increasing concentration is also given. The calibration plots give high linearity with an R^2 value of 0.997 for peak height. The limit of detection (LOD), calculated using 3 x standard deviation (3σ) divided by the slope [11] gave a value of 2.00 $\pm$ 0.01 μM.

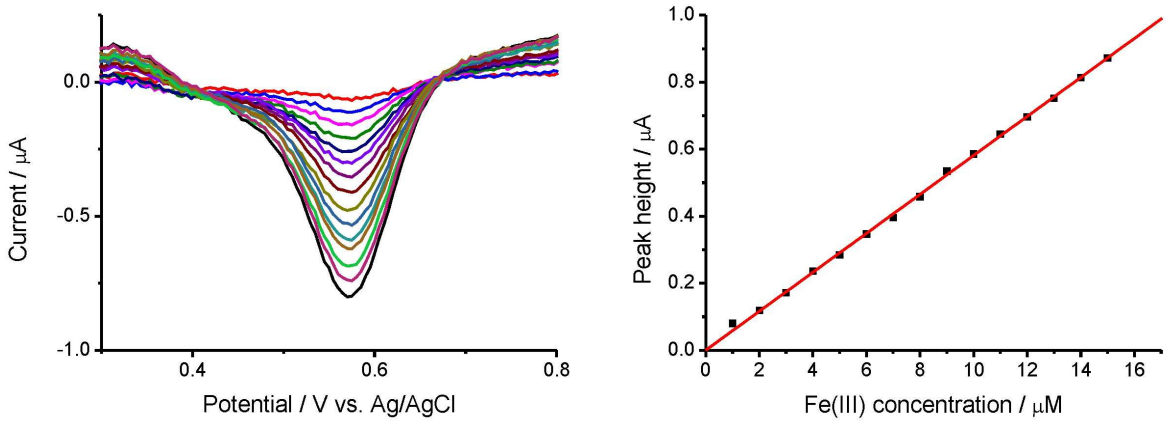


Figure 8.3: Left: Background subtracted version of Fe(III) additions on EPPG. Right: Linear plots of the peak height against concentration.

8.3.3 Analysis of Real Samples

After establishing the parameters needed for Fe(III) to be detected at an EPPG, a test sample of bottled mineral water was analysed. The predominating species within environmental samples is assumed to be Fe(III), however presence of other iron species may also exist in trace quantities.

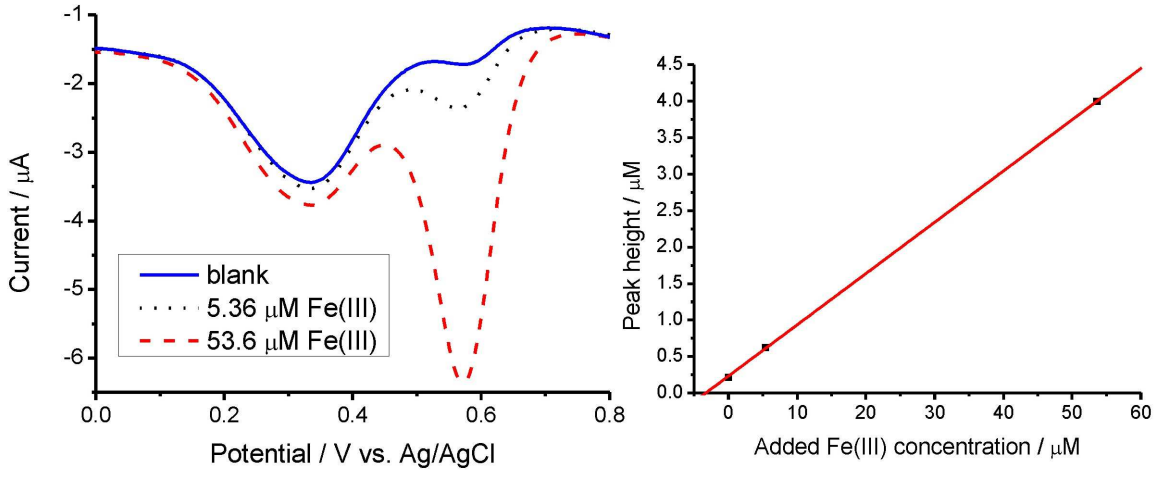


Figure 8.4: Voltammetric graph of blank acidified Buxton water with 5.36 μM and 53.6 μM Fe(III) spiked samples at an EPPG electrode

A 10 mL sample of supermarket Buxton still mineral water was acidified with HNO_3 and KNO_3 to the experimental conditions established previously, and scans were taken to determine the iron concentration within the test sample. A trace amount of iron could be seen to exist in the solution, and further amounts of Fe(III) were used to spike the sample with the upper and lower limits of acceptable concentrations of Fe(III) in drinking water as stated by the WHO, as seen in Figure 8.4.

A set of standard additions were added to a blank, 5.36 μM and 53.6 μM Fe(III) spiked solution of acidified Buxton water for recovery analysis to be performed. The form of the voltammetric peaks could be enhanced by subtracting the polynomial baseline and thus improving the peak shape without interference from the quinone reduction peak. Peak height against added Fe(III) concentration graphs were produced for the blank sample (Figure 8.5), 5.36 μM Fe(III) spiked sample (Figure 8.6) and 53.6 μM Fe(III) spiked sample (Figure 8.7).

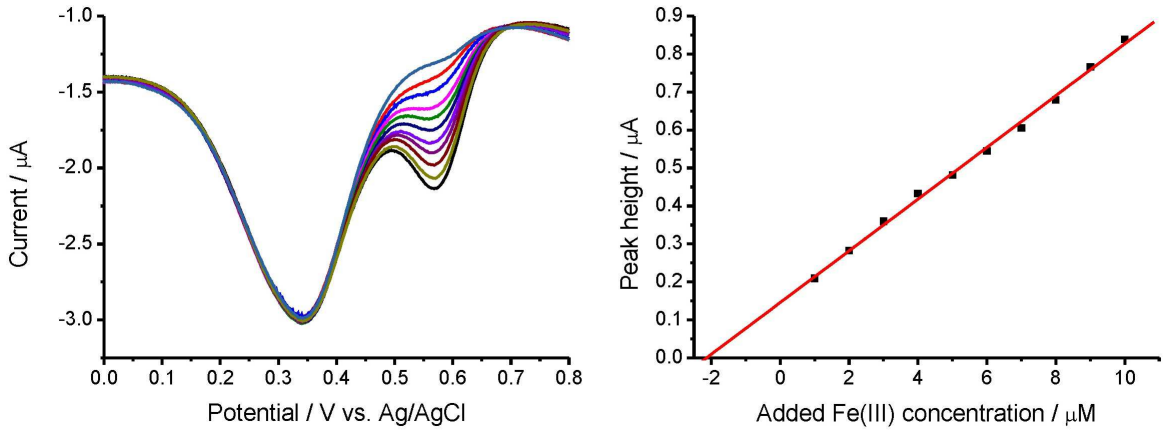


Figure 8.5: Left: 1 μM Fe(III) consecutive additions on EPPG electrode, added to blank acidified Buxton water. Right: extrapolated plot to determine concentration of Fe(III) in blank sample

Highly linear plots for the EPPG revealed that the solution contained 2.14 μM Fe(III)

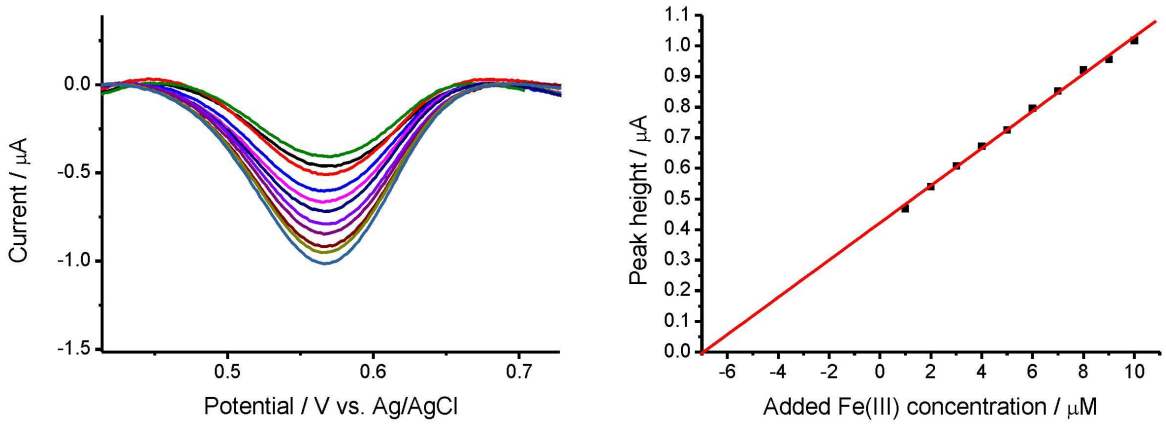


Figure 8.6: Left: Polynomial baseline subtracted voltammetric peaks of 1 μM Fe(III) consecutive additions at an EPPG electrode to spiked 5.36 μM Fe(III) in acidified Buxton water. Right: extrapolated plot to determine concentration of Fe(III) in spiked 5.36 μM Fe(III) sample

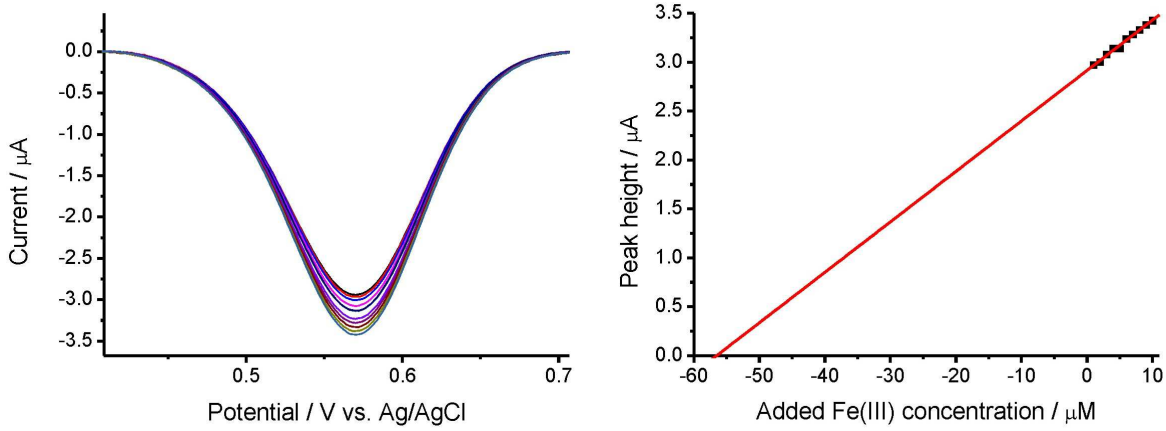


Figure 8.7: Left: Polynomial baseline subtracted voltammetric peaks of 1 μM Fe(III) consecutive additions at an EPPG electrode to spiked 53.6 μM Fe(III) in acidified Buxton water. Right: extrapolated plot to determine concentration of Fe(III) in spiked 53.6 μM Fe(III) sample

within the bottled sample, and the recovery percentages for the 5.36 μM and 53.6 μM additions were 103% and 107% respectively. The sensitivity of the unspiked sample was calculated to be 0.06 μA μM^{-1}, whilst in the spiked samples, values for the 5.36 μM and 53.6 μM additions were 0.07 μA μM^{-1} and 0.06 μA μM^{-1}, respectively. The response

characteristics of the bare EPPG demonstrated their high suitability for the determination of Fe(III) in water samples. Table 8.1 highlights the performance obtained with this method compared to a selection of results from other publications.

Technique [a]	Electrode [b]	Modifier/Complexing agent (if any) [c]	Speciation	*LOD* (M)	Sensitivity (μA μM^{-1})	Year	Reference
SWV	EPPG	N/A	Fe(III)	2.0 x 10^{-6}	0.06	2013	This method
CSV	Rotating GCE	N/A	Fe(III)	1.0 x 10^{-5}	NR	1972	[12]
MSWV	GCE	Nafion coated	Fe(II)	1.5 x 10^{-6}	0.24	2001	[13]
DPASV	Diamond paste electrode	N/A	Fe(III)	1.0 x 10^{-13}	NR	2003	[10]
CSV	Gold microwire	Mercury coated	Fe(III)	1.0 x 10^{-8}	NR	2006	[11]
CSV	GCE	Bismuth film, TEA	Fe(III)	7.7 x 10^{-9}	0.88	2005	[14]
SWAdSV	GCE	Bismuth film, PAN	Fe(III)	1.8 x 10^{-9}	NR	2008	[15]
CVA	CME	Gold modified	Fe(tot)	1.3 x 10^{-8}	NR	2012	[16]

Table 8.1: [a] SWV: square wave voltammetry, CSV: cathodic stripping voltammetry, DPASV: differential pulse anodic stripping voltammetry, SWAdSV: square wave adsorptive stripping voltammetry, MSWV: multiple square wave volammetry, CVA: cyclic voltammetric analysis [b] EPPG: edge plane pyrolytic graphite, GCE: glassy carbon electrode, CME: carbon microelectrode ensemble [c] TEA: triethanolamine, PAN: 1-(2-piridylazo)-2-naphthol

Further to this, screen printed electrodes (SPEs) were tested for their suitability in determining Fe(III) concentrations, as a means for a cheap and disposable electrode for trace Fe(III) detection. A cell containing 10 mL acidified Buxton water was prepared under degassed conditions, and 1 μM Fe(III) additions were added to the pot before subsequently transferred onto the surface of the SPE. A 20 μL aliquot of solution was pipetted onto the surface on the screen print electrode for analysis each time.

Sets of experiments were performed on a single SPE electrode, by carefully wiping off the sample solution using a tissue and transferring a new droplet onto the surface. The potential window was shifted to +0.5 $\rightarrow$ -0.5 V for the new electrode material, as the reduction peak was observed at a lower potential of 0.05 V. Analogous recovery experiments were performed on the SPE using 5.36 μM and 53.6 μM as the spiked concentrations. Linear peak height against added Fe(III) concentration plots were produced, as

seen in Figures 8.8 - 8.10, and the best fit line was extrapolated to calculate high recovery percentages, giving 98.6% and 95.0% respectively.

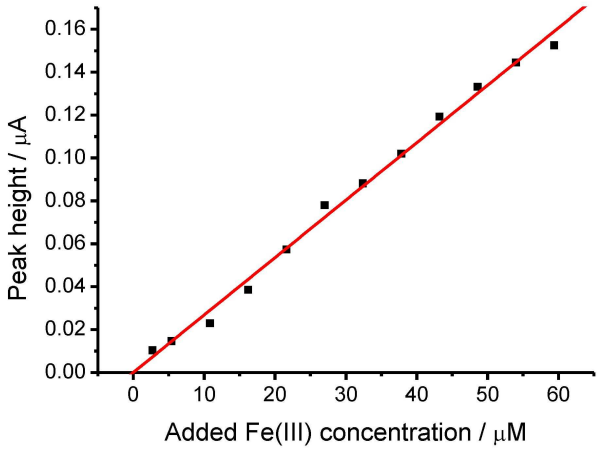


Figure 8.8: Linear extrapolation of acidified blank Buxton water sample on SPE

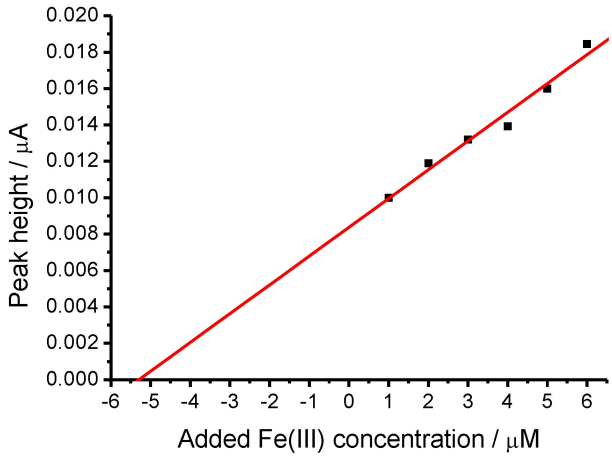


Figure 8.9: Linear extrapolation of 5.36 μM Fe(III) spiked solution of acidified Buxton water sample on SPE

The recovery percentage of iron was calculated using: Recovery % = $(x_s$ - $x)/x_{add}$ x 100%, where x_s = calculated concentration of spiked samples, x = calculated concentration of unspiked samples and x_{add} = amount of added analyte. For the SPE, the sensitivity of the unspiked sample was determined to be 0.003 μA μM^{-1}, whilst in the

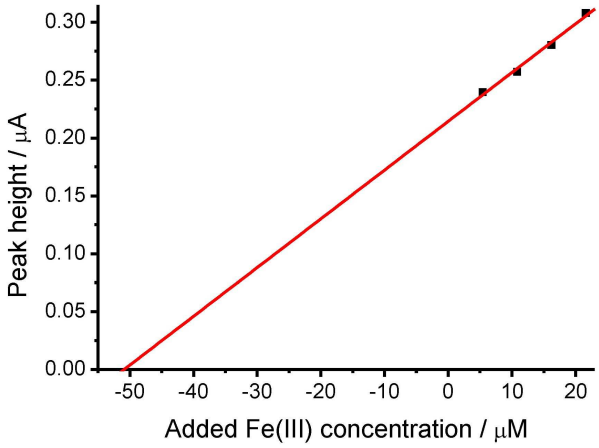


Figure 8.10: Linear extrapolation of 53.6 μM Fe(III) spiked solution of acidified Buxton water sample on SPE

5.36 μM and 53.6 μM spiked samples, the sensitivities were 0.002 μA μM^{-1} and 0.004 μA μM^{-1}, respectively.

8.4 Conclusions

Sensitive detection of Fe(III) can be carried out to levels below the WHO guideline limit of 5.36 μM (0.3 mg L^{-1}) and 53.6 μM (3.0 mg L^{-1}) at an unmodified edge plane pyrolytic graphite electrode and screen printed electrode using square wave voltammetry. The unmodified electrodes offer attractive properties such as low detection limit, affordability and simplicity which is highly valuable within electroanalytical work. The low detection limit of 2.00 μM on an EPPG allows the determination of iron in water samples to be possible, whilst the cheap and disposable nature of SPEs lead to the possibility for the design of portable voltammetric analysis for iron detection whilst being also the basis for a cheap mercury free approach to iron.

Aside from detecting analytes in solution, another important voltammetric sensor

involves the detection of pH of solutions. In the next chapter, a voltammetric pH sensor based on an edge plane pyrolytic graphite electrode is realised for a view to a novel carbon based pH sensor.

Bibliography

[1] S. Pehkonen, *Analyst (Cambridge, United Kingdom)* **120** (1995) 2655.

[2] M. Lu, N. V. Rees, A. S. Kabakaev and R. G. Compton, *Electroanalysis* **24** (2012) 1693.

[3] T. Miwa, *The Journal of Materials Science* **33** (1994) 374.

[4] R. F. Palmer, S. Blanchard, Z. Stein, D. Mandell and C. Miller, *Health place* **12** (2006) 203.

[5] F. Zahir, R. F. Zahir, S. J. Rizwi, S. K. Haq and R. H. Khan, *Environmental toxicology and pharmacology* **20** 351.

[6] S. E. W. Jones and R. G. Compton, *Current Analytical Chemistry* **4** (2008) 170.

[7] K. Kalcher, I. Svancara, R. Metelka, K. Vytras and A. Walcarius, *Section Title: Inorganic Analytical Chemistry*, volume 4, 283 (2006).

[8] C. E. Banks and R. G. Compton, *Analytical Sciences* **21** (2005) 1263.

[9] N. Y. Stozhko, N. A. Malakhova, M. V. Fyodorov and K. Z. Brainina, *Journal of Solid State Electrochemistry* **12** (2008) 1185.

[10] R.-I. Stefan, S. G. Bairu and J. F. van Staden, *Instrumentation Science & Technology* **31** (2003) 411.

[11] J. Gun, P. Salauen and C. M. G. van den Berg, *Analytica Chimica Acta* **571** (2006) 86.

[12] M. Stulikova and F. Vydra, *Journal of Electroanalytical Chemistry and Interfacial Electrochemistry* **38** (1972) 349.

[13] P. Ugo, L. M. Moretto, D. Rudello, E. Birriel and J. Chevalet, *Electroanalysis* **13** (2001) 661.

[14] A. Bobrowski, K. Nowak and J. Zarebski, *Analytical and Bioanalytical Chemistry* **382** (2005) 1691.

[15] R. Segura, M. I. Toral and V. Arancibia, *Talanta* **75** (2008) 973.

[16] G. N. Noskova, E. A. Zakharova, V. I. Chernov, A. V. Zaichko, E. E. Elesova and A. S. Kabakaev, *Analytical Methods* **3** (2011) 1130.

Chapter 9

Voltammetric pH Sensor based on an Edge Plane Pyrolytic Graphite Electrode

pH measurements have an extensive number of applications in virtually every industry. Here, a simple sensor for pH determination is reported using unmodified edge plane pyrolytic graphite (EPPG) electrodes. The analysis is based on the electro-reduction of surface quinone groups on the EPPG which was characterised using cyclic voltammetry (CV) and optimised with square-wave voltammetry (SWV). Under optimised conditions, a linear response is observed between the peak potential and pH with a gradient of *ca.* 59 mV per pH at 298 K, which corresponds well with Nernstian behaviour based on a 2 proton/2 electron system over the aqueous pH range 1.0 to 13.0. As such, an EPPG is suggested as a reagent free and robust pH sensing material.

The work presented in this chapter has been published in *Analyst*, 139, (2014), 2397-2403.

9.1 Introduction

The determination of pH is fundamental to the study of chemical and biochemical reactions in aqueous solution, with measurements carried out extensively in both industrial

and academic environments [1]. Its widespread application includes uses in the food industry, agriculture, the biopharmaceutical industry, medicine and water treatment [2–4].

pH sensors are mainly potentiometric or amperometric [5, 6], however methods for pH determination also include using fluorescent agents [7, 8] and NMR methods [9] amongst many others [10]. At present, the use of glass electrodes [11] is the most common potentiometric approach due to their high sensitivity and selectivity, reasonably fast response, availability from commercial sources, and if carefully handled, long lifetimes. They are, however, fragile due to their glass nature and can be impractical to use for in-field analysis. In addition, glass electrodes can suffer from instability and potential drift [12] as a result of decreased sensitivity towards hydrogen activity caused by dehydration of the glass membrane [13]. They also suffer from alkali errors [14]. This approach requires regular and frequent re-calibration prior to use. Amperometric pH sensors utilising polymer films [15, 16], enzymes [17] and organic redox species [13] have been explored to address the various drawbacks related to potentiometric sensing.

Amperometric electrochemical pH sensors featuring polymer films or chemical modification of the electrode often involve attaching quinone functionality onto the surface [18]. Tarasevich et al. [19] observed redox processes related to quinoid group reactions, and further investigations revealed the effect of pH on these redox processes. The voltammetric response can be quantified using the Nernst equation [20],

$$E_p = E^o_{formal} - \frac{2.3RTm}{nF}pH \tag{9.1}$$

where m, n = number of protons and electrons involved in the redox process, respectively. There is thus a correlation between the peak potential and pH for the reduction of

quinones. In particular, for $n = 2$, slopes of *ca.* 0, 30 and 60 mV per pH unit are seen for $m = 0$, 1 and 2. The response of the quinone reduction has been reviewed by Guin et al. [21] and forms the basis of many modified pH sensors. A schematic showing three possible reduction pathways of an ortho-benzoquinone, along with associated protonations is given in Figure 9.1 where $n = 2$ and $m = 0$, 1, 2.

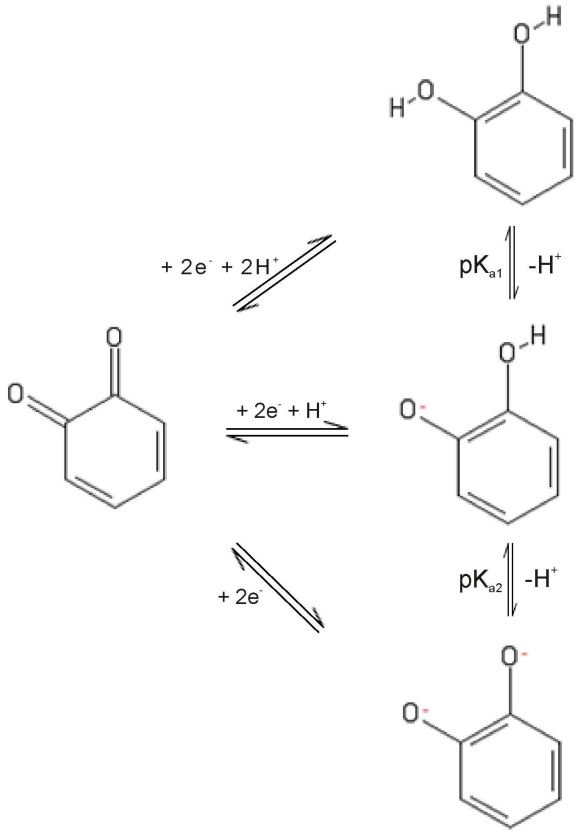


Figure 9.1: Schematic showing 3 pathways in which an orthoquinone molecule can be reduced in a $2e^-$ fashion with m = 0, 1 or 2

Literature pK_a values for ortho-benzoquinone are pK_{a1} 9.25 and pK_{a2} 13.0 in aqueous solution at 298 K [22]. Quinones and their electrochemical properties have been extensively studied previously, and the $2H^+/2e^-$ scheme of squares model [23] has been proposed assuming that electron transfer is the rate limiting step and the H^+ are at

equilibrium in well buffered media [24].

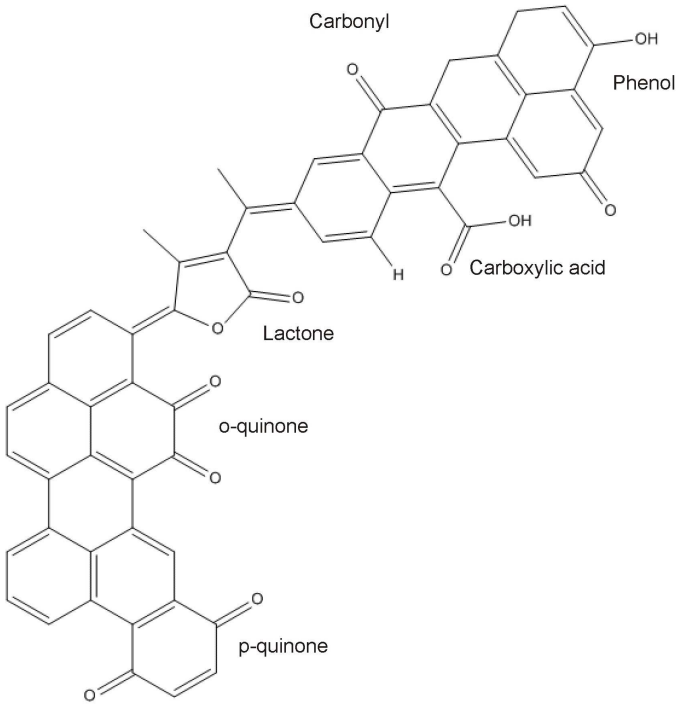


Figure 9.2: Representation of various functional groups present on graphitic carbon surfaces, adapted from [29]

Carbon is a highly attractive material, commonly employed in electrochemistry and widely used as an electrode material [25–27]. This can be attributed to its good conductivity, ready availability, versatility, wide working potential range and low cost. The surface chemistry of carbon is highly complex, extensive, and often decorated with many functional groups which sometimes can react easily with other molecules [28, 29]. A representation of various functional groups present on graphitic carbon surfaces is shown in Figure 9.2 [29].

Characterisation of the carbon surface has been studied by many researchers to identify surface oxo-groups [28, 30, 31]. In the case of edge plane pyrolytic graphite (EPPG) electrodes, the defect sites present on the carbon surface can easily react with oxygen

in the atmosphere to form a variety of oxo-groups on the surface, including quinonyl, carbonyl and hydroxyl functional groups [28] and these are suggested sites for electron transfer processes [32].

Carbon materials with surface modification and derivatization have been developed for reliable pH determination; Kahlert comprehensively summarises many of these methods [1]. Some patents have also been filed using functionalized carbon electrodes as a basis for electrochemical pH sensors [33–36].

In this chapter, in contrast and novelly, the intrinsic presence of quinone groups available on EPPG surfaces is exploited and cyclic voltammetry (CV) and square wave voltammetry (SWV) is used to study the effect of pH on the reduction of the surface quinones. It is surprising and somewhat unexpected, but very useful that a linear response was observed over the entire pH range. Given that the pK_a of ortho-benzoquinone is 9.25 in solution, one would expect a gradient consistent for $m = 2$ to be limited to *ca.* pH 9.0 and below; however here, a linear pH dependent response up to pH 13.0 at an EPPG electrode is reported. The observed shift in reduction peak potential is in good agreement with the theoretically predicted value of *ca.* 58 mV per pH for T = 298 K, for a Nernstian manner, suggesting the feasibility for the EPPG electrode to work as a pH sensor over the full pH range 1.0 to 13.0. Note that previous studies [37–39] have shown that very significant shifts for pK_a are possible for molecules tethered to carbon electrode surfaces and so in this light, the observed behaviour may be rationalised.

9.2 Experimental

9.2.1 Apparatus and Reagents

A standard three-electrode configuration consisting of a saturated calomel reference electrode (SCE), a platinum (Pt) mesh counter electrode and an edge plane pyrolytic graphite (EPPG) working electrode was used throughout.

All experiments were performed within a thermostatted Faraday cage (made in-house), to maintain a constant working temperature of 298 K. Temperature of the solutions were maintained at 298 ± 0.2 K throughout by placing the solutions within the Faraday cage for two hours to ensure thermal equilibrium. A constant temperature of 298 K was used to ensure that the reduction potential of the peaks do not shift with temperature. A thermometer was used for measurement of the solution during the experiment.

Buffer solutions were prepared as described in the Experimental Methods chapter.

9.2.2 Experimental Procedure

A range of buffer solutions were prepared and their pH determined using a pH meter prior to experiments. A small volume of each solution was taken and transferred into an electrochemical cell where a degassed system was established through thorough bubbling of pure N_2 into the vessel to remove dissolved oxygen in solution. The platinum mesh counter electrode was flamed before the experiment to ensure a clean set-up. The system was thermostatted to maintain temperature at 295 ± 0.2 K.

The surface of the EPPG electrodes were thoroughly polished using alumina slurry on soft lapping pads of decreasing grades, from 1.0 μm to 0.3 μm and finally 0.05 μm, followed by sonication and thorough rinsing using deionised water. With the EPPG

electrode acting as working electrode, cyclic voltammograms were performed to observe the redox properties of the surface quinones. However, optimised results were achieved by observing reductive cathodic scans with square wave voltammetry to more precisely determine the location of the peak potential. The optimised parameters for SWV were: frequency – 150 Hz, step potential – 2 mV, amplitude – 200 mV, over the entire pH range explored. The EPPG was used to scan in the cathodic direction, with the potential window adjusted for different pHs to best observe the reduction peak.

9.3 Results and Discussions

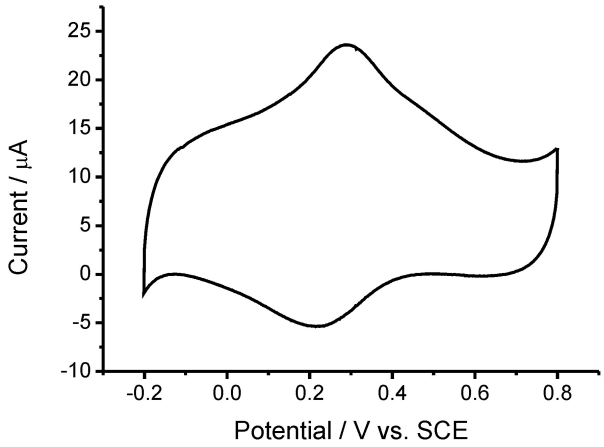


Figure 9.3: Typical CV of EPPG in 0.01 M HNO_3 + 100 mM KCl supporting electrolyte, from which surface coverage of quinone groups can be calculated

Initially, a cyclic voltammogram (CV) was recorded of the bare EPPG surface; a typical CV signal performed in 0.01 M HNO_3 with 100 mM KCl supporting electrolyte can be seen in Figure 9.3, with the peak potential of the quinone reduction occurring at 221 mV vs. SCE. From this, the surface coverage can be deduced by using the peak area of the reduction peak to determine the quinone surface coverage, according to $Q = nFA\Gamma$,

where Γ represents the surface coverage, n represents the number of electrons transferred per molecule, F is the Faraday constant and A is the electrode area. The average value for the surface coverage of quinones was calculated to be 5.9 x 10^{-11} ± 0.6 x 10^{-11} mol cm^{-2}, with $n = 2$. After establishing optimised parameters for the cathodic scans of the surface quinone reduction in square wave, all analyses were performed on the respective square wave voltammetric results.

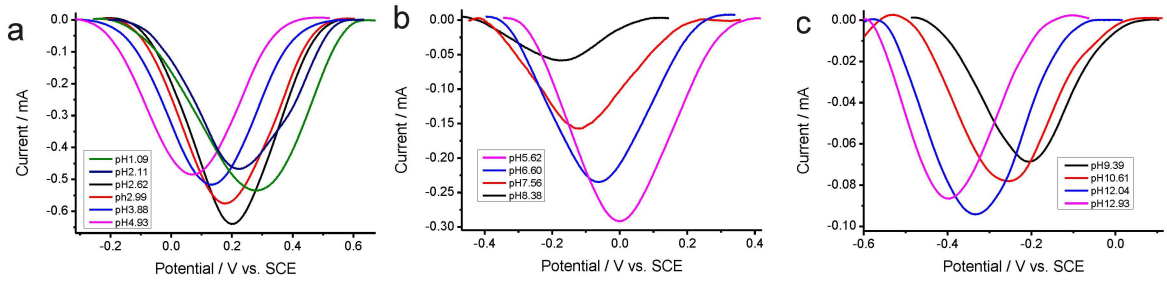


Figure 9.4: Quinone reduction peaks in square wave (SWV). 3 sets of peaks are shown, corresponding to the different media in which the reduction was performed; (a) 0.01 M HCl/KCl buffer and citrate buffer (pHs: 2.11, 2.62, 2.99, 3.88, 4.93), 0.1 M HCl/KCl buffer at pH 1.09 (b) 0.01 M phosphate buffer (pHs: 5.62, 6.60, 7.56, 8.38), (c) 0.01 M carbonate buffer and NaOH solutions (pHs: 9.39, 10.61, 12.04), 0.1 M NaOH buffer at pH 12.93. SWV performed under optimised conditions: frequency – 150 Hz, step potential – 2 mV, amplitude – 200 mV

Using a range of 0.01 M pH buffer solutions, a single peak was observed by scanning cathodically from positive to negative potentials in square wave voltammetry as shown in Figure 9.4. Since the pH for the 0.01 M HCl/KCl buffer solution was pH 2.11, and pH for the 0.01 M NaOH buffer solution was pH 12.04, a 0.1 M HCl/KCl and 0.1 M NaOH buffer solution was investigated and included for completeness to observe the response between the peak potential and full pH range. The pH of the 0.1 M HCl/KCl buffer in this case was 1.09. Three sets of reductions were performed which corresponds to solutions in the low (0.0 – 5.0), neutral (5.0 – 9.0) and high (9.0 – 14.0) pH range using HCl/KCl

and citrate buffer solutions, monosodium phosphate/disodium phosphate buffer solutions and sodium carbonate bicarbonate and sodium hydroxide solutions, respectively. Using HCl/KCl and citrate buffers, as in Figure 9.4(a), the reduction peak potential shifts from 222 mV at pH 2.11 to 71 mV at pH 4.93. Similarly, for other buffers shown in Figure 9.4(b) and (c), an increase in pH from 5.62 to 8.38 resulted in a peak potential shift from 1 mV to -172 mV, and for pH 9.39 to 12.9, the reduction peak potential changes from -207 mV to -402 mV, respectively. The potential window was increased for higher pH solutions to accommodate for the shift in potential with pH.

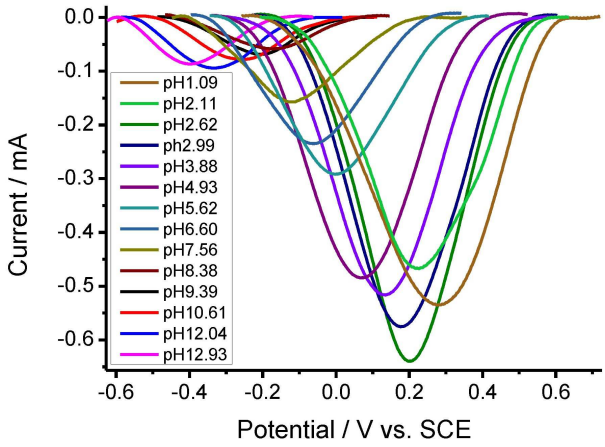


Figure 9.5: Quinone reduction peaks in square wave (SWV). Reduction peaks were obtained in different media (HCl/KCl buffer, citrate buffer, phosphate buffer, carbonate buffer and NaOH buffer solutions) at 0.01 M, ranging in pH from 2.11 to 12.04, 0.1M HCl/KCl buffer at pH 1.09 and 0.1 M NaOH at pH 12.93. SWV performed under optimised conditions: frequency – 150 Hz, step potential – 2 mV, amplitude – 200 mV

A composite of all the reductions peaks in different buffer solutions can be seen in Figure 9.5. It can be observed that by increasing pH, peak potentials shift in the cathodic direction towards more negative values. At high pH, there are fewer protons available for the $2H^+/2e^-$ reduction process, and as a result, probably limits the extent of quinone reduction resulting in less well resolved signals and lower currents. Background correction

and smoothing of the signals allowed enhancement of the peaks for analysis. Both methods were performed using GPES software; the background correction involved subtracting a 2^{nd} order polynomial baseline curve from the raw data, whilst background noise was smoothed using the Savitzky and Golay smoothing filter [40, 41].

Polishing of the EPPG electrode for 20 minutes prior to each experiment exposed surface quinone functional groups, which were used to explore the electrode response to varying pH. By measuring the peak potential of the reduction peaks in SWV and plotting against pH, a linear response could be seen in the pH 1.0 – 13.0 range, as shown in Figure 9.6. The gradient of the slope was 57.0 ± 1.0 mV per pH which is consistent with a linear Nernstian response corresponding to a two-electron, two-proton electrochemical process where m, n = number of protons and electrons involved in the redox process, respectively, T = 298 K.

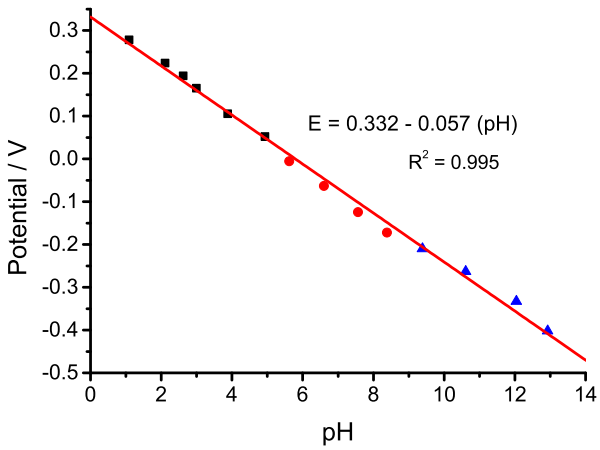


Figure 9.6: Calibration plot of SWV peak potential against pH for an EPPG in 0.01 M buffer solutions (with 0.1 M HCl KCl buffer solution at pH 1.09 and 0.1 M NaOH buffer solution at pH 12.93), showing a linear response with gradient of 57.0 mV per pH corresponding to a Nernstian behaviour. Black squares: low pH range, red circles: neutral pH range, blue squares: high pH range

The linear slope produced from the peak potential vs. pH graph highlights the pH

sensitive nature of the quinone groups on the surface of the EPPG electrode. By examining the pK_a values for ortho-benzoquinone in aqueous solution, pK_{a1} 9.25 and pK_{a2} 13.0 (Figure 9.1), it can inferred that significant differences in pK_a must exist between such molecules in bulk solution and similar structures present at the surface. If the surface quinones showed similar pK_a values to those displayed in solution, one would expect changes in gradient at high pH around pH 9.0 and 13.0. However, the gradient consistent for $m = 2$ was observed for the full aqueous pH 1.0 – 13.0 range. It can be assumed that deprotonation of the surface hydro-orthoquinone molecules does not occur below *ca.* pH 13, and so extensive pH measurements can be carried out even at high pH without the need for modification of the electrode to achieve a linear Nernstian response. We note that significant changes in pK_a have been reported for molecules immobilised on electrode surfaces [37–39, 42].

The mechanism of the quinone reduction in neutral solutions, involving a 2 proton/2 electron process, can lead to charged intermediates being possibly formed. At neutral pHs, this can be a semi-quinone species. Stabilization of semiquinone intermediates have been proposed in the literature [42].

To explore the possibilities of semi-quinones contributing to the SWV signal, the SWV parameters were altered, and the amplitude lowered from 200 mV to 20 mV. It was observed that phosphate buffers within the pH range 5.0 – 9.0 produced a double peak or splitting of the peak. Their reduction in SWV with amplitude 20 mV can be seen Figure 9.7(a) whilst the overcompensated scans at 200 mV amplitude can be seen in Figure 9.7(b). Lowered amplitude parameters with buffers outside of the neutral pH range were also investigated, but produced just one single peak, which suggests that the semiquinone intermediate is stabilised observed only in environments around pH 7.

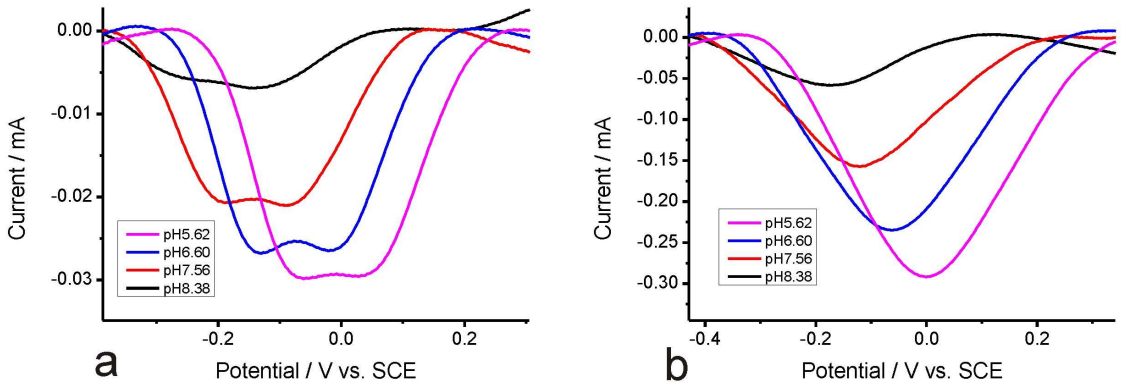


Figure 9.7: Reduction peaks on EPPG electrode in 0.01 M phosphate buffer solution, (a) shows reduction peaks with amplitude 20 mV, whereas (b)shows the peak under optimised conditions of amplitude 200 mV

The reduction potential of the double peaks shown in Figure 9.7(a) were plotted in Figure 9.8, together with the reduction peaks obtained with amplitude 200 mV. The red circles and black squares represent the two positions of the double peak reduction, whilst the blue triangles correspond to the peaks with amplitude 200 mV. It can be seen that the position of the reduction peaks at the higher amplitude is intermediate between the split peak values.

9.3.1 Investigating the Effects of changing Ionic Strength and Buffer Concentration

Having calibrated successfully for the 0.01 M buffer solutions, further investigation into higher concentration solutions were performed to see the effects of increasing ionic strength.

0.1 M citrate, phosphate and carbonate buffer solutions all produced a single reduction peak as seen in Figure 9.9. Taking the reduction peak potential and plotting against pH, as in Figure 9.10, the calibration gives a linear response with a gradient of 59.0 mV per pH.

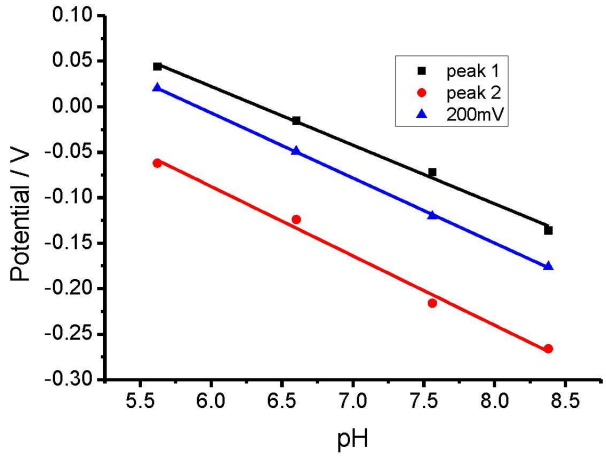


Figure 9.8: Calibration plot showing both peak 1 and peak 2 of the double peak reduction in 0.01 M phosphate buffer with amplitude 20 mV. Calibration for the reductions performed at 200 mV are shown as blue triangles, intermediate of the 2 peaks at 20 mV amplitude

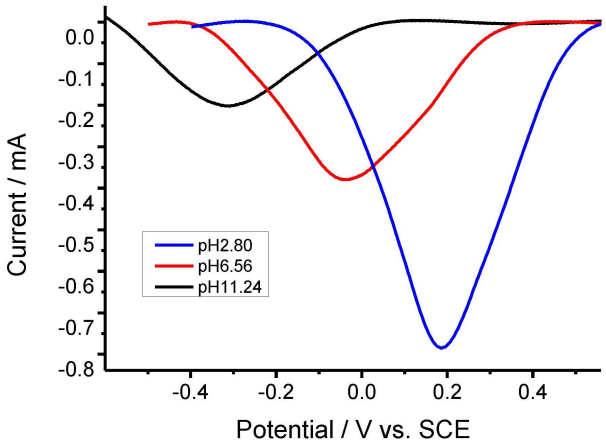


Figure 9.9: Reduction peaks of EPPG in 0.1 M buffer solutions (pH 2.80 citrate buffer solution, pH 6.56 phosphate buffer solution, pH 11.24 carbonate buffer solution)

By plotting these points against the original calibration plot across the entire pH range, it can seen from Figure 9.11 that the results (shown as blue triangles) fits well onto the previous results, given as black squares. A line of best fit going through both the 0.01 M and 0.1 M results with a gradient of 58 mV per pH could be produced using the parameters as specified earlier.

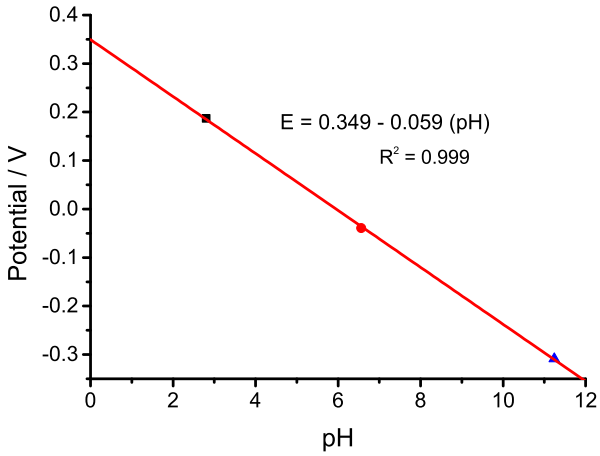


Figure 9.10: Calibration plot of the reduction peaks in 0.1 M buffer solutions. Back square corresponds to citrate buffer, red circle corresponds to phosphate buffer and blue triangle corresponds to carbonate buffer

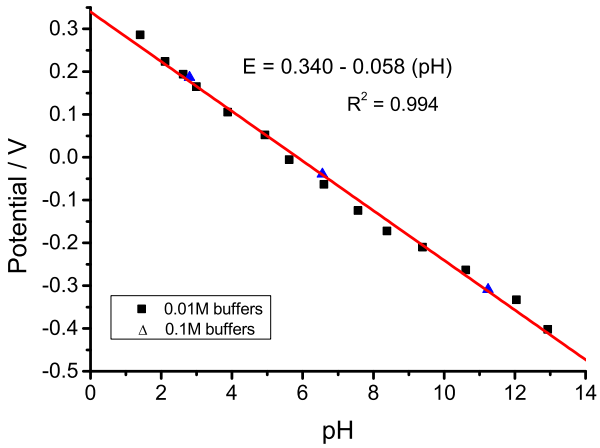


Figure 9.11: Calibration plot of the original reduction points in 0.01 M buffer solutions (black triangles), with reduction points of 0.1 M buffer solutions (blue triangles) added for comparison

It can be concluded that an EPPG electrode can be used as a pH sensor over the aqueous range 1.0 – 13.0 in solutions of variable ionic strength. Taking the reduction potential of the EPPG in SWV gave reduction peaks which can be easily analysed. Quantitative analysis of the reduction peak potential can thus be used to produce a linear reduction peak potential against pH calibration plot.

9.4 Conclusions

For an unmodified edge plane pyrolytic graphite electrode (EPPG), the SWV peak potential for the reduction of surface quinones has been shown to respond linearly with solutions of different pH such that a calibration plot ranging from pH 1.0 – 13.0 can be successfully formed. A Nernstian response corresponding to a 2 proton/2 electron system lends itself to the use of an EPPG as a simple, easy to use, reagentless and cheap pH sensing material.

Next, the pH response at a glassy carbon electrode is investigated. Given the pH sensitive quinone groups present at graphitic edge plane sites, it would be interesting to see whether the surface of glassy carbon presents similar characteristics as that of an edge plane pyrolytic graphite electrode.

Bibliography

[1] H. Kahlert, *Journal of Solid State Electrochemistry* **12** (2008) 1255.

[2] V. G. H. Lafitte, W. Wang, A. S. Yashina and N. S. Lawrence, *Electrochemistry Communications* **10** (2008) 1831.

[3] J. S. Bradley, J. O. Phillips, J. E. Cavanaugh and M. H. Metzler, *Critical Care Medicine* **26** (1998) 1905.

[4] C. Guyard, *Eau, l'Industrie, les Nuisances* **347** (2011) 87.

[5] D. R. Turner, M. Whitfield and A. G. Dickson, *Geochimica et Cosmochimica Acta* **45** (1981) 855.

[6] A. P. F. Turner, I. Karube and G. S. Wilson, *Biosensors: Fundamentals and Applications* (Oxford University Press, Oxford, 1987).

[7] B. K. Kanungo, M. Baral, R. K. Bera and S. K. Sahoo, *Monatshefte fuer Chemie* **141** (2010) 157.

[8] M. Kneen, J. Farinas, Y. Li and A. S. Verkman, *Biophysical journal* **74** (1998) 1591.

[9] R. B. Moon and J. H. Richards, *Journal of Biological Chemistry* **248** (1973) 7276.

[10] S. Nomura, *Bunseki* **8** (2011) 468.

[11] F. G. K. Baucke, *Journal of Non-Crystalline Solids* **73** (1985) 215.

[12] H. B. Kristensen, A. Salomon and G. Kokholm, *Analytical Chemistry* **63** (1991) 885.

[13] L. X. andChristopher Batchelor-McAuley and R. G. Compton, *Sensors and Actuators, B: Chemical* **159** (2011) 251.

[14] D. A. Skoog, D. M. West, J. Holler and S. R. Crouch, *Fundamentals of Electro-Analytical Chemistry* (2004), 8th ed. edition.

[15] G. Cui, J. S. Lee, S. J. Kim, H. Nam, G. S. Cha and H. D. Kim, *Analyst (Cambridge, United Kingdom)* **123** (1998) 1855.

[16] G. Cheek, C. P. Wales and R. J. Nowak, *Analytical Chemistry* **55** (1983) 380.

[17] R. M. Greenway, S. J. Gardiner, A. L. Hart and J. Dunlop, *Biosensors & bioelectronics* **9** (1994) 457.

[18] G. G. Wildgoose, M. Pandurangappa, N. S. Lawrence, L. Jiang, T. G. J. Jones and R. G. Compton, *Talanta* **60** (2003) 887.

[19] M. R. Tarasevich, V. A. Bogdanovskaya and N. M. Zagudaeva, *Journal of Electroanalytical Chemistry and Interfacial Electrochemistry* **223** (1987) 161.

[20] R. G. Compton and C. E. Banks, *Understanding Voltammetry* (Imperial College Press, London, 2011), 2nd ed. edition.

[21] P. S. Guin, S. Das and P. C. Mandal, *International Journal of Electrochemistry* **816202** (2011) 22.

[22] N. Schweigert, A. J. B. Zehnder and R. I. L. Eggen, *Environmental microbiology* **3** (2001) 81.

[23] J. Jacq, *Journal of Electroanalytical Chemistry and Interfacial Electrochemistry* **29** (1971) 149.

[24] C. Batchelor-McAuley, Q. Li, S. M. Dapin and R. G. Compton, *Journal of Physical Chemistry B* **114** (2010) 4094.

[25] C. E. Banks and R. G. Compton, *Analytical Sciences* **21** (2005) 1263.

[26] K. Kalcher, I. Svancara, R. Metelka, K. Vytras and A. Walcarius, *Section Title: Inorganic Analytical Chemistry*, volume 4, 283–429 (2006).

[27] V. Majer, J. Vesely and K. Stulik, *Journal of Electroanalytical Chemistry and Interfacial Electrochemistry* **45** (1973) 113.

[28] G. G. Wildgoose, P. Abiman and R. G. Compton, *Journal of Materials Chemistry* **19** (2009) 4875.

[29] R. L. McCreery, *Electroanalytical Chemistry* (1991).

[30] C. A. Thorogood, G. G. Wildgoose, J. H. Jones and R. G. Compton, *New Journal of Chemistry* **31** (2007) 958.

[31] C. A. Thorogood, G. G. Wildgoose, A. Crossley, R. M. J. Jacobs, J. H. Jones and R. G. Compton, *Chemistry of Materials* **19** (2007) 4964.

[32] X. Ji, C. E. Banks, A. Crossley and R. G. Compton, *Chemphyschem : a European journal of chemical physics and physical chemistry* **7** (2006) 1337.

[33] N. Lawrence and A. Meredith, *Electrochemical ph sensor.*, 2012.

[34] A. Star, *pH sensor systems and methods of sensing pH.*, 2013.

[35] N. Ushizawa, H. Yamaguchi and T. Shimomura, *Carbon electrode and its manufacture.*, 1991.

[36] S. P. McCormack and R. G. Compton, *Electrochemical sensors.*, 2005.

[37] P. T. Lee, J. C. Harfield, A. Crossley, B. S. Pilgrim and R. G. Compton, *RSC Advances* **3** (2013) 7347.

[38] A. T. Masheter, P. Abiman, G. G. Wildgoose, E. Wong, L. Xiao, N. V. Rees, R. Taylor, G. A. Attard, R. Baron, A. Crossley, J. H. Jones and R. G. Compton, *Journal of Materials Chemistry* **17** (2007) 2616.

[39] P. Abiman, G. G. Wildgoose, A. Crossley, J. H. Jones and R. G. Compton, *Chemistry - A European Journal* **13** (2007) 9663.

[40] A. Savitzky and M. J. E. Golay, *Anal. Chem.* **36** (1964) 1627.

[41] M. U. A. Bromba and H. Ziegler, *Analytical Chemistry* **53** (1981) 1583.

[42] Q. Li, C. Batchelor-McAuley, N. S. Lawrence, R. S. Hartshorne and R. G. Compton, *ChemPhysChem* **12** (2011) 1255.

Chapter 10

Voltammetric pH Sensing using Carbon Electrodes : Glassy Carbon behaves similarly to EPPG

Developing and building on the previous chapter based on a simple sensor for pH determination using unmodified edge plane pyrolytic graphite (EPPG) electrodes [1], voltammetric method for pH determination using a bare unmodified glassy carbon (GC) electrode is presented next. By exploiting the pH sensitive nature of quinones present on carbon edge-plane like sites within the glassy carbon, it is shown here how GC electrodes can be used to measure pH. The electro-reduction of surface quinone groups on the glassy carbon electrode was characterised using cyclic voltammetry (CV) and optimised with square-wave voltammetry (SWV) at 298 K and 310 K. At both temperatures, a linear correlation was observed, corresponding to a 2 proton/2 electron Nernstian response over the aqueous pH range 1.0 to 13.1. As such, unmodified glassy carbon electrodes are seen to be pH dependent, and the Nernstian response suggests its facile use for pH sensing. Given the widespread use of glassy carbon electrodes in eletroanalysis, the approach offers a method for the near-simultaneous measurement and monitoring of pH during such analyses.

The work presented in this chapter has been published in *Analyst*, 139, (2014), 4599-

4605.

10.1 Introduction

Chemical and biochemical reactions are often extremely sensitive to proton concentrations and even the slightest fluctuation in pH levels can result in significant changes of rate, so that pH often has to be carefully monitored and controlled [2–4].

There are a wide range of different pH sensors available, which can be voltammetric [5], amperometric [6–9] or potentiometric in nature [10, 11]. As an effort to move away from the conventional glass electrode, many different methods and materials have been explored [12, 13] and NMR methods [14], one of which is using carbon as an electrode material [15].

The characterisation of carbon surfaces has been extensively studied using both physical and chemical techniques [16]. Using methods such as XPS [17, 18], thermal decomposition methods [19], vibrational spectroscopy [20] and electrochemistry [21, 22] many functional groups have been realised. Edge plane sites present on graphitic carbons present many functional groups which can react with the oxygen in the atmosphere to form various surface oxo-groups [16]. These have been suggested as sites for electron transfer processes [23]. Of the range of functional groups present, such as carbonyl, quinonyl, hydroxyl, quinone groups have shown to be pH dependent and have been developed for the determination of pH. Many researchers have exploited this and patents using carbon electrodes for pH determination have been filed [24–27].

Figure 10.1 shows a schematic where there are three possible reduction pathways of an ortho-benzoquinone with their associated protonations, where $n = 2$ and $m = 0$, 1, 2. pK_a values for ortho-benzoquinone in aqueous solution at 298 K have been quoted in the

literature as 9.25 and 13.0 for pK_{a1} and pK_{a2}, respectively [28].

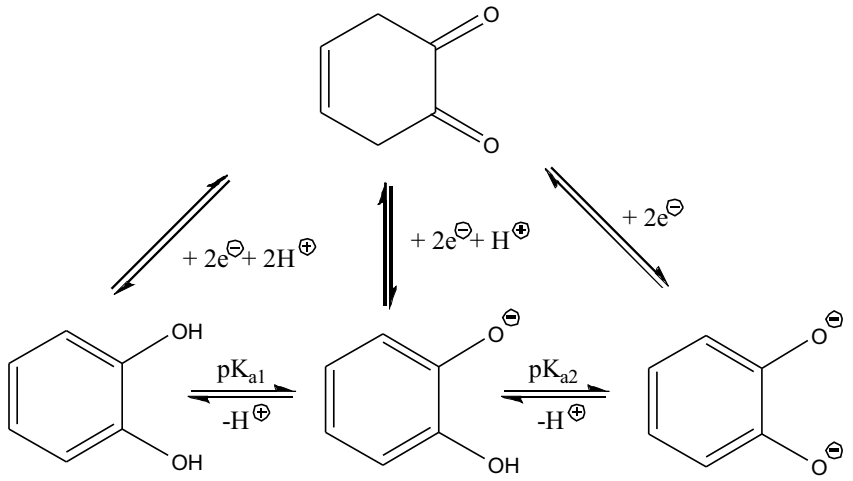


Figure 10.1: Schematic showing 3 pathways in which an orthoquinone molecule can be reduced in a 2e fashion with $m = 2$, 1 or 0

In this chapter, the use of a glassy carbon (GC) electrode and its ability to function as a pH sensor is investigate by highlighting the pH dependence of intrinsic quinone groups. Using an unmodified EPPG electrode as a simple method for pH determination has previously been reported [1] by exploiting the pH sensitive nature of intrinsic quinone groups on the surface edge place sites. The presence of quinone functional groups on graphitic carbon has been confirmed by XPS and chemical labelling by Thorogood et al. [29, 30]. Developing this, one can assume other forms of carbon with intrinsic edge-plane sites might behave in an analogous manner. Using the edge plane sites as a basis for quinone presence, investigation into the pH nature of a glassy carbon electrode is described. The glassy carbon electrode is a widely used carbon electrode material in electrochemistry due to its low electrical resistance, high temperature resistance and hardness. It is composed of sp^2 carbons, and upon polishing, edge plane surface functionalities may be revealed including pH dependent quinone functional groups.

Previously, Paixao et al. [31] have shown the use of electrochemically pre-treated glassy

carbon electrodes as pH sensors in potentiometric titrations, suggesting the presence of electrochemically reversible redox couples on the surface of glassy carbon. The authors found that the electrode could be used in pH potentiometric titrations with excellent agreement with corresponding measurements at a glass electrode. The potential varied linearly with pH over the range pH 1.0 to 13.1, with a slope of *ca.* 60 mV per pH, making it a suitable pH sensor for potentiometric experiments. Whilst potentiometric measurements are useful, in this chapter a method using voltammetric pH sensing at a glassy carbon electrode is described.

Cyclic voltammetry (CV) and square wave voltammetry (SWV) were used to study the behaviour of a bare GC electrode in a range of buffer solutions. The experiments were carried out at room temperature (298 K), and a higher temperature of 310 K. The response of the GC electrode at higher ionic strength was also investigated. A linear correlation was seen in all cases between the pH and peak potential, corresponding to a Nernstian response. One can therefore infer that glassy carbon electrodes have analogous edge-plane sites to edge plane pyrolytic graphite electrodes and can similarly function as a pH sensor through their intrinsic pH sensitive quinone functional groups.

It is common to use glassy carbon electrodes in electroanalysis. The method proposed in this chapter suggests a basis for a near-simultaneous measurement of pH during such analyses. The use of the same electrode for pH measurement and as a working electrode is extremely useful in electroanalytical measurements. A proof of concept of combined measurements at a single pH has been reported by Henstridge et al [32] whereby theory and experimental evidence shows that the single-electrode generator-collector approach is capable of detecting local pH changes adjacent to the electrode surface during a redox reaction. This approach can be applied to a wide range of electrochemical systems.

10.2 Experimental

10.2.1 Apparatus and Reagents

Experiments were performed using a standard three-electrode system consisting of a saturated calomel reference electrode (SCE), a platinum (Pt) mesh counter electrode and a glassy carbon working electrode.

A thermostatted Faraday cage, made in-house, was used to house all the experiments performed. Two temperatures were investigated and constant working temperatures of 298 K and 310 K were set within the Faraday cage whilst the temperature of the solutions were maintained at 298 ± 0.2 K and 310 ± 0.2 K, respectively. By placing the solutions within the Faraday cage for at least two hours, thermal equilibrium could be ensured. A thermometer was used for measurement of the solution during the experiment.

Buffer solutions were prepared as described in the Experimental Methods chapter.

10.2.2 Experimental Procedure

Fresh buffer solutions were prepared daily, and their pH determined using a pH meter prior to experiments. A small volume of each solution was transferred into an electrochemical cell where thorough bubbling of pure N_2 into the vessel was performed to remove dissolved oxygen in solution and a degassed system was established. A platinum mesh functioned as the counter electrode and was flamed before the experiment to ensure a clean set-up. The system was thermostatted to maintain temperature at 295 ± 0.2 K and 310 K ± 0.2 K, respectively.

The glassy carbon electrodes were polished to a mirror finish by using an alumina slurry on soft lapping pads of decreasing grades, from 1.0 μm to 0.3 μm and finally 0.05

μm, followed by thorough sonication and rinsing using deionised water. Since glassy carbon electrodes are made up of interwoven ribbons of sp^2 carbons, mechanical polishing using alumina slurry can be used to expose edge plane surface functionalities. After preparation of the GC electrode, cyclic voltammograms were performed followed by square wave voltammetry using optimised parameters. More sensitive results could be achieved using SWV, and by observing the reductive cathodic scans, their peak potentials could be precisely determined and plotted against pH. The optimised parameters for SWV were: frequency - 150 Hz, step potential - 2 mV, amplitude - 200 mV, over the entire pH range explored. The glassy carbon electrode was used to scan in the cathodic direction, and the potential window was adjusted for different pHs to best observe the reduction peak. Reported analysis of the reduction peaks were all carried in SWV.

10.3 Results and Discussions

Glassy carbon electrodes were polished to a mirror finish prior to each experiment. This is thought to provide surface quinone functional groups which were used to explore the electrode response to varying pH [33]. Surface renewal is essential to obtaining reproducible data. First, cyclic voltammograms (CVs) were performed on GC electrodes to characterise the surface quinones before SWV scans were taken. The optimised parameters for scanning in SWV are outlined in the experimental procedure above, and by scanning cathodically, this produced a single reduction SWV peak.

A range of 0.01 M pH buffer solutions at 298 K were used, and after scanning from a positive to a negative potential in SWV, a single reduction peak corresponding to the reduction of the surface quinone was produced for each buffer solution. With increasing

pH of the buffer, the reduction peak was seen to shift in the cathodic direction to lower potential values. The potential window was adjusted accordingly to accommodate the shift in potential and observe the response of the reduction peak. In Figure 10.2, it can be clearly seen that the peak potential shifts with pH.

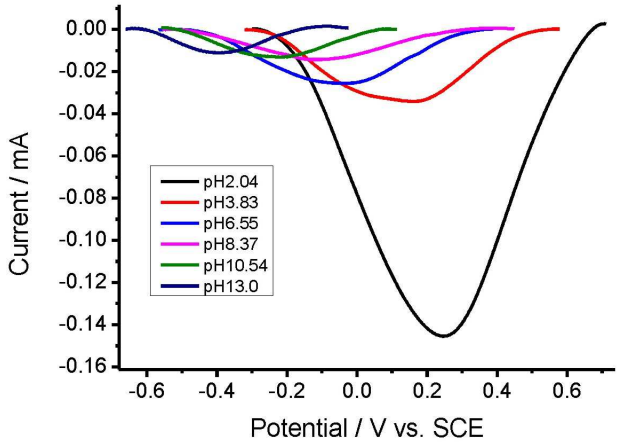


Figure 10.2: Quinone reduction peaks in square wave (SWV) on glassy carbon electrode at 298 K. Reduction peaks were obtained in different media (HCl/KCl buffer, citrate buffer, phosphate buffer, carbonate buffer at 0.01 M and NaOH buffer at 0.1 M), ranging in pH from 2.04 to 13.0. SWV performed under optimised conditions: frequency - 150 Hz, step potential - 2 mV, amplitude - 200 mV

0.01 M buffer solutions were prepared as discussed in the experimental section. To reach a higher pH, a 0.1 M sodium hydroxide buffer was used to make up the pH 13.0 solution. 100 mM KCl of supporting electrolyte was added to all solutions. It can be seen that the reduction peak potential shifts from 0.263 V at pH 2.04 to -0.397 V at pH 13.0. The gradual decrease in peak current may be explained by the fact there are fewer free protons available (lower concentration) for the $2H^+/2e^-$ reduction process at high pH, and thus this may limit the extent of quinone reduction producing peaks of smaller current. The electrochemical properties of quinones have been studied extensively using experiments and modelling [34]. A scheme of squares model for the 2 electron reduction of

quinones provides mechanistic pathways for the reduced species by assuming the electron transfer is the rate limiting step in well buffered media, and suggesting the presence of semiquinone intermediates.

Analysis of the results was carried out after background correction and smoothing of the signals, which enhanced the peaks for clearer analysis. Both methods were performed using GPES software; the background correction involved subtracting a 2^{nd} order polynomial baseline curve from the raw data, whilst background noise was smoothed using the Savitzky and Golay smoothing filter [35, 36]. In Figure 10.3, a plot of reduction peak potential against pH at 298 K shows a linear response with a gradient of 59.0 mV per pH, which agrees well with the Nernstian equation with T at 298 K. The linear slope reflects the sensitive nature of the quinone groups at the edge plane sites of the glassy carbon electrode.

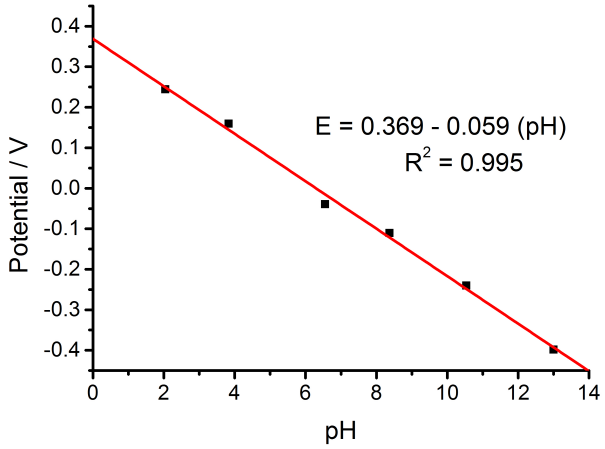


Figure 10.3: Calibration plot of SWV peak potential against pH for a glassy carbon electrode in 0.01 M buffer solutions (with 0.1 M NaOH buffer solution at pH 13.0), showing a linear response with gradient of 59.0 mV/pH corresponding to a Nernstian behaviour at T = 298 K

A consistent gradient, corresponding to a 2 $H^+/2e^-$ process, was seen across the entire pH range of pH 1.0 to pH 13.0. Literature values for the pK_a of free ortho-benzoquinone

molecules in aqueous solution were 9.25 and 13.0 for pK_{a1} and pK_{a2}, respectively. Lee et al. [37] reviewed the change in pK_{a1} for immobilised quinone groups compared to that in bulk solution. A significant change in pK_{a1} was seen, implying that significant differences in thermodynamic and chemical behaviour exist between molecules in bulk solution and that immobilised at an interface. Given that significant changes in pH at the two quoted pK_a values is not seen, it can be inferred that significant differences in acidity exist between surface bound and bulk orthoquinone moieties, whereby the deprotonation of surface hydro-orthoquinone groups is not seen below *ca.* pH 13.

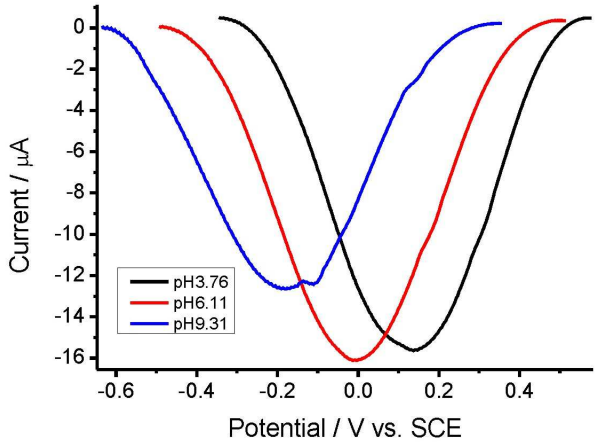


Figure 10.4: Reduction peaks at GC electrode in 0.1 M buffer solutions at 298 K (pH 3.76 citrate buffer solution, pH 6.11 phosphate buffer solution, pH 9.31 carbonate buffer solution)

After observing a linear response between the peak potential and pH for the 0.01 M buffer solutions, and seeing that the results agree well with the Nernst equation at 298 K, further investigation into the effects of increasing the ionic concentration was explored. The concentration of the solutions was increased ten-fold to 0.1 M, and a glassy carbon was used to see how the reduction peak potential would change with pH. 0.1 M citrate, phosphate and carbonate buffer solutions had pH values of 3.76, 6.11 and 9.31,

respectively, at 298 K. Figure 10.4 shows the quinone peak reduction in SWV at the above pHs. As with the 0.01 M solutions, the peaks can be seen to shift towards more negative potentials at higher pH. By plotting peak potential against pH and superimposing these results onto the previous calibration plot, Figure 10.5 shows that the points lie well on the line of best fit.

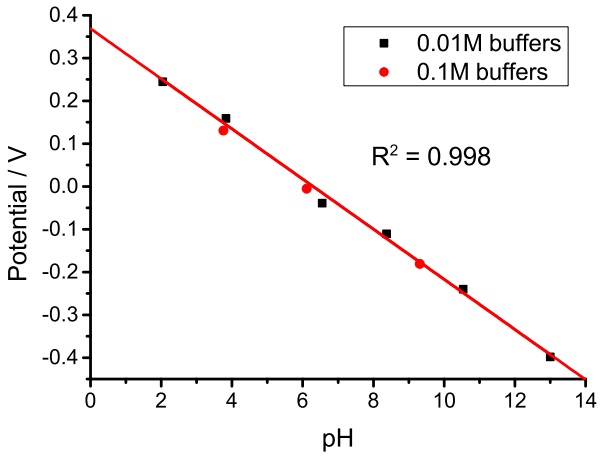


Figure 10.5: Calibration plot of the original reduction points in 0.01 M buffer solutions (black squares), with reduction points of 0.1 M buffer solutions (red circles), at 298 K, added for comparison

10.3.1 Investigating the GC Electrode Response to pH at Higher Temperature

The experiment was repeated at an increased temperature of 310 K and the glassy carbon electrode was investigated in different 0.01 M pH buffer solutions. The working temperature within the Faraday cage was maintained at 310 K, whilst the solutions and experimental apparatus were allowed to reach thermal equilibrium.

A set of square wave peaks were produced for a range of 0.01 M buffer solutions and it could be seen that with increasing pH, there was a corresponding reduction peak

potential shift towards more cathodic values, as expected. Taking the reduction peak potential values at 310 K and plotting the pH against potential, a linear response could be seen in the calibration plot across the entire pH range. The theoretical value for the gradient (2.303 RT/F) was calculated to be 61.4 mV/pH, and the calibration produced from the results at 310 K agreed very well this, giving a gradient of 61.0 mV/pH.

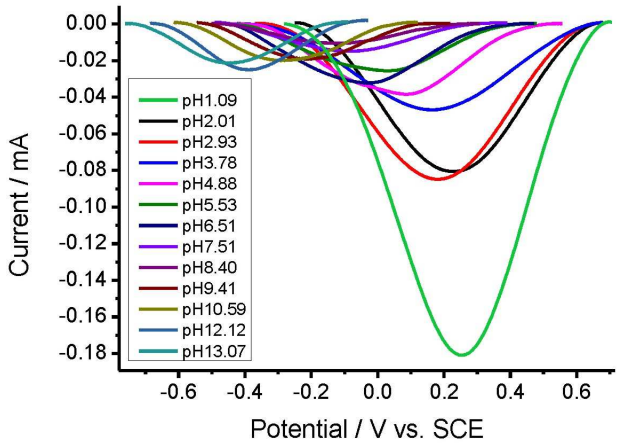


Figure 10.6: Quinone reduction peaks in square wave (SWV) on glassy carbon electrode at 310 K. Reduction peaks were obtained in different media (HCl/KCl buffer, citrate buffer, phosphate buffer, carbonate buffer at 0.01 M, 0.1 M HCl/KCl and NaOH buffers were included for completeness), ranging in pH from 1.09 to 13.07. SWV performed under optimised conditions: frequency - 150 Hz, step potential - 2 mV, amplitude - 200 mV

Figure 10.6 shows a set of SWV reduction peaks in a range of 0.01 M buffer solutions, (with 0.1 M HCl/KCl and NaOH buffer solutions included for completeness across the entire pH range). The peak potential value shifts from 0.253 V at pH 1.09 to -0.449 at pH 13.07. Again, the peak heights can be seen to decrease with increasing pH. This is attributed to the concentration of free protons available for quinone reduction with the number of H^+ ions being far less at high pH compared to low pH solutions. The effect of temperature on the size of currents is apparent by comparing Figure 10.6 with Figure 10.2. The peak heights are larger at higher temperature which may relate to faster

diffusion of H^+ ions. The plot of the peak reduction against pH at 310 K gave a very linear correlation with a gradient of 61.0 mV/pH, as seen in Figure 10.7. From this, it can seen that the plot highlights the temperature dependence of the Nernstian equation, and this can be exploited by observing the quinone reduction on carbon electrodes such as a GC electrode.

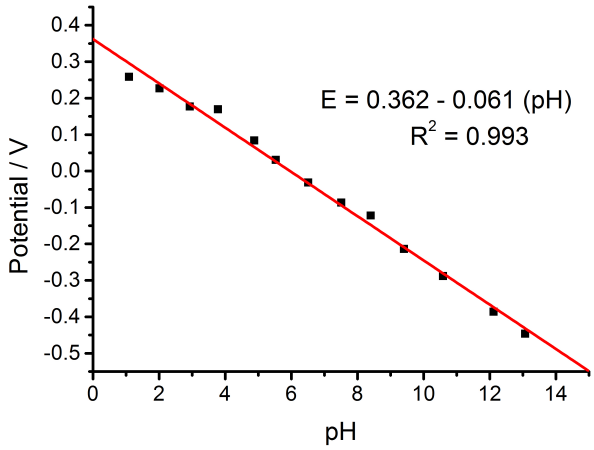


Figure 10.7: Calibration plot of SWV peak potential against pH for a glassy carbon electrode in 0.01 M buffer solutions (with 0.1 M HCl/ KCl and NaOH buffer solutions at pH 1.09 and pH 13.0, respectively), showing a linear response with gradient of 61.0 mV/pH corresponding to a Nernstian behaviour at T = 310 K

Using 0.1 M buffer solutions, investigation into the effects of higher ionic strength can be seen with respect to the reduction peak potentials seen. Buffer solutions of pH 3.98, pH 6.11 and pH 9.21 were made using citric acid/sodium citrate, monosodium phosphate/disodium phosphate and sodium carbonate/bicarbonate, respectively. In Figure 10.8, it can be seen that all three solutions at higher concentration produced a single reduction peak which also shifted towards cathodic potentials with increasing pH. By plotting the reduction potentials and overlaying them with the 0.01 M buffer solution results at 310 K, it can be seen from Figure 10.9 that the results agree very well with the

original calibration line.

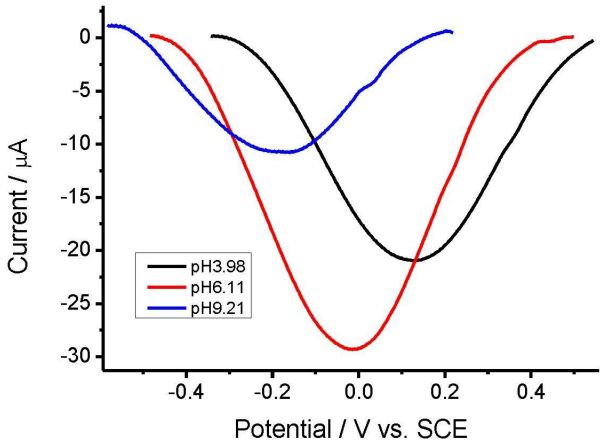


Figure 10.8: Reduction peaks at GC electrode in 0.1 M buffer solutions at 310 K (pH 3.98 citrate buffer solution, pH 6.11 phosphate buffer solution, pH 9.21 carbonate buffer solution)

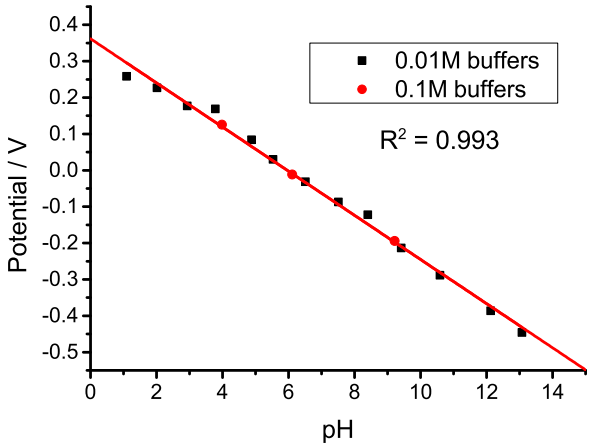


Figure 10.9: Calibration plot of the original reduction points in 0.01 M buffer solutions (black squares), with reduction points of new 0.1 M buffer solutions (red circles), at 310 K, added for comparison

It can therefore be concluded that a glassy carbon electrode works well as a pH sensor in aqueous solution across the entire pH range, at various ionic strength and at temperatures beyond room temperature of 298 K. By recording the reduction peaks in SWV,

quantitative analysis of the signals can be used to plot a very linear peak potential versus pH calibration graph.

10.4 Conclusions

Glassy carbon electrodes have shown an analogous behaviour to unmodified edge plane pyrolytic graphite (EPPG) electrodes when their SWV peak potential for the reduction of surface quinones is plotted against pH. This behaviour can be explained due to the common intrinsic nature of edge-plane sites that contain quinone functional groups. By using SWV, and analysing the reduction peak in different pH buffer solutions, at different temperatures and ionic strengths, a Nernstian response can be seen from the linear calibration plot. This suggests the presence of surface quinone groups at glassy carbon electrodes which show electrochemically reversible behaviour, and as such, by using SWV, lends itself to its use as a simple voltammetric pH sensor. In particular, since GC electrodes are widely used for voltammetric electroanalysis, the possibility of monitoring pH simultaneously with other electroanalytical measurements is viable.

Bibliography

[1] M. Lu and R. G. Compton, *Analyst (Cambridge, United Kingdom)* **139** (2014) 2397.

[2] V. G. H. Lafitte, W. Wang, A. S. Yashina and N. S. Lawrence, *Electrochemistry Communications* **10** (2008) 1831.

[3] J. S. Bradley, J. O. Phillips, J. E. Cavanaugh and M. H. Metzler, *Critical Care Medicine* **26** (1998) 1905.

[4] C. Guyard, *Eau, l'Industrie, les Nuisances* **347** (2011) 87.

[5] A. E. Musa, M. A. Alonso-Lomillo, F. J. del Campo, N. Abramova, O. Dominguez-Renedo, M. J. Arcos-Martinez and J. P. Kutter, *Talanta* **99** (2012) 737.

[6] G. Cui, J. S. Lee, S. J. Kim, H. Nam, G. S. Cha and H. D. Kim, *Analyst (Cambridge, United Kingdom)* **123** (1998) 1855.

[7] G. Cheek, C. P. Wales and R. J. Nowak, *Analytical Chemistry* **55** (1983) 380.

[8] H. C. Leventis, I. Streeter, G. G. Wildgoose, N. S. Lawrence, L. Jiang, T. G. J. Jones and R. G. Compton, *Talanta* **63** (2004) 1039.

[9] G. G. Wildgoose, M. Pandurangappa, N. S. Lawrence, L. Jiang, T. G. J. Jones and R. G. Compton, *Talanta* **60** (2003) 887.

[10] D. R. Turner, M. Whitfield and A. G. Dickson, *Geochimica et Cosmochimica Acta* **45** (1981) 855.

[11] A. P. F. Turner, I. Karube and G. S. Wilson, *Biosensors: Fundamentals and Applications* (Oxford University Press, Oxford, 1987).

[12] B. K. Kanungo, M. Baral, R. K. Bera and S. K. Sahoo, *Monatshefte fuer Chemie* **141** (2010) 157.

[13] M. Kneen, J. Farinas, Y. Li and A. S. Verkman, *Biophysical journal* **74** (1998) 1591.

[14] R. B. Moon and J. H. Richards, *Journal of Biological Chemistry* **248** (1973) 7276.

[15] H. Kahlert, *Journal of Solid State Electrochemistry* **12** (2008) 1255.

[16] G. G. Wildgoose, P. Abiman and R. G. Compton, *Journal of Materials Chemistry* **19** (2009) 4875.

[17] C. Kozlowski and P. M. A. Sherwood, *Journal of the Chemical Society, Faraday Transactions 1: Physical Chemistry in Condensed Phases* **80** (1984) 2099.

[18] R. I. R. Blyth, H. Buqa, F. P. Netzer, M. G. Ramsey, J. O. Besenhard, P. Golob and M. Winter, *Applied Surface Science* **167** (2000) 99.

[19] D. T. Fagan and T. Kuwana, *Analytical Chemistry* **61** (1989) 1017.

[20] M. A. Fryling, J. Zhao and R. L. McCreery, *Analytical Chemistry* **67** (1995) 967.

[21] S. S. Barton, G. L. Boulton and B. H. Harrison, *Carbon* **10** (1972) 395.

[22] T. Szabo, O. Berkesi, P. Forgo, K. Josepovits, Y. Sanakis, D. Petridis and I. Dekany, *Chemistry of Materials* **18** (2006) 2740.

[23] X. Ji, C. E. Banks, A. Crossley and R. G. Compton, *Chemphyschem : a European journal of chemical physics and physical chemistry* **7** (2006) 1337.

[24] N. Lawrence and A. Meredith, *Electrochemical ph sensor.*, 2012.

[25] A. Star, *pH sensor systems and methods of sensing pH.*, 2013.

[26] N. Ushizawa, H. Yamaguchi and T. Shimomura, *Carbon electrode and its manufacture.*, 1991.

[27] S. P. McCormack and R. G. Compton, *Electrochemical sensors.*, 2005.

[28] N. Schweigert, A. J. B. Zehnder and R. I. L. Eggen, *Environmental microbiology* **3** (2001) 81.

[29] C. A. Thorogood, G. G. Wildgoose, A. Crossley, R. M. J. Jacobs, J. H. Jones and R. G. Compton, *Chemistry of Materials* **19** (2007) 4964.

[30] C. A. Thorogood, G. G. Wildgoose, J. H. Jones and R. G. Compton, *New Journal of Chemistry* **31** (2007) 958.

[31] T. R. L. C. Paixao, L. Kosminsky and M. Bertotti, *Sensors and Actuators, B: Chemical* **87** (2002) 41.

[32] M. C. Henstridge, G. G. Wildgoose and R. G. Compton, *Journal of Physical Chemistry C* **113** (2009) 14285.

[33] I. F. Hu, D. H. Karweik and T. Kuwana, *Journal of Electroanalytical Chemistry and Interfacial Electrochemistry* **188** (1985) 59.

[34] Q. Li, C. Batchelor-McAuley, N. S. Lawrence, R. S. Hartshorne and R. G. Compton, *ChemPhysChem* **12** (2011) 1255.

[35] A. Savitzky and M. J. E. Golay, *Anal. Chem.* **36** (1964) 1627.

[36] M. U. A. Bromba and H. Ziegler, *Analytical Chemistry* **53** (1981) 1583.

[37] P. T. Lee, J. C. Harfield, A. Crossley, B. S. Pilgrim and R. G. Compton, *RSC Advances* **3** (2013) 7347.

Chapter 11

Summary and Conclusions

The work in this thesis sets out to investigate various forms of voltammetric sensing including the trace detection of antimony and iron using pulse methods, fabrication and use of a vibrating foil electrode and pH determination at unmodified carbon electrodes.

Optimised differential pulse stripping voltammetry of antimony (V) involving deposition beyond the hydrogen wave was found to be effective for the trace detection of antimony at an edge plane pyrolytic graphite (EPPG) electrode. By depositing at very negative potentials, hydrogen evolution at the working electrode could be avoided and anodic currents were produced without modification of the carbon electrode. This appears to be a new electroanalytical strategy with applications beyond antimony.

It was also found that square wave voltammetry at unmodified EPPG and screen print electrodes can be used to detect iron (III) in aqueous solution. Bottled water was successfully evaluated using this method and gave a calculated detection limit of Fe(III) to be 2.0 μM. This leads to a possible route for the design of a cheap and portable voltammetric sensor for iron detection.

Fabrication of a vibrating electrode was achieved through modification of a cheap and commercially available toothbrush with a platinum foil. Experiments at the vibrating electrode enhanced mass transport and current was found to change from a transient to

a steady state, which can then be useful for simple analysis. It can be realised that the described fabrication can be easily modified with other electrode materials and developed for alternative setups to address trace detection of analytes.

With a view for pH sensing, it was found that the reduction of surface ortho-quinone groups intrinsic to graphitic carbons was pH dependent. Using square wave voltammetry, a linear response was found to exist between the peak potential and pH at an unmodified EPPG electrode and corresponded well with Nernstian behaviour based on a 2 proton/2 electron system. A simple and novel carbon sensor for pH determination was thus developed and a patent has been filed based on this research. By extending this method to other graphitic edge plane sites, a glassy carbon electrode was investigated which showed an analogous behaviour to EPPG electrodes over the pH range 1.0 to 13.0. As such, the results from this thesis opens up a novel and different approach for pH determination.

The voltammetric sensing of trace analytes and their optimised techniques continue to be an important and extensive area of interest. Whilst the work in this thesis only touches on a couple of novel approaches at carbon electrodes, a vast number of electrode materials continue to be developed for the detection of many different analytes, leading to an exciting future for electroanalytical chemistry.